Topology of streamlines and vorticity contours for two - dimensional flows

Andersen, Morten

Publication date:
2013

Document Version
Publisher's PDF, also known as Version of record

Topology of streamlines and vorticity contours for two - dimensional flows

Morten Andersen

Supervisor: Professor Morten Brøns

Kongens Lyngby 2013
DTU Compute-PHD-2013-314

Technical University of Denmark
Applied Mathematics and Computer Science
Matematiktorvet, Building 303, DK-2800 Kongens Lyngby, Denmark
www.compute.dtu.dk

PHD: ISSN 0909-3192

Summary

Considering a coordinate-free formulation of helical symmetry rather than more traditional definitions based on coordinates, we discuss basic properties of helical vector fields and compare results from the literature. For inviscid flow where a velocity field is generated by a sum of helical vortex filaments with same pitch we use the established results to prove briefly that the velocity field is helical. We discuss the role of the stream function for the topology of the streamlines in incompressible, helical flows. On this basis, we perform a comprehensive study of the topology of the flow field generated by a helical vortex filament in an ideal fluid. The classical expression for the stream function obtained by Hardin (Phys. Fluids 25, 1982) contains an infinite sum of modified Bessel functions. Using the approach by Okulov (Russ. J. Eng. Thermophys. 5, 1995) we obtain a closed-form approximation which is considerably easier to analyse. Critical points of the stream function can be found from the zeroes of a single real function of one variable, and we show that three different flow topologies can occur, depending on a single dimensionless parameter. Including the self-induced velocity on the vortex filament by the localised induction approximation the stream function is slightly modified and an extra parameter is introduced. In this setting two new flow topologies arise, but not more than two critical points occur for any combination of the parameters. The analysis of the closed form show promise for analysing more complex flow with helical symmetry e.g. multiple helical vortex filaments inside a cylinder which has industrial relevance.

We then change focus and study creation, destruction and interaction of vortices in two dimensional flow. A vortex is advected above a wall causing a viscous response near the wall which generates a new vortex structure. The problem is studied numerically relying on the code developed by Prof. M. Thompson and his group at Monash University, Australia. We also investigate the problem

analytically using normal form theory. It is not a simple task to define a vortex in a proper way that allow the study of creation and destruction of vortices. We investigate three sound choices: the vorticity extrema, the streamline centers in a coordinate system with zero wall speed and the streamline centers in a frame moving with constant velocity as predicted by a point vortex above a wall in inviscid fluid. There is no reason to a priori expect equivalent results of the three vortex definitions. However, the study is mainly motivated by the findings of Kudela & Malecha (Fluid Dyn. Res. 41, 2009) who find good agreement between the vorticity and streamlines in the fixed wall system. For small Re no new vortices are observed. Creation of a vortex occurs for sufficiently large Re for all the applied vortex definitions. The new vortex alters the generating vortex motion by slowing its horizontal motion and lifting it further from the wall. In the fixed wall system vortex eruption happens through a characteristic 'figure 8' bifurcation. Considering the other coordinate system there is no topological change indicating when a vortex has left the boundary layer. However, here there is remarkable good agreement between streamlines and the vorticity contours even for short-lived vortices close to the wall.

The normal form approach does not reveal simple connections between the streamline topology and the vorticity contour topology. Only for a non simple degenerate on wall critical point may a bifurcation occur in both the streamlines and the vorticity contours. The streamline bifurcations in this normal form contain the lower part of the 'figure 8' bifurcation observed in numerics. The similarities and differences of the streamlines in the two different coordinate systems are well described by normal form theory.

We derive the criterion, $\boldsymbol{u} \cdot \nabla \omega = 0$, for exactly matching contours of the vorticity contours and streamlines. This is fulfilled when the Navier - Stokes equations and the heat equation have identical solutions.

Finally we focus on the superposition of two rotational invariant vortices in $\mathbb{R}^2$. The topology of the streamlines and the topology of the vorticity conturs are determined by the zeros of a single real function. For the canonical example of two Gaussian vortices three parameters exist. Three structurally stable topologies are observed. For the streamlines two of the topologies are well known for the corresponding situation of two point vortices when the singularities are treated as centers. The last topology is a single center which is consistent with the powerful result on the long time behaviour proved by Gallay & Wayne (Comm. in Math. Phys. 255, 2005). The case of three critical points of the streamlines is a subset of three critical points of the vorticity. This explains an observation in the simulations of vortex generation near a wall. Here, a long living erupted vortex disappears due to viscosity. This happens first considering the streamlines while being more robust when considering the vorticity formulation.

Resumé

Ved at benytte en koordinatfri formulering af helisk symmetri frem for mere traditionelle definitioner baseret på koordinater, diskuterer vi grundlæggende egenskaber for heliske vektor felter og sammenligner resultater fra litteraturen. For inviscid væske, hvor et hastighedsfelt er genereret af en sum af heliske hvirveltråde med samme pitch, benytter vi de opnåede resultater til at konstruere et kort bevis for, at hastighedsfeltet er helisk. Vi diskuterer strømfuntionens indflydelse på topologien af strømlinjerne for inviscid, helisk flow. På baggrund af dette laver vi en udførlig undersøgelse af topologien af et hastighedsfelt genereret af en helisk hvirveltrad i en idealvæske. Det klassiske udtryk for strømfunktionen opnået af Hardin (Phys. Fluids 25, 1982) indeholder en uendelig sum af modificerede Bessel funktioner. Ved at benytte metoden beskrevet af Okulov (Russ. J. Eng. Thermophys. 5, 1995) opnår vi en approksimation på lukket form, der er væsentlig lettere at analysere. Kritiske punkter for strømfunktionen kan findes som nulpunkterne af en enkelt reel funktion af en variabel, og vi viser, at tre forskellige toplogier kan forekomme, afhængig af en enkelt dimensionsløs parameter. Ved at inkludere den selvinducerede hastighed på hvirveltråden via 'den lokaliserede induktionstilnærmelse' bliver strømfunktionen lettere modificeret og en ekstra parameter introduceres. Nu fremkommer to nye topologier men der er højst to kritiske punkter for en vilkårlig kombination af parametrene. Analysen af den lukkede form er lovende for at undersøge mere komplekse strømninger med helisk symmetri, for eksempel flere heliske hvirveltråde inde i en cylinder, hvilket har industriel relevans.

Vi skifter fokus og undersøger dannelse, forsvinden og vekselvirkning af hvirvler for todimensionelle strømninger. En hvirvel strømmer over en væg, hvilket forårsager et viskøst respons nær væggen, hvilket genererer en ny hvirvelstruktur. Problemet undersøges numerisk ved brug af kode udviklet af Prof. M. Thompson

og hans gruppe på Monash Universitet, Australien. Vi undersøger også problemet analytisk ved brug af teori for normalformer. Det er ikke en simpel opgave at definere en hvirvel på en måde, der tillader studiet af dannelse og forsvinden af hvirvler. Vi undersøger tre fornuftige valg, vorticitetsekstrema, strømlinjecentre i et koordinatsystem, hvor væggen står stille, og strømlinjecentre i et koordinatsystem, der bevæger sig med konstant hastighed dikteret af hastigheden af en punkthvirvel over en væg i inviscid væske. Der er ingen grund til at forvente ens resultater af de tre hvirveldefinitioner a priori. Studiet er dog kraftigt motiveret af undersøgelserne af Kudela og Malecha (Fluid Dyn. Res. 41, 2009) som finder god overensstemmelse mellem vorticiteten og strømlinjer for koordinatsystemet, hvor væggen står stille. For små Re , ses ingen nye hvirvler. Hvirveldannelse sker for tilstrækkelig stor Re , for alle de anvendte hvirveldefinitioner. Den nye hvirvel løfter den oprindelige hvirvel længere væk fra væggen samt bremser dens horisontale bevægelse. I systemet, hvor væggen står stille, sker hvirveldannelse gennem en karakteristik "8-tals" bifurkation. I det andet koordinatsystem er der ingen toplogisk ændring, der indikerer, hvornår en hvirvel har forladt grænselaget. Derimod er der bemærkelsesværdig god overensstemmelse mellem strømlinjer og vorticitetskonturer selv for kortlivede hvirvler tæt på væggen.

Tilgangen med normalformer afslører ingen simple sammenhænge mellem strømlinjetopologien og vorticitetstoplogien. Kun for et ikke-simpel degenereret kritisk punkt på væggen kan en bifurkation forekomme både i strømlinjetopologien og vorticitetstoplogien. Strømlinjebifurkationerne i denne normal form indeholder den nedre del af "8-talsbifurkationen", der ses i simuleringerne. Lighederne og forskellene i strømlinjetopologierne for de to koordinatsystemer er velbeskrevet med normalforms teori.

Vi udleder kravet, $\boldsymbol{u} \cdot \nabla\omega = 0$, for perfekt matchende strømlinjer og vorticitetskonturer. Dette er opfyldt når Navier - Stokes ligningerne og varmeligningen har samme løsninger.

Til slut fokuserer vi på superposition af to rotationsinvariante hvirvler i $\mathbb{R}^2$. Topologien af vorticitetskonturerne og strømlinjerne er begge bestemt af nulpunkterne af en reel funktion af en variabel. For det kanoniske eksempel med to Gaussiske hvirvler findes tre parametre. Tre strukturelt stabile topologier observeres. For strømlinjerne er to af topologierne velkendte for den tilsvarende situation med to punkthvirvler, når singulariteterne opfattes som centre. Den sidste topologi er et enkelt center som er konsistent med et kraftfulde resultat bevist af Gallay & Wayne (Comm. In Math. Phys. 255, 2005). Tilfældet med tre kritiske punkter for strømlinjerne er en delmængde af tre kritiske punkterne for vorticiteten. Dette forklarer observationen i simuleringerne af hvirveldannelse nær en væg. En ny hvirvel, der er drevet væk fra væggen forsvinder grundet viskositet. Dette ses først, når man betragter strømlinjedefinitionen, mens hvirvlen er mere robust ud fra vorticetsdefinitionen.

Preface

This thesis was prepared at the Department of Mathematics which after a fusion process was a part of Department of Applied Mathematics and Computer Science at the Technical University of Denmark in partial fulfilment of the requirements for acquiring the Ph.D. degree. The PhD project was supervised by Professor Morten Brøns and was funded by the department/DTU.

Based on the findings in chapter 2 a manuscript has been submitted as joint work with Professor Morten Brøns to Journal of European Mathematical Society.

I would like to thank Professor Valery Okulov, DTU Mechanical Engineering, for bringing my attention to the closed form approximation of the velocity field generated by a helical vortex filament.

During the past three years I spent five months working with Mark Thompson at the Department of Mechanical and Aerospace Engineering, Monash University, Melbourne, Australia. I am grateful that Mark spent time teaching me to use the advanced numerical code they have developed and fine tuned at his department.

A special thanks to my supervisor Professor Morten Brøns. You have always had the time to discuss my PhD project and the fruitful discussions have been crucial for the outcome of my studies as well as your welcoming attitude has made the every day work life pleasant.

Morten Andersen
Lyngby, September 2013

Contents

Chapter 1

Introduction

1.1 Fundamentals of fluid dynamics

The following is a brief review of some important basics of fluid dynamics which can be found in any textbook on the subject e.g. [10, 65, 2].

The dynamics of a fluid may be described by considering a large collection of small 'fluid parcels' interacting through Newton's law. The aim is often to know the velocity field at any given time and point in the fluid i.e. $\boldsymbol{u}(\boldsymbol{x}, t)$. For a fluid with constant density this leads to a cornerstone of fluid dynamics - the Navier - Stokes equations (ν is the kinematic viscosity of the fluid, ρ is the fluid density, p is the pressure)

$$\frac{\partial \boldsymbol{u}}{\partial t} + \boldsymbol{u} \cdot \nabla \boldsymbol{u} = \nu \Delta \boldsymbol{u} - \frac{1}{\rho} \nabla p \tag{1.1}$$

along with boundary conditions and the incompressibility condition

$$\nabla \cdot \boldsymbol{u} = 0 \tag{1.2}$$

forcing the density ρ to be constant. The left hand side of equation (1.1) represents the acceleration of the fluid and the right hand side the forces per

unit mass acting on the fluid - a viscous term and a pressure term but more forces could be added.

The vorticity, $\boldsymbol{\omega}$, defined as the curl of the velocity field

$$\boldsymbol{\omega} = \nabla \times \boldsymbol{u} \tag{1.3}$$

is an important quantity. Is is a measure of the local 'swirl' or rotation of the fluid. For instance a solid body rotation $\boldsymbol{u} = \Omega \times \boldsymbol{x}$ has vorticity $\boldsymbol{\omega} = 2\boldsymbol{\Omega}$. However, the 'swirling' interpretation of vorticity does not always hold. Consider a laminar flow along a wall of the form $\boldsymbol{u} = (y, 0, 0)$ yielding constant, nonzero vorticity while no 'global rotation' appears.

Taking the curl of equation (1.1) and using some vector identities one get an evolution equation for the vorticity, 'the vorticity equation'

$$\frac{\partial \boldsymbol{\omega}}{\partial t} - \boldsymbol{\omega} \cdot \nabla \boldsymbol{u} + \boldsymbol{u} \cdot \nabla \boldsymbol{\omega} = \nu \nabla^2 \boldsymbol{\omega}\,, \tag{1.4}$$

where the pressure term from equation (1.1) has vanished when taking the curl. In fact this happens for any included force that can be written as a potential i.e. for any conservative force. The term $\boldsymbol{\omega} \cdot \nabla \boldsymbol{u}$ is called 'the vorticity stretching term' and it can be thought of as deforming the vorticity due to variations in the velocity field (though the variations in the velocity field is coupled to the variations in the vorticity field).

For the idealisation of no viscous forces the term with ν disappears and equation (1.4) simplifies to the Euler equation written in terms of the vorticity

$$\frac{\partial \boldsymbol{\omega}}{\partial t} + \boldsymbol{u} \cdot \nabla \boldsymbol{\omega} = \boldsymbol{\omega} \cdot \nabla \boldsymbol{u}\,. \tag{1.5}$$

However, vanishing viscosity means the highest order derivative vanishes, thus the number of boundary conditions is reduced. For the Euler equation a body in the fluid impose a *no flux condition* while for the Navier-Stokes equations typically also the tangential velocity component vanishes on the body - the *no slip condition*.

The operator on the left hand side of equation (1.1) and equation (1.5) is called the material derivative

$$\frac{D}{Dt} = \frac{\partial}{\partial t} + \boldsymbol{u} \cdot \nabla\,. \tag{1.6}$$

It consists of a term describing the time change at a fixed position plus a convection term describing that a fluid parcel is carried along with the flow. The material derivative describes the change of a quantity as it is convected in a

flow. An important result is then that if the material derivative of a quantity is zero then the quantity is *conserved* in time following a given fluid parcel. Reconsidering the Euler equation 1.5 it can be expressed

$$\frac{D\boldsymbol{\omega}}{Dt} = \boldsymbol{\omega} \cdot \nabla \boldsymbol{u}\,, \tag{1.7}$$

This implies that if the vorticity is initially zero it stays zero for that fluid element (Lagrange's theorem).

Some important set of curves can be used to describe the flow. The (instantaneous) *streamlines* of a flow are curves that are tangent to the velocity field, $\boldsymbol{v}(\boldsymbol{x}, t)$, at any fixed time, t_0, hence satisfying the differential equations

$$\frac{\mathrm{d}\boldsymbol{x}}{\mathrm{d}t} = \boldsymbol{v}(\boldsymbol{x}, t_0)\,. \tag{1.8}$$

If the time evolution of a velocity field is computed numerically the output is typically the velocity field at some time steps which exactly corresponds to the right hand side of equation (1.8). Then, the streamlines may be obtained by post processing. Hence, studying streamlines corresponds to how the fluid motion 'looks' at a given time instant.

Another set of curves describing structures in the flow are *pathlines* which solves the equation

$$\frac{\mathrm{d}\boldsymbol{x}}{\mathrm{d}t} = \boldsymbol{v}(\boldsymbol{x}, t)\,. \tag{1.9}$$

The motion of massless tracers in the fluid satisfy this equation.

A third kind of curves are the *streaklines*. The path connecting fluid particles all having the position $\boldsymbol{x}_0$ at some time. Hence, if one is standing on a bridge pouring dye in a river, the convected dye form a streakline.

For steady flow i.e. time independent flow, all three sets of curves coincide. The focus in this thesis is on the streamlines and on vorticity.

1.1.1 Two - dimensional flow

In case of two - dimensional flow, $\boldsymbol{u} = (u(x, y, t), v(x, y, t), 0)$ the vorticity is basically a scalar $\boldsymbol{\omega} = (0, 0, \omega)$ which is clear from equation (1.3). This means $\boldsymbol{\omega}$ is orthogonal to $\nabla \boldsymbol{u}$ so the vorticity stretching term vanishes. The Navier - Stokes equations then reduce to

$$\frac{\partial \omega}{\partial t} + \boldsymbol{u} \cdot \nabla \omega = \nu \nabla^2 \omega\,. \tag{1.10}$$

One may want to express the velocity in terms of the vorticity i.e. invert equation (1.3) which can be done using the Biot - Savart law in the case of unbounded fluid

$$\boldsymbol{u}(\boldsymbol{x},t) = \frac{1}{4\pi}\int_{\mathbb{R}^2} \frac{(\boldsymbol{x}-\tilde{\boldsymbol{x}})^{\perp}}{|\boldsymbol{x}-\tilde{\boldsymbol{x}}|^2}\cdot\omega(\tilde{\boldsymbol{x}},t)d\tilde{\boldsymbol{x}}\,, \tag{1.11}$$

with $\boldsymbol{x}^{\perp} = (-y,x)$. For a fluid satisfying the Euler equation, the material derivative of the vorticity vanishes by equation (1.7). This means the vorticity is invariant following a fluid particle which is popularly described as 'the vorticity being frozen in the fluid'. Vorticity is typically created at a no - slip boundary where viscous forces are important and then convected to flow domains where one may disregard viscosity on sufficient short time scales that nevertheless may be long enough for interesting dynamics to occur. In two - dimensional flow it is then of interest to investigate how concentrated 'patches' of vorticity interact in an inviscid fluid. The inviscid fluid cannot create new vorticity. It is merely a medium that allows the existing vorticity to interact. The simplest model using this idea relies on point vortices, where the vorticity is assumed to be a finite sum of delta function weighted with different strengths. The velocity field is then found from equation (1.11) as a superposition of all point vortex contributions where the velocity at the point vortex positions are singular.

The centers of the point vortices move in a field dictated by the remaining point vortices hence the dynamics is governed by a finite set of ordinary differential equations. This is a huge simplification which opens for many analytical results facilitated by existence of several time invariants of the dynamical system. The idea of point vortices date back to Helmholtz [52] and have been widely studied since e.g. in [8, 77].

In chapter 5 we use a similar approach allowing for viscous diffusing vortex cores. Still, a flow field is generated and the vortex cores move in response to this.

For incompressible, two - dimensional flow a stream function, $\psi : \mathbb{R}^2 \to \mathbb{R}$, exists with the property

$$u = \frac{\partial\psi}{\partial y}\,, \quad v = -\frac{\partial\psi}{\partial x}\,, \tag{1.12}$$

which automatically ensures the incompressibility condition is satisfied since

$$\nabla\cdot\boldsymbol{u} = \frac{\partial u}{\partial x}+\frac{\partial v}{\partial y} = \frac{\partial}{\partial x}\frac{\partial\psi}{\partial y}+\frac{\partial}{\partial y}\left(-\frac{\partial\psi}{\partial y}\right) = 0\,, \tag{1.13}$$

as the derivatives commute assuming a smooth velocity field. Comparing equation

(1.12) to equation (1.8) the differential equations for the streamlines is then

$$\frac{\mathrm{d}x}{\mathrm{d}t} = \frac{\partial \psi}{\partial y}\,, \quad \frac{\mathrm{d}y}{\mathrm{d}t} = -\frac{\partial \psi}{\partial x}\,. \tag{1.14}$$

The existence of the stream function means the vorticity by direct computation can be expressed

$$\omega = -\Delta\psi\,. \tag{1.15}$$

In chapter 3 we will see an example of a fluid showing a remarkable similarity in the vorticity contours and streamlines which is not to be expected in general from equation (1.15).

In chapter 2 we will see an example of a flow possessing a stream function without the flow being two - dimensional. However, a symmetry does imply simplifications enabling existence a stream function.

1.2 Framework and vocabulary from dynamical systems theory

The structure of fluid flows are investigated using tools from dynamical system theory which can be found in e.g. [73, 102].

An important approach is to assume that a velocity field is at hand and then to study the changes in the structure of the velocity field as parameters are varied. These parameters may be viscosity (Reynolds number, *Re* for normalised Navier - Stokes equations), angle of attack, aspect ratio, Péclet number, changing boundary conditions etc. The term 'changing structure' of a flow field has to be specified. This is done by first defining 'same structure' through the term topological equivalence.

Definition 1.1 Two velocity fields $\boldsymbol{v}$ and $\boldsymbol{v}'$ are *topologically equivalent* if there exists a continous, bijective map, h, with continous inverse, that maps the streamlines of $\boldsymbol{v}$ onto the streamlines of $\boldsymbol{v}'$ such that the sense of time is preserved. If h is defined in a subset of the flow domain only, $\boldsymbol{v}$ and $\boldsymbol{v}'$ are *locally topologically equivalent.*

The streamlines of two topological equivalent two - dimensional flows are shown in figure 1.1. A critical point, $\boldsymbol{x}_0$ satisfies by definition $\boldsymbol{v}(\boldsymbol{x}_0) = 0$. As a simple consequence of definition 1.1, two topological equivalent flows have the same

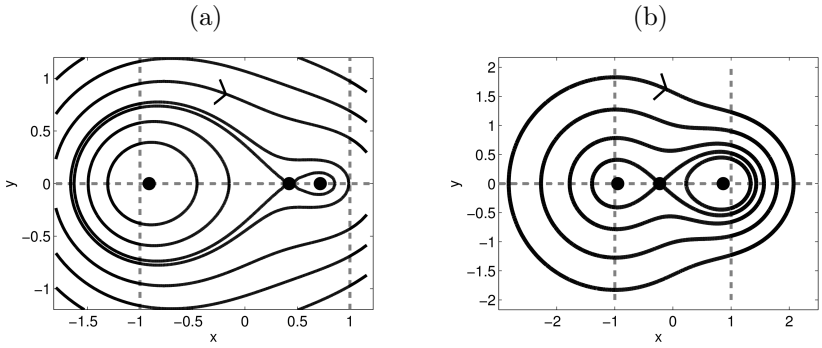

Figure 1.1: Streamlines of two topologically equivalent velocity fields.

number of critical points. A rescaling of time leads to the same streamlines, only the speed along an orbit is changed. Hence, a rescaling of time results in topological equivalent flows. This becomes useful when studying fluid structures close to a wall in chapter 4.

If a velocity field is perturbed one can compare the perturbed to the unperturbed case. If they are topologically equivalent for any small perturbation, the vector field is *structurally stable*. Otherwise it is structurally unstable with obvious meaning of locally structurally stable/unstable.

Therefore, a structurally stable velocity field captures the meaning of being robust. As an example a saddle point is robust, a small perturbation of the vector field can change the position of the saddle point but not the existence nor are new critical points created near by. On the other hand a critical point of the type *cusp* is structurally unstable. A perturbation can lead to a saddle and a center i.e. two critical points or to no critical points - see figure 1.2.

Fortunately, most points in a fluid are structurally stable, in fact if $\boldsymbol{x}_0$ is not a critical point then $\boldsymbol{x}_0$ is a locally structurally stable point. In order to detect a local change in a flow pattern we are then forced to consider the critical points of a fluid. Since the structurally unstable vector fields are related to critical points singularity theory is useful (here [42] is an excellent reference). For a given stream function $\psi_0(x, y)$ and for a given family of stream functions $\psi(x, y, \boldsymbol{p})$, depending on the parameter vector $\boldsymbol{p} \in \mathbb{R}^k$ such that $\psi(x, y, \boldsymbol{0}) = \psi_0(x, y)$, we say that ψ is an *unfolding* of ψ_0. In that case we can think of the unfolding as a perturbation to ψ_0 which gets small for $\boldsymbol{p}$ small. We are then interested in the smallest parameter space (smallest k) such that all small perturbations to ψ_0 are topologically equivalent to $\psi(x, y, \boldsymbol{p})$ for some $\boldsymbol{p}$. Assuming such a situation exists, the dimension k is called the *codimension* of ψ_0 - see figure 1.2 for an

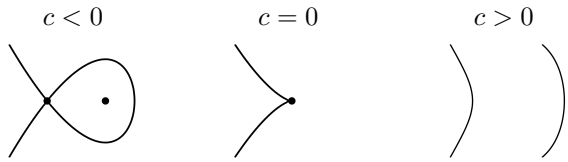

Figure 1.2: Unfolding of the *cusp* seen for $c = 0$ depends on one unfolding parameter, c, and hence has codimension 1. The structurally unstable cusp may be perturbed to a saddle and a center ($c < 0$) or to no critical points ($c > 0$)

example of an unfolding with a one - dimensional unfolding space. Studying such a complete set of unfoldings result in a complete bifurcation diagram showing all possible behaviours that may occur when perturbing a critical point. Imagine we have the unfolding $\psi(x, y, \boldsymbol{p})$ of $\psi_0(x, y,)$ with the smallest possible dimension of $\boldsymbol{p}$. Then, k gives number of parameter values that have to vanish simultaneously to produce the critical point. Hence, the higher the codimension of a critical point the 'less expected' is it. The normal form for a critical point is typically a low order, polynomial expression expressing the behaviour near the critical point. *Normal form theory* is useful for writing up a simple (the simplest) expression for an unfolding using a polynomial expression. In chapter 4 normal forms are used to describe the streamline and vorticity topology near critical points.

1.3 Outline

The thesis is organised in four main parts. Chapter 2 is about a coordinate free approach to helical symmetry and a topological analysis of a closed form approximation to the flow generated by a helical vortex filament. A helical vortex filament has vorticity pointing in along the tangent of one helix in three dimensional, inviscid flow. Hence, the problem is close to the ball game of point vortex dynamics but with three dimensional flow implications.

Chapter 3,4 and 5 are disjoint from this work in research area but the mathematical approach is similar. The overall aim is to study and compare vortices as seen from streamlines and vorticity formulations. In chapter 3 motion of a vortex above a wall in a flow governed by the Navier - Stokes equations is studied numerically. Due to viscous effects this creates new vortices. Instantaneous streamlines in two coordinate systems as well as extrema of vorticity are used to study creation of vortices. The remarkable agreement between streamlines and vorticity found in [64] motivates this study. The connections between vorticity and streamlines are also investigated from an analytical perspective in chapter 4.

Normal form theory is used to study the simplest form of the flow field locally given certain conditions.

In chapter 5 we study the vorticity and instantaneous streamlines of the superposition of two rotational invariant vortices, later exemplified by two Gaussian vortices. The motivation is an idealisation of an erupted vortex interaction with the 'generating vortex' as observed in chapter 3. In the case of two Gaussian vortices three independent parameters matter simultaneously. We then consider the time evolution, assuming that the center of one vortex moves in the field generated by the other vortex, an assumption well known from point vortex theory.

Chapter 2

Topology of helical fluid flow

2.1 Introduction

Helical flows (flows with helical symmetry) arise behind propellers and wind turbines [48, 70] and helical vortices are important for helicopter rotor performance [43, 96, 82]. Helical pipe flow has a general engineering interest [28, 68, 56, 99, 41] and has also been studied as a model for a blood vessel with non-vanishing curvature and torsion [104, 105].

Helical symmetry combines translational and rotational symmetries and have these as limiting cases. In general, however, flows with helical symmetry are more complicated than what can occur in each of these cases separately. Often helical symmetry is described from a certain coordinate relation [55, 104, 37, 93, 98, 24]. In contrast to this, we will use a coordinate-free approach from which the basic properties of fields with helical symmetry can be obtained in a simple and transparent way. This approach was first used by Ettinger & Titi [36] to investigate global uniqueness and existence of solutions for inviscid, helical flow. Using the coordinate free approach we give a short proof that the velocity field generated by a helical vortex filament is helical and we show consistency to helical formulations that rely on coordinates.

We then focus on the topological structure of helical flows, and, in particular, bifurcations in the streamline patterns. A topological approach has been used to characterize two-dimensional flows [14, 17, 31] and axisymmetric flows [16, 15]. For an incompressible helical flow a stream function can be defined, and we discuss to which extent the topology of the streamlines can be inferred from this. As a specific case, we consider the flow induced by a helical vortex filament. At a given helix, the vorticity is tangent to the helix and elsewhere the flow is potential. Hardin [48] found an expression for the stream function in terms of infinite series of products of modified Bessel functions. Okulov [80] and Fukumoto & Okulov [37] have obtained an efficient closed form approximation to such series and we use this to obtain a topological classification of the flow with the pitch of the helix as a bifurcation parameter.

The flow induced by a vortex filament impacts the location of the vortex filament itself. This can be taken into account using the localised induction approximation (LIA). When LIA is used [88, 86, 87] a helical filament has the interesting property that the self-induced motion does not spoil the helical shape. However, the filament translates and rotates as shown by e.g. Batchelor [10]. LIA results in a minor modification of the stream function discussed above where the speed of the helix appears as an extra parameter which was investigated by Mezic et al. [76]. We construct a closed form approximation and make a topological analysis of the flow field in this case as well.

This chapter is organised as follows. In §2.2 the notions of helical vector fields and helical scalar functions are introduced as well as the helical vortex filament. Helical coordinates are then described. The stream function and the geometric implications of its topology are discussed. In §2.3 the stream function calculated by Hardin, ψ_H, is introduced. We find a closed form approximation of the stream function, $\psi_{H,c}$, and analyse the topology of the induced flow. The velocity field generated by a translating and rotating helical vortex filament is approximated and analysed in §2.4. In §2.5 conclusions are drawn.

2.2 Helical vector fields and scalar functions

Let $\boldsymbol{e}_3$ be a unit vector in $\mathbb{R}^3$ and let R_ρ denote the counter-clockwise rotation by the angle ρ around $\boldsymbol{e}_3$. For a fixed $d \in \mathbb{R}$ we define a family of helical transformations with respect to $\boldsymbol{e}_3$ by

$$S_\rho \boldsymbol{x} \equiv R_\rho \boldsymbol{x} + \rho d \boldsymbol{e}_3 \,. \tag{2.1}$$

For a fixed $\boldsymbol{x}$, the curve $\rho \to S_\rho \boldsymbol{x}$ is a helix with pitch $2\pi d$. In a right-handed cartesian coordinate system $\boldsymbol{e}_1, \boldsymbol{e}_2, \boldsymbol{e}_3$, which we will use from now on, we have

$$R_\rho \boldsymbol{x} = \begin{pmatrix} \cos(\rho) & -\sin(\rho) & 0 \\ \sin(\rho) & \cos(\rho) & 0 \\ 0 & 0 & 1 \end{pmatrix} \boldsymbol{x} \,. \tag{2.2}$$

A helical transformation is distance preserving. For a fixed pitch, $2\pi d$, $\mathbb{R}^3$ may be filled by disjoint helices. Following Ettinger & Titi [36] we make two basic definitions

Definition 2.1 A scalar function $f : \mathbb{R}^3 \mapsto \mathbb{R}$ is called helical if

$$f(S_\rho \boldsymbol{x}) = f(\boldsymbol{x}) \,, \;\; \forall\, \rho \in \mathbb{R} \,, \;\; \forall \boldsymbol{x} \in \mathbb{R}^3 \,. \tag{2.3}$$

Thus, the value of a helical scalar function is constant along any helix.

Definition 2.2 The vector field $\boldsymbol{v} : \mathbb{R}^3 \mapsto \mathbb{R}^3$ is called helical if

$$\boldsymbol{v}(S_\rho \boldsymbol{x}) = R_\rho \boldsymbol{v}(\boldsymbol{x}) \,, \;\; \forall\, \rho \in \mathbb{R} \,, \;\; \forall\, \boldsymbol{x} \in \mathbb{R}^3 \,. \tag{2.4}$$

Both helical functions and helical vector fields are completely determined by their values in the xy-plane: If $\boldsymbol{x} = (x, y, z)$ and $\rho' = -z/d$, the point $S_{\rho'}(\boldsymbol{x})$ lies in the xy-plane and we find from (2.3) and (2.4)

$$f(\boldsymbol{x}) = f\left(S_{\rho'} \boldsymbol{x}\right) \,, \quad \boldsymbol{v}(\boldsymbol{x}) = R_{-\rho'} \boldsymbol{v}\left(S_{\rho'} \boldsymbol{x}\right) \,. \tag{2.5}$$

The vector field of normalised tangents $\tilde{\boldsymbol{t}}$ to the helices that disjointly fill $\mathbb{R}^3$ turns out to provide a useful way to determine if a scalar or vector field is helical. The vector field is found by differentiating equation (2.1) with respect to ρ,

$$\tilde{\boldsymbol{t}}(S_\rho \boldsymbol{x}) = \frac{\partial}{\partial \rho} S_\rho(\boldsymbol{x}) \,. \tag{2.6}$$

Using the definition of $S_\rho(\boldsymbol{x})$ from equation (2.1) and $S_0 \boldsymbol{x} = \boldsymbol{x} = (x, y, z)$ we get

$$\tilde{\boldsymbol{t}}(\boldsymbol{x}) = -y\boldsymbol{e}_1 + x\boldsymbol{e}_2 + d\boldsymbol{e}_3 \,. \tag{2.7}$$

with $\boldsymbol{e}_1, \boldsymbol{e}_2, \boldsymbol{e}_3$ being the usual basis in cartesian coordinates.

The following lemmas, proved by Ettinger & Titi [36], are useful for establishing helical symmetry.

Lemma 2.3 *The function $f : \mathbb{R}^3 \mapsto \mathbb{R}$ is helical if and only if*

$$\tilde{\boldsymbol{t}} \cdot \nabla f = 0\,. \tag{2.8}$$

Lemma 2.4 *Denote the Cartesian coordinates of the vector field $\boldsymbol{v}$ by (v_x, v_y, v_z). Then $\boldsymbol{v}$ is helical if and only if*

$$\tilde{\boldsymbol{t}} \cdot \nabla v_x = -v_y \tag{2.9a}$$
$$\tilde{\boldsymbol{t}} \cdot \nabla v_y = v_x \tag{2.9b}$$
$$\tilde{\boldsymbol{t}} \cdot \nabla v_z = 0\,. \tag{2.9c}$$

In the theorem below we collect a number of basic properties fulfilled by helical functions and vector fields.

Theorem 2.5 *Conservation of helical properties*

1. *If f is a nonzero helical scalar function then $1/f$ is a helical scalar function.*
2. *The product of helical scalar functions is a helical scalar function.*
3. *A linear combination of helical scalar functions is a helical scalar function.*
4. *For $i \in \{1, ..., n\}$ let $f_i(\boldsymbol{x})$ be a helical scalar function and $\boldsymbol{v}_i(\boldsymbol{x})$ be a helical vector field. Then $\boldsymbol{w}(\boldsymbol{x}) = \sum_{i=1}^{n} f_i(\boldsymbol{x})\boldsymbol{v}_i(\boldsymbol{x})$ is a helical vector field.*
5. *The dot product of helical vector fields is a helical scalar function.*
6. *Let $\boldsymbol{u}(\boldsymbol{x}) = \sum_{i=1}^{3} f_j(\boldsymbol{x})\boldsymbol{v}_j(\boldsymbol{x})$ where the $\boldsymbol{v}_j(\boldsymbol{x})$ are helical vector fields constituting a basis for $\mathbb{R}^3$. Then $\boldsymbol{u}(\boldsymbol{x})$ is a helical vector field if and only if the $f_j(\boldsymbol{x})$ are helical scalar functions.*
7. *The cross product of two helical vector fields is a helical vector field.*
8. *The curl of a helical vector field is a helical vector field.*
9. *The gradient of a helical scalar function is a helical vector field.*

Properties (1)–(6) follow directly from the definitions (2.1) and (2.2).

For example property (4) is proven as follows:

PROOF.

$$\begin{aligned}\boldsymbol{w}(S_\rho \boldsymbol{x}) &= \sum_{i=1}^{n} f_i(S_\rho \boldsymbol{x}) \boldsymbol{v}_i(S_\rho \boldsymbol{x}) = \sum_{i=1}^{n} f_i(\boldsymbol{x}) R_\rho \boldsymbol{v}_i(\boldsymbol{x}) = R_\rho \sum_{i=1}^{n} f_i(\boldsymbol{x}) \boldsymbol{v}_i(\boldsymbol{x}) \\ &= R_\rho \boldsymbol{w}(\boldsymbol{x}) \,. \end{aligned} \tag{2.10}$$

The first and last equality sign is by definition of $\boldsymbol{w}$. The second equality sign is due to f and $\boldsymbol{v}$ being helical. The third equality sign is due to a rotation being a linear transformation. □

As another example property (6) is proved.

PROOF. If $f_j(\boldsymbol{x})$ is a helical scalar function then $\boldsymbol{u}$ is a helical vector field by property (4). Since

$$\boldsymbol{u}(S_\rho \boldsymbol{x}) = \sum_{i=1}^{3} f_j(S_\rho \boldsymbol{x}) \boldsymbol{v}_j(S_\rho \boldsymbol{x}) \,, \tag{2.11}$$

then, if $\boldsymbol{u}$ is a helical vector field we have:

$$R_\rho \boldsymbol{u}(\boldsymbol{x}) = R_\rho \sum_{i=1}^{3} f_j(\boldsymbol{x}) \boldsymbol{v}_j(\boldsymbol{x}) = \sum_{i=1}^{3} f_j(\boldsymbol{x}) R_\rho \boldsymbol{v}_j(\boldsymbol{x}) = \sum_{i=1}^{3} f_j(\boldsymbol{x}) \boldsymbol{v}_j(S_\rho \boldsymbol{x}) \,. \tag{2.12}$$

The first equality sign is due to rotations being linear functions, the second equality sign is due to $\boldsymbol{v}_j$ being helical. Since $\boldsymbol{u}$ is a helical vector field then equation (2.12) is equal to equation (2.11):

$$0 = \sum_{i=1}^{3} \left(f_j(S_\rho \boldsymbol{x}) - f_j(\boldsymbol{x}) \right) \boldsymbol{v}_j(S_\rho \boldsymbol{x}) \,. \tag{2.13}$$

Since $\boldsymbol{v}_1$, $\boldsymbol{v}_2$, $\boldsymbol{v}_3$ is a basis for $\mathbb{R}^3$ then $f_j(S_\rho \boldsymbol{x}) - f_j(\boldsymbol{x}) = 0$ such that f_j are helical scalar functions for $j = 1, 2, 3$. □

Property (6) shows a vector field $\boldsymbol{u}$ is helical if and only if the coordinates of $\boldsymbol{u}$ in any helical basis are helical scalar functions. Examples of helical vector fields are $\boldsymbol{e}_r, \boldsymbol{e}_\theta, \boldsymbol{e}_z$, and the normalised tangent to the helices, equation (2.7), $\boldsymbol{t} = \left(1 + \frac{r^2}{d^2}\right)^{-1/2} \left(\boldsymbol{e}_z + \frac{r}{d} \boldsymbol{e}_\theta\right)$ whereas $\boldsymbol{e}_1$ and $\boldsymbol{e}_2$ are not helical.

Properties (7) - (9) can be proved using lemma 2.4 and the product rule for $f : \mathbb{R}^3 \mapsto \mathbb{R}$

$$\tilde{\boldsymbol{t}} \cdot \frac{\partial}{\partial i} (\nabla f) = \frac{\partial}{\partial i} (\tilde{\boldsymbol{t}} \cdot \nabla f) - \frac{\partial \tilde{\boldsymbol{t}}}{\partial i} \cdot \nabla f \,, \quad i \in \{x, y, z\} \,. \tag{2.14}$$

Although much of theorem 2.5 may seem evident, its coordinate free form can help to pinpoint effects of helical symmetry.

2.2.1 The helical vortex filament

To illustrate the use of the coordinate free description we turn to a specific case – the flow induced by a helical vortex filament. In an inviscid fluid a helical filament is placed with vorticity pointing along the tangent of the helix. The vorticity is zero except at the filament. Assuming the velocity goes to zero at infinite distance the velocity field $\boldsymbol{u}$ can be calculated from the Biot-Savart law. Using the coordinate free form we give a simple proof that the velocity field generated by a number of helical vortex filaments is helical.

The vector potential $\boldsymbol{A}$ satisfies the relation

$$\boldsymbol{u} = \nabla \times \boldsymbol{A}\,. \tag{2.15}$$

For any vortex filament c in an inviscid fluid $\boldsymbol{A}$ can be found from

$$\boldsymbol{A} = \frac{\Gamma}{4\pi}\int_c \frac{1}{||\Delta \boldsymbol{r}||} d\boldsymbol{l}, \tag{2.16}$$

see e.g. [6] where $d\boldsymbol{l}$ is the tangent to the filament and $\Delta\boldsymbol{r}$ is the distance from $\boldsymbol{x}$ to a point on the filament which is parametrised by l. A helical filament can be parametrised as $S_l(\boldsymbol{y})$ for a fixed $\boldsymbol{y}$ and since $d\boldsymbol{l} = \boldsymbol{t}(S_l\boldsymbol{y})dl = R_l\boldsymbol{t}(y)dl$ we have

$$\boldsymbol{A}(\boldsymbol{x}) = \frac{\Gamma}{4\pi}\int_{-\infty}^{\infty} \frac{1}{||\boldsymbol{x} - S_l\boldsymbol{y}||}\boldsymbol{t}\left(S_l\boldsymbol{y}\right) dl = \frac{\Gamma}{4\pi}\int_{-\infty}^{\infty} \frac{1}{||\boldsymbol{x} - S_l\boldsymbol{y}||} R_l\boldsymbol{t}\left(\boldsymbol{y}\right) dl\,. \tag{2.17}$$

Lemma 2.6 *The vector potential $\boldsymbol{A}$ given by equation (2.17) is helical.*

Proof. The proof is by direct use of definition 2.2. Fix any $\rho \in \mathbb{R}$:

$$R_\rho\boldsymbol{A}(\boldsymbol{x}) = \frac{\Gamma}{4\pi}R_\rho\int_{-\infty}^{\infty} \frac{1}{||\boldsymbol{x} - S_l\boldsymbol{y}||} R_l\boldsymbol{t}\left(\boldsymbol{y}\right) dl = \frac{\Gamma}{4\pi}\int_{-\infty}^{\infty} \frac{1}{||\boldsymbol{x} - S_l\boldsymbol{y}||} R_{\rho+l}\boldsymbol{t}\left(\boldsymbol{y}\right) dl\,. \tag{2.18}$$

This is now compared to:

$$\boldsymbol{A}(S_\rho\boldsymbol{x}) = \frac{\Gamma}{4\pi}\int_{-\infty}^{\infty} \frac{1}{||S_\rho\boldsymbol{x} - S_l\boldsymbol{y}||} R_l\boldsymbol{t}\left(\boldsymbol{y}\right) dl\,. \tag{2.19}$$

Changing the integration variable $l = \rho + s$ in equation (2.19) yields

$$\boldsymbol{A}(S_\rho \boldsymbol{x}) = \frac{\Gamma}{4\pi} \int_{-\infty}^{\infty} \frac{1}{||S_\rho \boldsymbol{x} - S_{\rho+s} \boldsymbol{y}||} R_{\rho+s} \boldsymbol{t}(\boldsymbol{y})\, ds\,. \tag{2.20}$$

Since $S_{\rho+s}\boldsymbol{y} = S_\rho(S_s \boldsymbol{y})$ we get using that a helical transformation conserves distance i.e. $|\boldsymbol{y} - \boldsymbol{x}| = |S_\rho \boldsymbol{y} - S_\rho \boldsymbol{x}|$:

$$\boldsymbol{A}(S_\rho \boldsymbol{x}) = \frac{\Gamma}{4\pi} \int_{-\infty}^{\infty} \frac{1}{||\boldsymbol{x} - S_s \boldsymbol{y}||} R_{\rho+s} \boldsymbol{t}(\boldsymbol{y})\, ds\,, \tag{2.21}$$

which is identical to equation (2.18). □ The argument generalises to multiple

helical vortex filaments with the same pitch since equation (2.16) is then a sum of helical terms. Furthermore, since the curl of a helical vector field is helical by property (8) of theorem 2.5 it follows that $\boldsymbol{u}$ in equation (2.15) is helical.

2.2.2 Helical coordinates

Consider cylindrical coordinates (r, θ, z) and define the corresponding helical coordinates $\boldsymbol{\xi} = (\xi, \eta, \zeta)$ through the following relations:

$$\xi = r \tag{2.22a}$$

$$\eta = \theta - \frac{1}{d} z \tag{2.22b}$$

$$\zeta = \frac{1}{d} z\,. \tag{2.22c}$$

Since cylindrical coordinates are not well defined on the z-axis neither are helical coordinates. Helical coordinates are convenient since the radius ξ and the 'helical angle' η are constant on a helix.

Moving on a helix corresponds to changing only ζ. A helix is a straight line parallel to the ζ axis in the (ξ, η, ζ) coordinate system. Since a helical scalar function is invariant along a helix, this means a scalar function is helical if and only if it is independent of ζ. Hence we have

Lemma 2.7 *A scalar function $f : \mathbb{R}^3 \mapsto \mathbb{R}$ is helical if and only if $\frac{\partial f(\xi,\eta,\zeta)}{\partial \zeta} = 0$.*

A vector field is helical if and only if the coordinates in a helical basis are helical scalar functions according to property (6):

Lemma 2.8 *A vector field is helical if and only if the coordinates in a helical basis differentiated with respect to ζ vanishes.*

Since $\boldsymbol{e}_r$, $\boldsymbol{e}_\theta$ and $\boldsymbol{e}_z$ constitute a helical basis a vector field expressed in cylindrical coordinates (u_r, u_θ, u_z), is helical if and only if $\frac{\partial}{\partial\zeta}u_r = \frac{\partial}{\partial\zeta}u_\theta = \frac{\partial}{\partial\zeta}u_z = 0$.

Finally we have

Lemma 2.9 *If f is a smooth helical scalar function then $\frac{\partial^i\partial^j\partial^k}{\partial\xi^i\partial\eta^j\partial\zeta^k}f$ is a helical scalar function.*

Lemma 2.9 is proved using lemma 2.7 and that taking derivatives commutes.

Fixing two of three helical coordinates and varying the third, a curve in $\mathbb{R}^3$ is generated. The tangent to such a curve, normalised to unity, is the corresponding unit vector to the coordinate direction. We find

$$\boldsymbol{e}_\xi = \boldsymbol{e}_r\,, \quad \boldsymbol{e}_\eta = \boldsymbol{e}_\theta\,, \quad \boldsymbol{e}_\zeta = \boldsymbol{t}\,. \tag{2.23}$$

$\boldsymbol{e}_\xi$, $\boldsymbol{e}_\eta$, $\boldsymbol{e}_\zeta$ are helical vector fields and they constitute a basis for $\mathbb{R}^3$ except at the z-axis. Notice that for points in the xy-plane $\zeta = 0$ and $(\xi, \eta) = (r, \theta)$ are standard polar coordinates.

2.2.3 Stream function

Assuming the velocity field is incompressible, $\nabla\cdot\boldsymbol{u} = 0$, a stream function can be constructed. In cylindrical coordinates the incompressibility condition is

$$\frac{1}{r}\frac{\partial}{\partial r}(ru_r) + \frac{1}{r}\frac{\partial u_\theta}{\partial\theta} + \frac{\partial u_z}{\partial z} = 0\,. \tag{2.24}$$

The velocity field in cylindrical coordinates can be represented by the velocity field in helical coordinates

$$u_r = u_\xi\,, \quad u_\theta = u_\eta + \frac{\xi}{\sqrt{d^2+\xi^2}}u_\zeta\,, \quad u_z = \frac{d}{\sqrt{d^2+\xi^2}}u_\zeta\,, \tag{2.25}$$

and inserted in equation (2.24)

$$\frac{1}{\xi}\frac{\partial}{\partial\xi}(\xi u_\xi) + \frac{1}{\xi}\frac{\partial}{\partial\theta}\left(u_\eta + \frac{\xi}{\sqrt{d^2+\xi^2}}u_\zeta\right) + \frac{\partial}{\partial z}\left(\frac{d}{\sqrt{d^2+\xi^2}}u_\zeta\right) = 0\,. \tag{2.26}$$

From equation (2.22) the chain rule yields

$$\frac{\partial}{\partial r} = \frac{\partial}{\partial \xi}, \quad \frac{\partial}{\partial \theta} = \frac{\partial}{\partial \eta}, \quad \frac{\partial}{\partial z} = \frac{1}{d}\left(-\frac{\partial}{\partial \eta} + \frac{\partial}{\partial \zeta}\right), \tag{2.27}$$

from which we can transform equation (2.26)

$$\frac{1}{\xi}\left(\frac{\partial}{\partial \xi}\left(\xi u_\xi\right) + \frac{\partial}{\partial \eta} u_\eta\right) + \frac{1}{\sqrt{d^2+\xi^2}}\frac{\partial}{\partial \zeta} u_\zeta = 0\,. \tag{2.28}$$

For a helical vector field the last term vanishes by lemma 2.8. Then equation (2.28) yields

$$\frac{\partial\left(\xi u_\xi\right)}{\partial \xi} + \frac{\partial u_\eta}{\partial \eta} = 0\,, \tag{2.29}$$

from which it follows that a stream function $\psi : \mathbb{R}^2 \to \mathbb{R}$ exists such that

$$\frac{\partial \psi}{\partial \eta} = \xi u_\xi\,, \qquad -\frac{\partial \psi}{\partial \xi} = u_\eta\,. \tag{2.30}$$

It follows that $u_\xi \boldsymbol{e}_\xi + u_\eta \boldsymbol{e}_\eta$ is parallel to the tangent of the level curves of the stream function.

A helical, incompressible velocity field thus only depends on two single valued functions $\psi(\xi, \eta)$ and $u_\zeta(\xi, \eta)$ and can always be written

$$\boldsymbol{u} = \frac{1}{\xi}\frac{\partial \psi(\xi,\eta)}{\partial \eta}\boldsymbol{e}_r - \frac{\partial \psi(\xi,\eta)}{\partial \xi}\boldsymbol{e}_\theta + u_\zeta(\xi,\eta)\boldsymbol{t}\,. \tag{2.31}$$

If the velocity is known in the xy-plane it is easy to calculate the entire velocity field from equation (2.5).

As $d \to \infty$, $\boldsymbol{t} \to \boldsymbol{e}_z$ and $\eta \to \theta$, and the flow will have translational symmetry along the $\boldsymbol{e}_3$-axis. This agrees with equation (2.31) where we recover the standard stream function formulation in cylindrical coordinates for flows with translational symmetry. If further $u_\zeta = u_z = 0$, the flow is two-dimensional. It is common to use a stream function depending on ξ and η spanned in the plane normal to the tangent vector [37, 70, 5, 104, 67, 30]. References are often to the work of Landman [66] and Dritschel [35] where a helical, incompressible velocity field is decomposed in the form

$$\boldsymbol{u} = \nabla f_1 \times \boldsymbol{B} + f_2 \boldsymbol{B}\,. \tag{2.32}$$

Landman [66] requires f_1 and f_2 are helical scalar functions i.e. depend on ξ, η (and time). Dritschel [35] does not explicitly require f_1 and f_2 being helical. Here f_1 plays the role of the stream function. From theorem 2.5 it is clear that $\boldsymbol{u}$ in equation (2.32) is helical for helical f_1 and f_2. However, we have found no

proof in literature why all helical velocity field can be written in the form of equation (2.32). Actually, Childress et al. [24] define a helical velocity field to be one that obeys equation (2.32). This definition is equivalent to our definition 2.2:

Lemma 2.10 *An incompressible vector field, $\boldsymbol{u}$, is helical if and only if there exists helical scalar functions f_1 and f_2 such that equation (2.32) holds.*

Proof. The proof relies on that any helical, incompressible vector field can be written in the form of equation (2.31). First assume f_1 and f_2 are helical scalar functions. Using the gradient for cylindrical coordinates and equation (2.27), equation (2.23) and

$$\boldsymbol{t} = \frac{1}{\sqrt{1+\frac{r^2}{d^2}}}\left(\boldsymbol{e}_z + \frac{r}{d}\boldsymbol{e}_\theta\right) \tag{2.33}$$

then equation (2.32) can be written as

$$\boldsymbol{u} = \frac{1}{\xi}\frac{\partial f_1}{\partial \eta}\boldsymbol{e}_r - \frac{\partial f_1}{\partial \xi}\boldsymbol{e}_\eta + \frac{1}{\sqrt{1+\frac{\xi^2}{d^2}}}\left(\frac{\xi}{d}\frac{\partial f_1}{\partial \xi} + f_2\right)\boldsymbol{t}\,. \tag{2.34}$$

Choosing

$$\psi = f_1\,, \quad u_\varsigma = \frac{1}{\sqrt{1+\frac{\xi^2}{d^2}}}\left(\frac{\xi}{d}\frac{\partial f_1}{\partial \xi} + f_2\right)\,, \tag{2.35}$$

equation (2.31) is recovered. To prove the converse statement assume ψ and u_ς are helical scalar functions. Invert equation (2.35) to define f_1 and f_2 which are helical scalar functions by lemma 2.9 and theorem 2.5. Then we get equation (2.34) which is equivalent to equation (2.32). □

2.2.4 Interpretation of level curves of ψ

Figure 2.1(a) shows an example of a contour plot of ψ in the xy plane. Three critical points are shown, two elliptic and one hyperbolic. A critical point of ψ is characterised by $\frac{\partial}{\partial \xi}\psi(\xi,\eta) = \frac{\partial}{\partial \eta}\psi(\xi,\eta) = 0$ i.e. $u_\xi = u_\eta = 0$ so in the three dimensional flow only u_ς may be nonzero. The velocity field at some height $z = z_1$ is merely a rotation around the z -axis of the velocity field at $z = 0$. It is appreciable that the stream function lives in the xy-plane since we just have to rotate this around the z - axis as well. This is illustrated in figure 2.1.

A critical point of ψ in a plane with constant z-value corresponds to flow tangential to a helix in the three dimensional flow. Since a helical flow does

not depend on ζ the flow has constant magnitude along any helix including this special 'critical point helix'. This is illustrated for the middle critical point in figure 2.1. The tangent to a contour of ψ gives two velocity coordinates according to the properties of the stream function. In two dimensions (figure 2.1(a)) a closed curve of ψ separates the flow. The same is true in three dimensions corresponding to a helix tube that separates the flow. This is shown in figure 2.1 for the closed curve surrounding the middle critical point in two dimensions. Thus, a critical point of ψ corresponds to a stream line in the three dimensional flow and a level curve of ψ corresponds to a stream surface of the three dimensional flow.

Through each point in the xy - plane passes exactly one helix. On each of these helices u_ζ is constant. However, u_ζ may change for different points in the xy - plane. The helical tube in figure 2.1 thus may have different u_ζ for different helices. The value of u_ζ can not be deduced from the stream function in general.

There is an important difference between the interpretation of level curves of the stream function in helical symmetry and in translation symmetry relating to the vorticity $\boldsymbol{\omega} = \nabla \times \boldsymbol{u}$. From Kelvin's circulation theorem we have

$$\Gamma = \int_C \boldsymbol{u} \cdot \boldsymbol{dl} = \int_S \boldsymbol{\omega} \cdot \boldsymbol{n} ds \,, \tag{2.36}$$

with C being a closed curve with tangent $\boldsymbol{dl}$ and surface S with normal $\boldsymbol{n}$. For a smooth vorticity distribution and a small surface with area S this yields for the the normal component of the vorticity $\omega_\perp$

$$\Gamma \approx \omega_\perp S \,. \tag{2.37}$$

Therefore, nonzero Γ means nonzero vorticity. Now, considering a case where a level curve of ψ is a closed curve as in figure 2.1(a). We choose the curve C to be this curve. First imagine this is a translational symmetric case which implies the third basis vector is $\boldsymbol{e}_3$. Then the value of u_3 has no impact on $\boldsymbol{u} \cdot \boldsymbol{dl}$. The xy - component of the flow is parallel to the tangent to the level curve of ψ. This means $\boldsymbol{u} \cdot \boldsymbol{dl}$ is nonzero and has constant sign for any point on the curve. Therefore, for a closed level curve of ψ, Γ is nonzero. Thus, in the translation symmetric case an elliptic critical point guarantees nonzero vorticity.

In a helical flow using $\boldsymbol{e}_r$, $\boldsymbol{e}_\theta$, $\boldsymbol{t}$ as a basis the situation is different since the third basis vector $\boldsymbol{t}$ is not orthogonal to the xy - plane. Computing $\boldsymbol{u} \cdot \boldsymbol{dl}$ also has a term including u_ζ. Therefore, a closed level curve of ψ in itself is no indicator of the presence of vorticity.

The character of a critical point can be determined by the second derivative test

$$H = \frac{1}{\xi^2} \left(\frac{\partial^2 \psi}{\partial \xi^2} \frac{\partial^2 \psi}{\partial \eta^2} - \left(\frac{\partial^2 \psi}{\partial \xi \partial \eta} \right)^2 \right) , \tag{2.38}$$

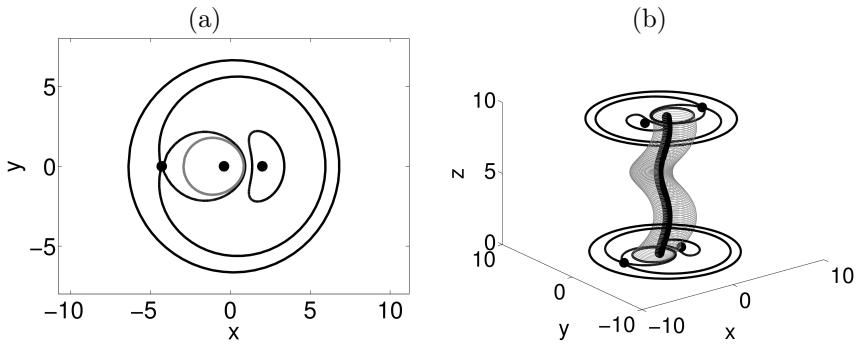

Figure 2.1: (a) Example of contourplot of the stream function. The tangent to the contour curves of ψ gives two of the velocity coordinates. (b) The corresponding three dimensional picture. A critical point in (a) corresponds to a helix in (b) with a constant velocity vector parallel to the tangent of the helix. A closed curve in (a) corresponds to a helix tube in (b) with no cross flow.

where the right side is evaluated at the critical point. If $H > 0$ the critical point is elliptic. If $H < 0$ the critical point is hyperbolic.

2.3 The velocity field generated by a helical vortex filament

Hardin [48] found the stream function for the flow generated by the vortex filament of strength Γ, radius a and pitch d as an infinite series involving modified Bessel functions,

$$\psi_H = \frac{\Gamma}{2\pi}\begin{pmatrix} \frac{\xi^2}{2d^2} \\ -\ln(\xi)+\ln(a)+\frac{a^2}{2d^2} \end{pmatrix} - \frac{\Gamma a \xi}{\pi d^2}\sum_{m=1}^{\infty}\begin{pmatrix} K'_m\left(m\frac{a}{d}\right) I'_m\left(m\frac{\xi}{d}\right) \\ K'_m\left(m\frac{\xi}{d}\right) I'_m\left(m\frac{a}{d}\right) \end{pmatrix}\cos(m\eta)\,. \tag{2.39}$$

Here the top line is valid for $\xi < a$ (the inner solution) and the lower line is valid for $\xi > a$ (the outer solution). We have included a constant $\ln(a) + \frac{a^2}{2d^2}$ not in the original expression by Hardin to ensure ψ_H is continuous at the helix cylinder $\xi = a$.

We introduce scaled variables

$$\tilde{\xi} = \frac{\xi}{d}\,, \quad \lambda = \frac{a}{d}\,, \tag{2.40}$$

such that the helix cylinder is at $\tilde{\xi} = \lambda$, and define $\tilde{\psi}_H(\tilde{\xi}, \eta) = \frac{\pi}{\Gamma}\psi_H(d\tilde{\xi}, \eta)$:

$$\tilde{\psi}_H(\tilde{\xi}, \eta) = \frac{1}{2}\begin{pmatrix} \frac{\tilde{\xi}^2}{2} \\ -\ln(\tilde{\xi}) + \ln(\lambda) + \frac{\lambda^2}{2} \end{pmatrix} - \tilde{\xi}\lambda \sum_{m=1}^{\infty} \begin{pmatrix} K'_m(m\lambda)\, I'_m\left(m\tilde{\xi}\right) \\ K'_m\left(m\tilde{\xi}\right) I'_m(m\lambda) \end{pmatrix} \cos(m\eta)\,, \tag{2.41}$$

We now skip the tilde for convenience (whenever λ is appearing we are using scaled variables). In the rest of the paper we focus on the topology of the flow induced by helical vortex filaments and proceed to state a few basic facts about the critical points of ψ_H which can be obtained from equation (2.41).

It is immediately clear that $\eta = 0$ and $\eta = \pi$ solve $\frac{\partial}{\partial\eta}\psi_H = 0$. Whether there are further solutions is not clear, but a numerical investigation by Mezic et al. [76] finds no critical points at other values of η.

The modified Bessel functions are solutions to the equation

$$x^2y'' + xy' - (x^2 + m^2)y = 0\,. \tag{2.42}$$

Using this and the well-known properties $K_m(x) > 0$, $I_m(x) > 0$, $I'_m(x) > 0$, $K'_m(x) < 0$ for $x > 0$ one finds that $\frac{\partial}{\partial\xi}\psi(\xi, 0)$ has constant sign in the inner and the outer domain. Thus, there are no critical points at $\eta = 0$, but they may occur at $\eta = \pi$. The type of a critical point is determined by the Hessian (2.38). It is easily seen that

$$\frac{\partial^2}{\partial\eta\partial\xi}\psi_H(\xi, \pi) = 0\,, \tag{2.43}$$

while the signs of $\frac{\partial^2}{\partial\xi^2}\psi_H(\xi, \pi)$ and $\frac{\partial^2}{\partial\eta^2}\psi_H(\xi, \pi)$ are not obvious.

2.3.1 Closed form approximation of ψ_H

The infinite sum appearing in ψ_H makes analysis hard, but there are also numerical issues due to the asymptotic behaviour of the Bessel functions. While I'_m goes to infinity for large arguments, K'_m goes to zero. Hence products of the form $I'_m(mx)K'_m(my)$ may be impossible to evaluate numerically from each of the factors. Mezic et al. [76] use a finite number of terms to represent the

infinite series without addressing this issue while Ijzermans et al. [55] use an asymptotic expansion which is only briefly discussed. This asymptotic expansion may be related to the approach by Okulov [80] and Fukumoto & Okulov [37] we discuss now. In this approach approximations for the modified Bessel functions for large arguments are used, see Abramowitz & Stegun [[1], p. 378] and Olver [83, 84] for a derivation. The resulting closed-form approximation to ψ_H is most useful, but unfortunately there are some misprints. In the following we rederive the closed-form approximation for equation (2.41).

Define

$$f(x) = \sqrt{1+x^2} + \ln\left(\frac{x}{1+\sqrt{1+x^2}}\right). \tag{2.44}$$

For later use we notice that f is strictly increasing for positive x. Then for large m

$$I'_m(mx) \approx \frac{1}{\sqrt{2\pi m}} \frac{\left(1+x^2\right)^{\frac{1}{4}}}{x} e^{mf(x)} \tag{2.45a}$$

$$K'_m(my) \approx -\sqrt{\frac{\pi}{2m}} \frac{\left(1+y^2\right)^{\frac{1}{4}}}{y} e^{-mf(y)}. \tag{2.45b}$$

With these we obtain (Re denotes real part)

$$\begin{aligned}
&\sum_{m=1}^{\infty} K'_m(my)\, I'_m(mx) \cos(m\eta) = \mathrm{Re}\left(\sum_{m=1}^{\infty} K'_m(my)\, I'_m(mx)\, e^{\mathrm{i}m\eta}\right) \\
&\approx -\mathrm{Re}\left(\sum_{m=1}^{\infty} \sqrt{\frac{\pi}{2m}} \frac{\left(1+y^2\right)^{\frac{1}{4}}}{y} e^{-mf(y)} \frac{1}{\sqrt{2\pi m}} \frac{\left(1+x^2\right)^{\frac{1}{4}}}{x} e^{mf(x)} e^{\mathrm{i}m\eta}\right) \\
&= -\frac{\left(\left(1+x^2\right)\left(1+y^2\right)\right)^{\frac{1}{4}}}{2xy} \mathrm{Re}\left(\sum_{m=1}^{\infty} \frac{1}{m} e^{-m(f(y)-f(x)-\mathrm{i}\eta)}\right).
\end{aligned} \tag{2.46}$$

This can be further simplified by noting that the well-known formula

$$\sum_{m=1}^{\infty} (-1)^{m+1} \frac{x^m}{m} = \ln(1+x) \quad \text{for } |x| < 1 \tag{2.47}$$

yields

$$\sum_{m=1}^{\infty} \frac{1}{m} e^{-m(\alpha-\mathrm{i}\beta)} = -\ln\left(1-e^{-\alpha+\mathrm{i}\beta}\right) \quad \text{for } \alpha > 0. \tag{2.48}$$

Note that Okulov [81] and Fukumoto & Okulov [37] have a sign error in this expression. Consider now equation (2.46) with $y > x$. Then $f(y) > f(x)$ so

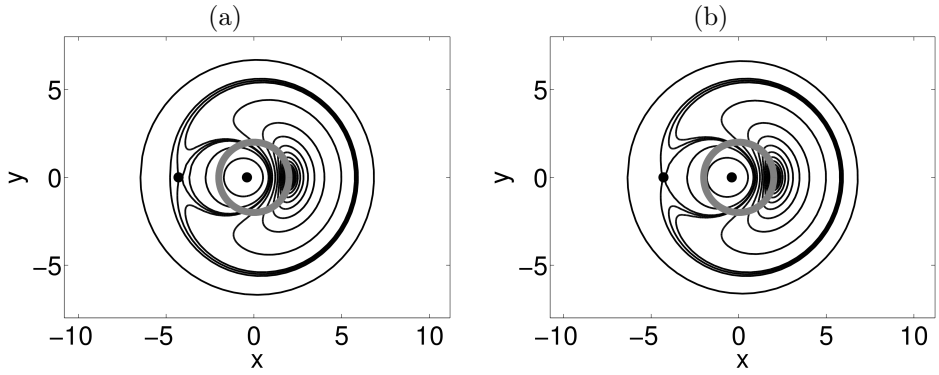

Figure 2.2: Level curves of the stream function, with the cylinder $r = \lambda = 2$ marked as a grey circle. Critical points of $\psi_{H,c}$ are marked with black dots. (a) Level curves of ψ_H, equation (2.41), including 300 terms (b) Level curves of $\psi_{H,c}$, equation (2.51).

equation (2.48) can be used to get the approximation

$$\sum_{m=1}^{\infty} K_m'(my)\, I_m'(mx)\cos(m\eta) \approx \frac{\left(\left(1+x^2\right)\left(1+y^2\right)\right)^{\frac{1}{4}}}{2xy}\mathrm{Re}\left(\ln\left(1-e^{f(x)-f(y)+\mathrm{i}\eta}\right)\right). \tag{2.49}$$

Denoting

$$\alpha = \alpha(\xi,\eta) = f(\xi) - f(\lambda) \tag{2.50}$$

we apply equation (2.49) to equation (2.41) to finally get a closed form approximation (denoted by subscript c) of Hardin's solution,

$$\psi_{H,c}(\xi,\eta) = \frac{1}{2}\begin{pmatrix} \frac{\xi^2}{2} \\ -\ln(\xi) + \ln(\lambda) + \frac{\lambda^2}{2} \end{pmatrix} - \frac{1}{2}\left(\left(1+\lambda^2\right)\left(1+\xi^2\right)\right)^{\frac{1}{4}}\mathrm{Re}\left(\ln\left(1-e^{\pm\alpha+\mathrm{i}\eta}\right)\right). \tag{2.51}$$

The limit of equation (2.51) as ξ tends to λ exists for nonzero η. There only is a problem on the filament itself $(\xi,\eta) = (\lambda, 0)$ where the velocity field diverges similar to the situation in point vortex dynamics.

An typical example of level curves for ψ_H and $\psi_{H,c}$ is shown in figure 2.2. In this example, and in many other we have tested, a very good agreement between the series and the closed form is achieved.

2.3.2 Topological analysis of the closed form expression

We now analyse the topology of the flow induced by the closed form expression equation (2.51). To find critical points we compute first the partial derivative

$$\frac{\partial}{\partial\eta}\psi_{H,c}(\xi,\eta)=\frac{1}{2}\left(\left(1+\lambda^2\right)\left(1+\xi^2\right)\right)^{\frac{1}{4}}\operatorname{Re}\left(\frac{\mathrm{i}e^{\pm\alpha+\mathrm{i}\eta}}{1-e^{\pm\alpha+\mathrm{i}\eta}}\right), \tag{2.52}$$

which is zero only when $\eta=0,\pi$. These values are also zeroes for the original expression equation (2.41), but for the closed form it is clear that there are no other solutions. The other partial derivative is

$$\begin{aligned}\frac{\partial}{\partial\xi}\psi_{H,c}(\xi,\eta)&=\frac{1}{2}\begin{pmatrix}\xi\\-\frac{1}{\xi}\end{pmatrix}\\-\frac{1}{2}(1+\lambda^2)^{\frac{1}{4}}&\left(\frac{1}{2}\frac{\xi}{(1+\xi^2)^{\frac{3}{4}}}\operatorname{Re}(\ln(1-e^{\pm\alpha+\mathrm{i}\eta}))\mp\frac{(1+\xi^2)^{\frac{3}{4}}}{\xi}\operatorname{Re}\left(\frac{e^{\pm\alpha+\mathrm{i}\eta}}{1-e^{\pm\alpha+\mathrm{i}\eta}}\right)\right).\end{aligned} \tag{2.53}$$

Inserting $\eta=0$, we obtain

$$\begin{aligned}\frac{\partial}{\partial\xi}\psi_{H,c}(\xi,0)&=\frac{1}{2}\begin{pmatrix}\xi\\-\frac{1}{\xi}\end{pmatrix}\\&-\frac{1}{2}(1+\lambda^2)^{\frac{1}{4}}\left(\frac{1}{2}\frac{\xi}{(1+\xi^2)^{\frac{3}{4}}}\ln(1-e^{\pm\alpha})\mp\frac{(1+\xi^2)^{\frac{3}{4}}}{\xi}\frac{e^{\pm\alpha}}{1-e^{\pm\alpha}}\right).\end{aligned} \tag{2.54}$$

Lemma 2.11 *There are no critical points of $\psi_{H,c}(\xi,0)$ off the filament.*

Proof. We will show that $\frac{\partial}{\partial\xi}\psi_{H,c}(\xi,0)$ has one sign away from the helix cylinder. It is easy to see that

$$\frac{\partial}{\partial\xi}\psi_{H,c}(\xi,0)>0\ \text{ for }\xi<\lambda\,, \tag{2.55}$$

since all three terms in equation (2.54) are positive.

To show that $\frac{\partial}{\partial\xi}\psi_{H,c}(\xi,0)\neq 0$ also for $\xi>\lambda$ we go back to equation (2.51). We see that $\frac{\partial}{\partial\xi}\psi_{H,c}(\xi,0)<0$ if $\frac{\partial}{\partial\xi}\left(-\left(1+\xi^2\right)^{\frac{1}{4}}\operatorname{Re}\left(\ln\left(1-e^{-\alpha}\right)\right)\right)<0$. From equation (2.48) we get

$$-\left(1+\xi^2\right)^{\frac{1}{4}}\operatorname{Re}\left(\ln\left(1-e^{-\alpha}\right)\right)=\left(1+\xi^2\right)^{\frac{1}{4}}\sum_{m=1}^{\infty}\frac{1}{m}e^{-m\alpha}\,. \tag{2.56}$$

Then

$$\frac{\partial}{\partial\xi}\left(-\left(1+\xi^2\right)^{\frac{1}{4}}\operatorname{Re}\left(\ln\left(1-e^{-\alpha}\right)\right)\right)= \sum_{m=1}^{\infty} e^{-m\alpha}\left(\frac{1}{2m}\frac{\xi}{(1+\xi^2)^{\frac{3}{4}}}-\frac{(1+\xi^2)^{\frac{3}{4}}}{\xi}\right). \quad (2.57)$$

It is not difficult to see that each term in equation (2.57) is negative for $\xi > 0$ such that

$$\frac{\partial}{\partial\xi}\psi_{H,c}(\xi,0) < 0 \text{ for } \xi > \lambda\,, \quad (2.58)$$

so combining (2.55) and (2.58) we see that no critical points exist at $\eta = 0$. □

We now turn to $\eta = \pi$ and introduce

$$F(\xi,\lambda) \equiv \frac{\partial}{\partial\xi}\psi_{H,c}(\xi,\pi) = \frac{1}{2}\begin{pmatrix} \xi \\ -\frac{1}{\xi} \end{pmatrix} - \frac{1}{2}(1+\lambda^2)^{\frac{1}{4}}\left(\frac{1}{2}\frac{\xi}{(1+\xi^2)^{\frac{3}{4}}}\ln(1+e^{\pm\alpha}) \pm \frac{(1+\xi^2)^{\frac{3}{4}}}{\xi}\frac{e^{\pm\alpha}}{1+e^{\pm\alpha}}\right), \quad (2.59)$$

the zeroes of which represent critical points. To determine the type of a possible critical point we find by direct computation

$$\frac{\partial^2\psi_{H,c}(\xi,\pi)}{\partial\xi\partial\eta} = \frac{\partial F(\xi,\lambda)}{\partial\eta} = 0\,, \frac{\partial^2\psi_{H,c}(\xi,\pi)}{\partial\eta^2} > 0\,, \text{ for } \xi \neq \lambda\,. \quad (2.60)$$

such that the sign of the Hessian (2.38) is solely determined by the sign of $\frac{\partial^2\psi_{H,c}(\xi,\pi)}{\partial\xi^2} = \frac{\partial F(\xi,\lambda)}{\partial\xi}$. If it is positive the critical point is a center and if it is negative it is a saddle. Hence, the function F contains all information about existence and properties of critical points.

Lemma 2.12 *$F(\xi,\lambda)$ is negative for fixed λ and ξ small or ξ large.*

Proof. We consider first small ξ. Using L'Hospital's rule on

$$\xi\ln\left(1+e^{\alpha}\right) = \frac{\ln\left(1+e^{f(\xi)-f(\lambda)}\right)}{\frac{1}{\xi}} \quad (2.61)$$

which appears in equation (2.59) we get

$$\lim_{\xi\to 0}\xi\ln\left(1+e^{\alpha}\right) = \lim_{\xi\to 0} -\xi\sqrt{1+\xi^2}\frac{e^{f(\xi)-f(\lambda)}}{1+e^{f(\xi)-f(\lambda)}} = 0\,. \quad (2.62)$$

The limits of the rest of the terms in equation (2.59) are easily obtained, yielding

$$\lim_{\xi\to 0} F(\xi,\lambda) = -\frac{1}{4}\left(1+\lambda^2\right)^{\frac{1}{4}} e^{1-f(\lambda)} < 0\,. \tag{2.63}$$

For large ξ we also have $F(\lambda,\xi) < 0$: In the outer region we have, by disregarding a negative term,

$$F(\xi,\lambda) < -\frac{1}{2\xi} + \frac{1}{2}(1+\lambda^2)^{\frac{1}{4}}\frac{(1+\xi^2)^{\frac{3}{4}}}{\xi}\frac{e^{-\alpha}}{1+e^{-\alpha}} \tag{2.64}$$

$$= \frac{-\left(e^{\alpha}+1\right)+\left(1+\lambda^2\right)^{\frac{1}{4}}\left(1+\xi^2\right)^{\frac{3}{4}}}{2\xi\left(e^{\alpha}+1\right)}. \tag{2.65}$$

As $\xi > \lambda$ it further follows that

$$F(\xi,\lambda) < \frac{-\left(e^{\alpha}+1\right)+1+\xi^2}{2\xi\left(e^{\alpha}+1\right)} = \frac{-\frac{e^{f(\xi)}}{\xi^2}+e^{f(\lambda)}}{\frac{2}{\xi}e^{f(\lambda)}\left(e^{\alpha}+1\right)}. \tag{2.66}$$

Since the denominator in the last fraction in equation (2.66) is positive, we can show that $F < 0$ if the numerator is negative. As $e^{f(\xi)}/\xi^2 \to \infty$ for $\xi \to \infty$, we see that this is indeed the case for ξ sufficiently large and fixed λ. □ It follows

from lemma 2.12 that there will in general be an even number (possibly zero) critical points of ψ at $\eta = \pi$. The innermost will be a centre since $\partial F/\partial\xi > 0$ here, the next one will be a saddle, and so on.

We now address the existence of critical points in the limits of small and large λ. We consider first the limit of small λ. Then the helix is an almost straight line and therefore no critical points are expected.

Lemma 2.13 *There are no zeros of $F(\xi,\lambda)$ for small λ.*

Proof. First we consider the region $\xi < \lambda$ and we aim for an upper bound on $F(\xi,\lambda)$. The second term in $F(\xi,\lambda)$ is disregarded

$$F(\xi,\lambda) \le \frac{1}{2}\xi - \frac{1}{2}\left(1+\lambda^2\right)^{\frac{1}{4}}\left(1+\xi^2\right)^{\frac{1}{4}}\frac{\sqrt{1+\xi^2}}{\xi}e^{f(\xi)}\frac{e^{-f(\lambda)}}{1+e^{f(\xi)-f(\lambda)}}\,. \tag{2.67}$$

Using $1+e^{\alpha} < 2$, $\xi > \lambda$, $\left(1+\lambda^2\right)^{\frac{1}{4}}\left(1+\xi^2\right)^{\frac{1}{4}} > 1$ and $\frac{\sqrt{1+x^2}}{x}e^{f(x)}$ is increasing for all positive x and $\lim_{x\to 0}\frac{\sqrt{1+x^2}}{x}e^{f(x)} = \frac{e}{2}$ so $\frac{\sqrt{1+\xi^2}}{\xi}e^{f(\xi)} > \frac{e}{2}$ we get from inequality (2.67)

$$F(\xi,\lambda) \le \frac{1}{2}\lambda - \frac{e^{1-f(\lambda)}}{8}\,. \tag{2.68}$$

Since $e^{f(x)}$ goes to zero for x going to zero then $F(\xi, \lambda) < 0$ for $\xi < \lambda$ and λ small.

For $\xi > \lambda$ we return to the estimate (2.66). There exists a $c > 0$ such that the function $e^{f(\xi)}/\xi^2 > c$ for all $\xi > 0$. Since $e^{f(\lambda)} \to 0$ for $\lambda \to 0$ it follows that $F < 0$ for λ sufficiently small.

We now turn to the case of large λ. Then the helix is densely wound and is close to being a cylindrical vortex sheet.

Lemma 2.14 *There is at least two zeros of $F(\xi, \lambda)$ for large λ. One zero is located inside the helical cylinder and corresponds to a center, and one is located outside the helical cylinder and corresponds to a saddle.*

Proof. Since F is continuous we can evaluate it at the vortex cylinder using the lower part of equation (2.59),

$$F(\lambda, \lambda) = -\frac{1}{2\lambda} - \frac{\lambda}{4\sqrt{1+\lambda^2}} \ln(2) + \frac{1}{4}\left(\frac{1+\lambda^2}{\lambda}\right), \tag{2.69}$$

which is positive for large λ. Since $F(\xi, \lambda)$ is negative for small and large ξ an elliptic critical point in the inner region and a hyperbolic critical point in the outer region must exist for large λ.

We now complement our analytical results by a numerical investigation. The main results are shown in figure 2.3. In agreement with the results above, no critical points exist for small values of λ. However, at $\lambda = 1.265$ a saddle-node bifurcation occurs and a centre and a saddle are created in the outer region. At $\lambda = 1.313$ the elliptic fixed point moves into the inner region. Increasing λ yields no further bifurcations. While the location of a critical inside or outside the helix cylinder is not strictly speaking a topological property, it seems important physically to keep track of this. With this understanding, we conclude that three different flow topologies may occur in this flow.

The streamline patterns have reflection symmetry around the x-axis. This arises from the invariance of $\eta \to -\eta$ in equation (2.51) (and also in the original expression given by equation (2.41)). This symmetry is due to special properties of the field induced by a helical vortex filament and is not a general feature of helical flow fields.

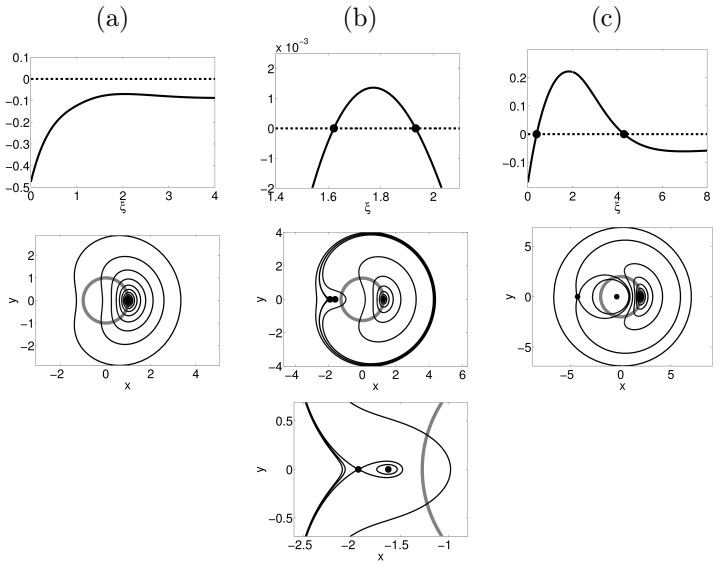

Figure 2.3: The three observed flow topologies of the closed form stream function $\psi_{H,c}$ equation (2.51). The top row shows graphs of $F(\xi, \lambda)$. The middle row shows isolines of the stream function $\psi_{H,c}$. Note the different scaling of the axes. The grey circle has radius λ and represents the filament cylinder. (a) $\lambda = 1.00$. No critical points of the stream function. (b) $\lambda = 1.27$. Two critical points in the outer region. The panel in the third row is a detail near the critical points. (c) $\lambda = 2.00$. The elliptic critical point is now located in the inner region.

2.4 Topological effects of self-induced velocity

The self-induced velocity on a vortex filament has been considered in e.g. [88, 86, 87, 10, 76]. Using the localised induction approximation (LIA) the self induced velocity on a helix with nonzero core size carrying vorticity is proportional to the binormal of the helix [76]:

$$\boldsymbol{v}_{\text{hel}} = \frac{\kappa\Gamma}{4\pi} \ln\left(\frac{1}{\epsilon}\right) \boldsymbol{b}_{\text{hel}} \,, \tag{2.70}$$

where ϵ is a non-dimensional core radius defined by the physical core radius σ and the curvature κ,

$$\epsilon = \sigma\kappa \,. \tag{2.71}$$

This means $0 < \epsilon \leq 1$. Notice that $\boldsymbol{v}_{\text{hel}}$ is not defined for the core radius being zero. Equation (2.70) is valid up to order $\mathcal{O}(1)$ terms in ϵ. Introducing

$$\gamma = \frac{1}{4} \ln\left(\frac{1}{\epsilon}\right) \,, \tag{2.72}$$

the velocity of the helix may be written

$$\boldsymbol{v}_{\text{hel}} = \kappa\frac{\Gamma}{\pi}\gamma\boldsymbol{b}_{\text{hel}} \,. \tag{2.73}$$

Therefore, increasing γ increases the speed of the helix. By equation (2.72) an increase in γ corresponds to a decrease in ϵ and thereby improves the accuracy of LIA.

By equation (2.73) the velocity of the vortex filament has constant components along the $\boldsymbol{e}_z$ and $\boldsymbol{e}_\theta$ directions (the component in the $\boldsymbol{e}_r$ direction is zero). Thus, any point on the helix is translated in the z-direction with the same speed, and rotated around the z-axis with same (negative) rotation frequency. Therefore, including finite core thickness in this way, the helix remains a helix as time varies. This hinges on $\boldsymbol{b}$ being a helical vector field.

2.4.1 Topology of velocity field generated by constantly rotating and translating helical vortex filament

Now we consider an thin helical vortex filament that translates along the center axis with constant speed and rotates around the center axis with constant speed. The case emerges from the selfinduced velocity on the helix for nonzero core size. However, the assumption is that the core size only affects the velocity of the

filament itself and through that the entire flow. The ratio of rotation speed and translation speed is fixed as a consequence of LIA so the velocity is given by one parameter.

Introducing a non-negative parameter δ by

$$\delta = \gamma \frac{1}{\sqrt{1+\lambda^2}}\,, \tag{2.74}$$

the stream function considered by Mezic et al. [76] (subscript M) can be written

$$\psi_M\left(\xi,\eta\right) = \psi_H\left(\xi,\eta\right) - \frac{1}{2}\delta\xi^2\,. \tag{2.75}$$

2.4.2 Closed form approximation of ψ_M

Since the same products of modified Bessel functions appear in the expressions of Hardin and Mezic it is easy to construct a closed form approximation (subscript c) $\psi_{M,c}$ from equation (2.75),

$$\psi_{M,c} = \psi_{H,c} - \frac{1}{2}\delta\xi^2\,, \tag{2.76}$$

with $\psi_{H,c}$ is given by equation (2.51). Many of the properties of $\psi_{H,c}$ are also valid for $\psi_{M,c}$ and are shown in the same way.

Since $\frac{\partial\psi_{M,c}}{\partial\eta} = \frac{\partial\psi_{H,c}}{\partial\eta}$, $\eta = 0$ and $\eta = \pi$ are the only possible values of η where critical points can occur. All information about critical points is contained in the function

$$G(\xi,\eta,\lambda,\delta) \equiv \frac{\partial}{\partial\xi}\psi_{M,c}(\xi,\eta) = \frac{\partial}{\partial\xi}\psi_{H,c}(\xi,\eta) - \delta\xi\,, \tag{2.77}$$

with $\eta = 0, \pi$. The zeroes of G as a function of ξ correspond to critical points, and the sign of the slope $\frac{\partial G}{\partial\xi}$ determines whether it is a center or a saddle. For $\eta = 0$ we have

$$\begin{aligned} G(\xi,0,\lambda,\delta) =& \frac{1}{2}\begin{pmatrix} \xi \\ -\frac{1}{\xi} \end{pmatrix} - \frac{1}{2}\left(\left(1+\lambda^2\right)\left(1+\xi^2\right)\right)^{\frac{1}{4}}\left(\frac{1}{2}\frac{\xi}{1+\xi^2}\ln\left(1-e^{\pm\alpha}\right)\right. \\ & \left.\mp f'(\xi)\frac{e^{\pm\alpha}}{1-e^{\pm\alpha}}\right) - \delta\xi\,. \end{aligned} \tag{2.78}$$

The conclusion is the same as before, zeroes of $G(\xi,0,\lambda,\delta)$ corresponds to critical points and the slope at a critical point determines the type. However, for small

ξ, $G(\xi,0,\lambda,\delta) > 0$ whereas $G(\xi,\pi,\lambda,\delta) < 0$. There is also a sign change in the second order derivative with respect to η. Since the type of critical point is determined by the sign of $\frac{\partial^2}{\partial\eta^2}G(\xi,\eta,\lambda,\delta)\frac{\partial^2}{\partial\xi^2}G(\xi,\eta,\lambda,\delta)$ then in case of critical points the same conclusion applies, the first critical point is elliptic and the next is hyperbolic.

As for the model of Hardin for a given parameter set an even number of critical point is guaranteed and no critical points exist for small λ.

We now investigate if critical points at $\eta = 0$ and $\eta = \pi$ are possible for the same parameter set (λ,δ). By inequality (2.58) we have no critical points at $\eta = 0$ in the outer region

$$G(\xi,0,\lambda,\delta) \leq \frac{\partial}{\partial\xi}\psi_{H,c}(\xi,0) < 0\,, \quad \text{for } \xi > \lambda. \tag{2.79}$$

From equation (2.78) for $\xi < \lambda$ the only negative term is $-\delta\xi$. In order to have $G(\xi,0,\lambda,\delta) = 0$ this term must at least dominate the other term that is linear in ξ, namely $\frac{1}{2}\xi$. Therefore $\delta > \frac{1}{2}$ is a necessary condition for a critical point at $\eta = 0$. Comparing to the case at $\eta = \pi$

$$G(\xi,\pi,\lambda,\delta) = \frac{1}{2}\begin{pmatrix} \xi - 2\delta\xi \\ -\frac{1}{\xi} - 2\delta\xi \end{pmatrix} - \frac{1}{2}\left(\left(1+\lambda^2\right)\left(1+\xi^2\right)\right)^{\frac{1}{4}}\left(\frac{1}{2}\frac{\xi}{1+\xi^2}\ln\left(1+e^{\pm\alpha}\right) \pm f'(\xi)\frac{e^{\pm\alpha}}{1+e^{\pm\alpha}}\right), \tag{2.80}$$

it is immediately clear that for $\delta \geq \frac{1}{2}$ the first term is non positive and the rest of the terms are negative for $\xi < \lambda$ which spoils the possibility of critical points in the inner region. Considering the outer region and throwing away the logarithmic term;

$$G(\xi,\pi,\lambda,\delta) \leq \frac{1}{2}\left(-\frac{1}{\xi} - 2\delta\xi\right) + \frac{1}{2}\left(\left(1+\lambda^2\right)\left(1+\xi^2\right)\right)^{\frac{1}{4}} f'(\xi)\frac{e^{-\alpha}}{1+e^{-\alpha}}\,, \quad \text{for } \xi > \lambda\,. \tag{2.81}$$

From equation (2.50) and $\xi > \lambda$ then $\frac{e^{-\alpha}}{1+e^{-\alpha}} \leq \frac{1}{2}$. Using this and $\delta \geq \frac{1}{2}$ in inequality (2.81):

$$G(\xi,\pi,\lambda,\delta) \leq \frac{1}{2}\left(-\frac{1}{\xi} - \xi\right) + \frac{1}{2}\left(1+\xi^2\right)^{\frac{1}{2}} f'(\xi)\frac{1}{2}\,, \quad \text{for } \xi > \lambda\,. \tag{2.82}$$

Since $\sqrt{1+\xi^2}f'(\xi) = \frac{1}{\xi} + \xi$ then

$$G(\xi,\pi,\lambda,\delta) \leq \frac{1}{2}\left(\frac{1}{\xi} + \xi\right)\left(-1 + \frac{1}{2}\right) < 0\,, \quad \text{for } \xi > \lambda\,. \tag{2.83}$$

Thus, for $\delta < \frac{1}{2}$ the only critical point possibility is at $\eta = \pi$. For $\delta > \frac{1}{2}$ the only critical point possibility is at $\eta = 0$, and no critical point exists at $\delta = \frac{1}{2}$. By changing a parameter, the only way to get from a critical point at $\eta = \pi$ to a critical point at $\eta = 0$ is through a region with no critical points.

We summarise analytical results about the zeroes of G in the following theorem.

Theorem 2.15 *Properties of G*

1. *There are no zeroes of G when λ is small and δ is fixed for $\eta = 0, \pi$.*
2. *There are at least two critical points of $G(\xi, 0, \delta, \lambda)$ for large δ and λ fixed.*
3. *Zeroes for G at $\eta = 0$ can exist only when $\delta > \frac{1}{2}$.*
4. *Zeroes for G at $\eta = \pi$ can exist only when $\delta < \frac{1}{2}$.*
5. *There are no zeroes for G in the outer region $\xi < \lambda$ for $\eta = 0$.*
6. *The innermost critical point, if it exists, is elliptic, the next is hyperbolic, and so on. This holds separately at $\eta = 0, \pi$.*

A main difference from the case considered in § 2.3.2 is that critical points can also occur at $\eta = 0$. However, they never exist simultaneously with critical points at $\eta = \pi$. This is a strict mathematical statement for $\psi_{M,c}$ whereas Mezic et al. [76] argue the same holds for ψ_M invoking a numerical argument.

We now turn to a numerical investigation of $\psi_{M,c}$. Two new topologies are found. Figure 2.4(a) shows that for positive δ the hyperbolic critical point may be located in the inner domain. A critical point is possible for $\eta = 0$ as shown in figure 2.4(b). Here the elliptic critical point is still closest to the origin but now the hyperbolic critical point is between the elliptic critical point and $(\lambda, 0)$. Only two critical points are observed at a given set of of parameters and the only bifurcations occurring are saddle-node bifurcations.

The reflection symmetry around the x - axis is inherited from the invariance of $\eta \to -\eta$ in the stream function of Hardin and also the closed form formulation.

The critical point pattern as a function of the parameters is summarised in a bifurcation diagram, figure 2.5. Here the parameter $\gamma = \sqrt{1 + \lambda^2}\delta$ is used to facilitate comparison with the results of Mezic et al. [76] - the results compare very well. For small δ the topologies observed in the model of Hardin shown in figure 2.3 are recovered. However, the topology with two critical points in the inner region at $\eta = \pi$ exists only for $\gamma < 0.07$. For $\gamma > 2.15$ critical points

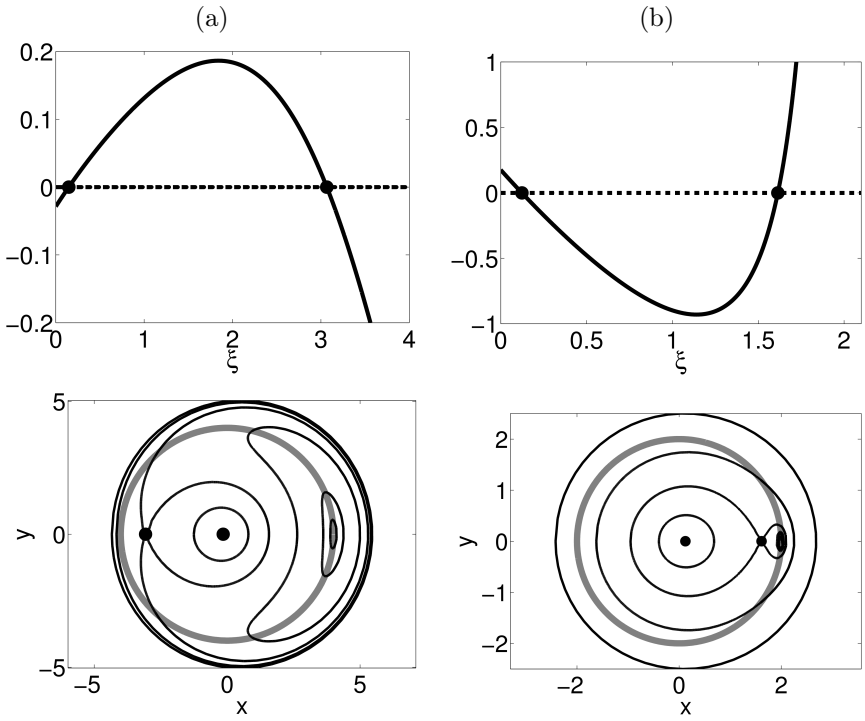

Figure 2.4: The two topologies of $\psi_{M,c}$ not existing for $\psi_{H,c}$. (a) $\lambda = 4$, $\delta = 0.3$. The top panel shows $G(\xi, \pi, 4, 0.3)$. The bottom panel shows the contour plot of $\psi_{M,c}$. There are two critical points in the inner region $\xi < \lambda$. (b) $\lambda = 2$, $\delta = 2$. Top panel shows $G(\xi, 0, 2, 2)$. There are two critical points in the inner region but here the saddle point is closest to $(\lambda, 0)$.

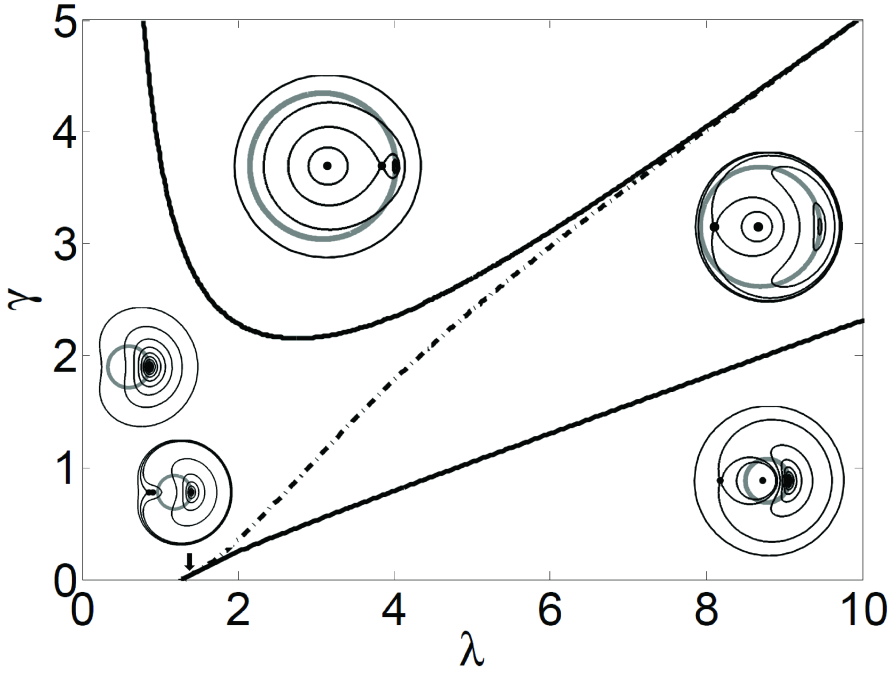

Figure 2.5: Bifurcation diagram for $\psi_{M,c}$. The top full curve is saddle-node bifurcation of critical points at $\eta = 0$. The curve approaches the γ axis asymptotically as shown in Theorem 2.15 (a) and (b). The dashed curve is saddle-node bifurcation of critical points at $\eta = \pi$. The lower full curve marks where the hyperbolic critical point at $\eta = \pi$ moves from the inner to the outer region. Between the upper full curve and the dashed curve is the curve (not shown) $\delta = \frac{1}{2}$ i.e. $\gamma = \frac{1}{2}\sqrt{1+\lambda^2}$ where no critical points can occur.

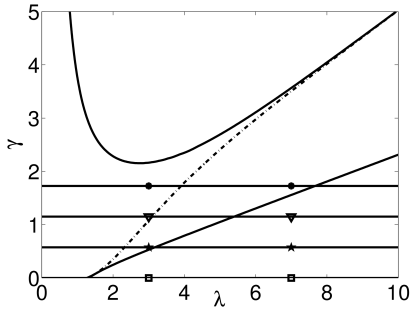

Figure 2.6: The bifurcation diagram from figure 2.5 with horizontal lines showing how well LIA works for the corresponding filament speed - see section 2.4. Circles: $\epsilon = 10^{-3}$, triangles : $\epsilon = 10^{-2}$, stars: $\epsilon = 10^{-1}$, squares : $\epsilon = 1$. Demanding $\epsilon \leq 10^{-3}$ only the part of the bifurcation diagram above the upper horizontal line is valid. Then the topology with two outer critical points is not accessible.

also exist for $\eta = 0$. The two top bifurcation curves appear to have a common asymptote which must be the line $\delta = \frac{1}{2}$, i.e. $\gamma = \frac{1}{2}\sqrt{1+\lambda^2}$ where no critical points can exist according to Theorem 2.15.

Increasing γ improves the accuracy of LIA as discussed in section 2.4. In figure 2.6 the bifurcation diagram in figure 2.5 is superimposed with horizontal lines corresponding to various values of ϵ in equation (2.72). Decreasing ϵ corresponds to increasing the accuracy of LIA. The velocity field generated by the zero thickness helical vortex filament generates infinite speed of the vortex filament which is unphysical (as well as a zero thickness core). However, Hardin's solution is useful for the velocity field away from the vortex filament. Using LIA the velocity field is no longer infinite on the filament. By demanding a high accuracy of LIA the topology with two critical points in the outer domain is not possible.

2.5 Conclusions

In theoretical mechanics coordinate-free formulations are generally very useful for highlighting fundamental consequences of symmetries. This point of view, however, seems to have had a quite limited impact on the research in helical fluid flows. We have extended the coordinate-free approach by Ettinger & Titi [36] and shown how it clarifies the basic properties of these flows.

A main purpose was a topological analysis of the streamlines in flows induced by

helical vortex filaments. Using the closed-form approximation by Okulov [80] and Fukumoto & Okulov [37] a significant simplification of the stream function was obtained, making a very complete analytical study of the flow topology possible. We have shown that a relatively small set of flow topologies can occur, even if self-induction of the filament is taken into account. Nevertheless, compared to the flow topology induced by rectilinear vortex filaments helical flow is much richer, underlining how complex these flows are.

There are obvious extensions of the topological analysis of the present investigation, e.g. the flow induced by several helical vortex filaments [81, 82] and the flow in a domain bounded by a cylinder [55]. Also, the topological analysis is not limited to inviscid flows. The same approach has previously been used to classify flow topologies in vortex breakdown in viscous axisymmetric flows, using both numerical computations [16, 15] and experimental data [69]. This could easily be extended to flows with helical symmetry.

Chapter 3

Boundary layer eruption

3.1 Introduction

A vortex convected close to a wall induces a viscous response from the near wall fluid (the boundary layer) due to the no slip boundary conditions on the wall - see figure 3.1. For sufficiently high Reynolds number this creates built up of vorticity in the boundary layer leading to ejection of fluid from the boundary layer with large absolute vorticity into the surrounding fluid thereby resulting in a new vortex structure. Thus, a vortex interacting with a boundary layer can create new vortices. We investigate this phenomena numerically by solving the two dimensional Navier - Stokes equations for Reynolds numbers up to 10000. Kudela & Malecha [64] found good agreement between streamlines and vorticity contours for such a problem. This surprising result was a key motivation to investigate this phenomenon further.

The described phenomena has been called various names such as *eruption* of boundary layer [64], *unsteady separation* [78, 103] or *bursting* [90]. The behaviour is typical for a range of set-ups such as vortex rings, vortex pairs, convected rectilinear vortex filaments and convected thick vortex cores and the eruption occurs over a range of Reynolds numbers [33, 32, 40]. Unsteady separation is important in many contexts. Any obstacle to a flow creates a boundary layer with the possibility of eruption. Other examples are wake - rotor interactions in

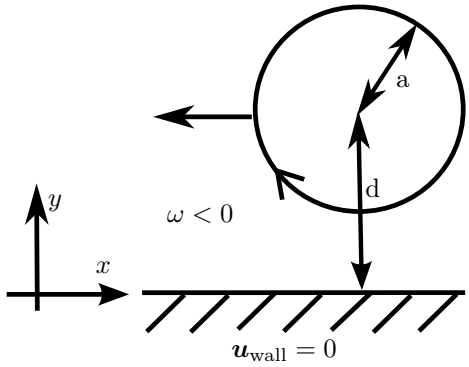

Figure 3.1: A vortex with negative vorticity close to a wall. d is the distance to the wall, and a is the characteristic length for the Gaussian distribution.

turbines or impulsive motion of bluff bodies [29]. Likewise for engineering vehicles in any environment the understanding of lift and drag induced by separation is important [26]

Of course any experiment like the one by [32] is conducted in the three dimensional world, but the characteristic behaviour of unsteady separation can be found also in two dimensional models [33, 40]. Since the eruption phenomenon is observed for many different vortex configurations close to a wall, the present study in two dimensions of vortex creation can therefore be considered a building block for more complex vortex - boundary layer interactions.

The first idea of a boundary layer dates back to [85] who considered steady two dimensional flow close to a solid body.

For large Reynolds numbers it is assumed that viscosity matters only very close to a solid body in a boundary layer. Then the inviscid equations are used outside the boundary layer. Inside the boundary layer a rapid change in the velocity component parallel to the solid body exist as one moves in normal direction to the solid body. This is due to the no slip boundary condition on the body whereas the inviscid equations only has a no flux boundary condition. Thus even for the viscosity considered 'small' (or Re 'large') then close to the solid body the spatial derivatives of the velocity are large making the viscous term in the Navier - Stokes equation non negligible. The success of the boundary layer equations relies on the identification of two different length scales. The thickness of the boundary layer provides a length scale for the direction perpendicular to the wall, and the length of the solid body provides a (much larger) length scale in the direction tangential to the solid body. This leads to omission of some of

the derivatives in the Navier - Stokes equations. The pressure in the boundary layer is typically assumed to be independent of y (the direction perpendicular to the wall) and is dictated by the outer, inviscid flow. This means that the pressure is an uncoupled 'source term' in the boundary layer equations such that one can say that the pressure 'causes' a certain behaviour of the velocity field. In the two dimensional Navier - Stokes equations the velocity and pressure are coupled both ways i.e. they dynamically evolve dependently.

The boundary layer equations have been widely studied - especially before it was possible to perform simulations of the Navier - Stokes equations with large Reynolds numbers [27, 34, 29, 101, 20, 22, 18]. Separation in the boundary layer equations described in Lagrangian coordinates have been studied by [29] and [100].

A relation between Reynolds number and a laminar boundary layer can be constructed from balancing two terms in the Navier - Stokes equation given a boundary layer of thickness δ, a length of a solid body L, and a mean flow U. The two terms to match are the viscous term $\nu\nabla\boldsymbol{u}$ which dominates close to the solid body where large velocity gradients occur and the advective term $(\boldsymbol{u}\cdot\nabla)\,\boldsymbol{u}$ which dominates in the inviscid region far from the body. The advective term is of order $\frac{U^2}{L}$ and the viscous term is of order $\nu\frac{U}{\delta^2}$.

$$1 \approx \frac{\frac{U^2}{L}}{\nu\frac{U}{\delta^2}} = \frac{\delta^2}{L^2}\frac{LU}{\nu} = \frac{\delta^2}{L^2}\mathrm{Re}\,. \tag{3.1}$$

When this order of magnitude argument holds the boundary layer grows like $\mathrm{Re}^{-\frac{1}{2}}$. This means the boundary layer is thinning for increasing Re. Many papers describing boundary layers include a scaling of y by $\mathrm{Re}^{-\frac{1}{2}}$ which may be reasonable from the above argument. However, the argument does not take into account the rapid changes in the vorticity structure and boundary layer during the eruption event thus making a scaling with $\mathrm{Re}^{-\frac{1}{2}}$ less favourable. The unsteady boundary layer equations have been widely studied - also for understanding separation.

Prandtl discussed steady boundary layer separation as a consequence of a increasing pressure in the flow direction. Due to the no slip condition an adverse pressure gradient promotes reversed flow close to the wall. Prandtl derives the condition for separation that $\frac{\partial u(x,0)}{\partial y} = 0$ i.e. vanishing shear on a wall point(we are only considering Newtonian fluids). In case of no separation, the flow is mainly parallel to the wall i.e. u has constant sign close to the wall. In case of a separation, to the left of the separation point close to the wall then u is positive and to the right of the separation point close to the wall then u is negative. Due to the no slip condition this means that $\frac{\partial u}{\partial y}$ changes sign when passing the separation point along the wall - see figure 3.2.

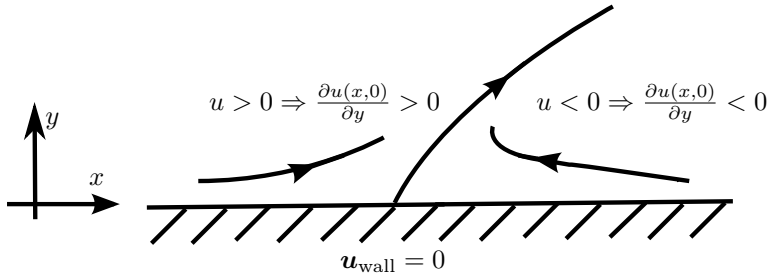

Figure 3.2: The boundary layer separation of steady flow considered by Prandtl

A separation of the boundary layer has vast implications for the flow description. This is the only way non zero vorticity particles can enter the inviscid domain. Therefore, a separation event is a signal that the original simplification of an inviscid outer domain and a viscous boundary layer fails such that the boundary layer equations no longer holds.

A consequence of the boundary layer equations is that in the boundary layer u is much larger than v i.e. the flow is almost parallel to the wall. This cannot be fulfilled when a separation is present since a sign change of u is needed. Therefore, a breakdown of the boundary layer equations are expected after or during separation. However, according to Sears & Telionis [94] the breakdown of the boundary layer equations provide a good indicator for the actual separation.

Gargano et al. [40] compare solutions of the boundary layer equations with the Navier - Stokes equations for a rectilinear vortex filament convected close to a wall. The recirculating region is also observed in the boundary layer equations even though the solution becomes untrustworthy when actual injection of concentrated vorticity in the outer flow happens. A similar observation is made by Walker [101] who also study the boundary layer due to a rectilinear vortex.

For unsteady flows Prandtl's separation criteria is not reliable as discussed in e.g. [94] and considered in Lagrangian coordinates by Cowley et al. [26]. Especially, vanishing wall shear is not an indicator of separation for unsteady flow. In case of moving walls a suggested criteria for separation is the MRS - criterion (named after Moore, Rott and Sears) $\frac{\partial u(x,y)}{\partial y} = 0$ and $u = 0$ where u is moving with speed of the separation point that is situated in the boundary layer. While $\frac{\partial u(x,y)}{\partial y} = 0$ is Galilean invariant and equal to the zero vorticity contour in the boundary layer, the question of choosing the right coordinate system for vanishing u is more delicate. Also [9] discuss how the MRS - criterion is insufficient for a vortex generated close to a wall described using normal form theory.

A sign change in u is not a good measure of separation as noted in [101] when using a coordinate system moving with the generation vortex filament. This is due to existence of a saddle point in the velocity field much earlier and at a different location than one would define a recirculation zone. Therefore, he defines the separation as the first time a recirculation zone is present.

From a dynamical system approach Haller [45] formulates criteria for unsteady separation in two dimensions as an extension of Prandtl's separation criteria and of the Lagrangian approach conducted by Cowley et al. [26]. The result of Haller [45] is formulated in Eulerian quantities and for various cases of separation. In one of the simplest cases the separation happens at a fixed spatial location on the wall but the separation profile (the unstable manifold of the separation point on the wall) may have arbitrary smooth shape as long as it is not parallel to the boundary. Hence, the separation profile on figure 3.2 is an example of this. Two criteria needed for separation are formulated assuming no slip wall, mass conservation and existence of the separation profile as a time dependent graph with a fixed wall attachment. These reduce to Prandtl's criteria for steady flow. Haller [45] discusses criteria of a moving separation point which is a separation point of varying location and existence. Here understanding of finite-time unstable manifolds are needed - see [44]. A finite time unstable manifold may be interpreted as a material line that attracts all nearby fluid particles over a finite time interval. Then, if a close material line becomes a finite time unstable manifold in the following time interval then a sliding separation profile can be observed. The moving separation criterion is non trivial and one difficulty is the non uniqueness of the finite time unstable manifolds.

Another approach to unsteady separation than using the MRS criteria is carried through by Cassel [20]. Here a thick vortex core above a wall is used to study unsteady separation. The separation is believed to occur in various asymptotic stages that are governed by subsets of the Navier - Stokes equation. This is put in relation to various instabilities in [22, 79, 21]. Another instability suggested in relation to a vortex interacting with a shear layer is described by Sengupta et al. [95] who study the so called disturbance energy.

Our scope is to study the topology of the vortices generated by a vortex close a wall. Optimally, this can lead to a catalogue of the possible 'patterns' that can be observed.

3.1.1 Vortex center criteria

A useful toolbox for analysing vortex creation is bifurcation theory. Here, we may restrict our attention to vortex centers i.e. a single point identifying a

vortex. Using bifurcation theory the creation and destruction of vortex centers can be formulated in a rigorous mathematical context. One challenge in order to do this is a useful definition of a vortex center.

The definition of a vortex center is not trivial. Relevant definitions relating to the two dimensional flow considered here will be discussed in relation to studying vortex creation near a wall.

There are various criteria in literature defining a vortex as illustrated by Chong et al. [25]: '*It is unlikely that any definition of a vortex will win universal acceptance.*' In the analysis we focus on vortex centers which facilitate the study of creation of vortices. Some criteria are found from considerations regarding the transpose of the Jacobian of the velocity field, $\nabla \boldsymbol{u}$ also known as the velocity gradient tensor or the rate-of-deformation tensor with elements $\frac{\partial v_i}{\partial x_j}$. Chong et al. [25] define a vortex as a region in space where the velocity gradient tensor has complex eigenvalues. This definition is Galilean invariant. According to Jeong & Hussain [58] the definition implies that for a critical point in the flow there are locally closed or spiralling streamlines if the critical point fulfils the vortex criterion. This interpretation is closely related to the approach we will use when considering closed streamlines. Any point in the flow is a critical point in the comoving frame. Therefore, the vortex definition may be formulated as existence of closed or spiralling streamlines if the coordinate system is chosen such that the point in question is a critical point. This is also well aligned with a vortex definition mentioned by Robinson [89]: ' *A vortex exists when instantaneous streamlines mapped onto a plane normal to the vortex core exhibit a roughly circular or spiral pattern, when viewed from a reference frame moving with the center of the vortex core*'.

The velocity gradient tensor can be split as a sum of a symmetric part, $S_{i,j} = \frac{1}{2}\left(\frac{\partial v_i}{\partial x_j} + \frac{\partial v_j}{\partial x_i}\right)$, and an antisymmetric part $\Omega_{i,j} = \frac{1}{2}\left(\frac{\partial v_i}{\partial x_j} - \frac{\partial v_j}{\partial x_i}\right)$. The antisymmetric part ($\boldsymbol{\Omega}$) is the vorticity tensor and the symmetric part, ($\boldsymbol{S}$) is the strain rate tensor. The eigenvalues of a symmetric matrix are real so the effect of applying $\boldsymbol{S}$ is 'stretching'. The eigenvalues of an antisymmetric, realvalued matrix are imaginary (possibly zero), so the effect of applying $\boldsymbol{\Omega}$ is rotation.

A Galilean invariant that measures the stretching versus rotation is Q

$$Q = \frac{1}{2}\left(||\boldsymbol{\Omega}||^2 - ||\boldsymbol{S}||^2\right) , \tag{3.2}$$

where $||\boldsymbol{\Omega}||^2 = \mathrm{tr}\left(\boldsymbol{\Omega}\boldsymbol{\Omega}^T\right)$ and $||\boldsymbol{S}||^2 = \mathrm{tr}\left(\boldsymbol{S}\boldsymbol{S}^T\right)$. The sum of the squared norm of the eigenvalues of $\boldsymbol{\Omega}$ is $||\boldsymbol{\Omega}||^2$ and $||\boldsymbol{S}||^2$ is the sum of the squared norm of the eigenvalues of $\boldsymbol{S}$. Therefore Q is a measure of the 'stretching' relative to the rotation given by a single number. Large Q can thus be interpreted as vorticity

dominating strain. Hunt et al. [53] use positive Q as a vortex definition along with the requirement that the pressure must be lower than the ambient value.

An often used vortex criteria is the one formulated by Jeong & Hussain [58]. They define a vortex core as a connected region with two negative eigenvalues of $\boldsymbol{S}^2 + \boldsymbol{\Omega}^2$. For two dimensional flow some of the vortex definitions are identical

Lemma 3.1 *For planar flow the following conditions are equivalent:*

- *Two negative eigenvalues of* $\boldsymbol{S}^2 + \boldsymbol{\Omega}^2$.
- *Imaginary eigenvalues of* $\nabla \boldsymbol{u}$.
- $Q > 0$.

The lemma is proven by Jeong & Hussain [58] by direct computation. For planar flow Q is easily computed as

$$Q = \frac{\partial u}{\partial x}\frac{\partial v}{\partial y} - \frac{\partial u}{\partial y}\frac{\partial v}{\partial x}\,. \tag{3.3}$$

Thus, Q reduces to the determinant of $\nabla \boldsymbol{u}$. This equals the determinant of the Hessian of the stream function which determines the type of a non degenerate critical point of the stream function. To put it another way, any nondegenerate center of any Galilean transformed stream function has positive Q.

For a no slip condition on a wall at $y = 0$ then $u(x, 0) = v(x, 0) = 0$ which implies $\frac{\partial u(x,0)}{\partial x} = \frac{\partial v(x,0)}{\partial x} = 0$. This means Q vanishes on a no slip wall, thus there are no vortices on a wall using the vortex definition of Jeong & Hussain [58].

Haller [46] also defines a spatially extended vortex which is done in a Galilean and rotationally invariant way. In this definition a time derivative is present which makes it harder to study.

Considering the velocity 'frozen' at some time instant, the elliptic critical points can be interpreted as indicators of a vortex. Especially if they persist in time [71]. However, one must be careful with inferring mass transport properties from a 'frozen' velocity field [54].

Fluid dynamics may be described using a field which is referred to as the Eulerian approach or using the trajectories of some fluid particles referred to as the Lagrangian approach. If the aim is to study material transport modelled as passive tracers the Lagrangian approach has been successful. Vortical motion may

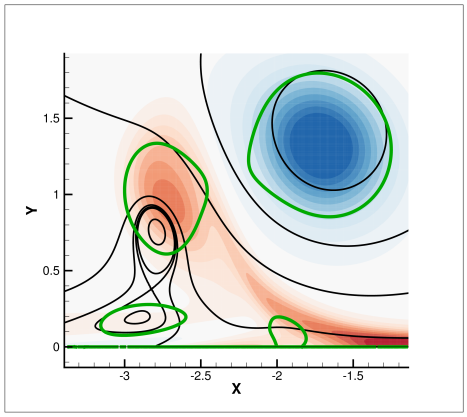

Figure 3.3: Comparison of different vortex center indicators at Reynolds number 1000 at time $t = 61$. Red - blue flooded contours are vorticity, black solid curves are isocurves of ψ_w, orange solid curves are isocurves of ψ_p. Green curves are contours of $Q = 0$. All centers of the stream functions are contained in regions with positive Q.

be put in the category of coherent structures which have covered a wide range of physical descriptions of visually 'obvious' flow characteristics [47]. Patterns emerging from studying advection of passive tracers is often labelled Lagrangian coherent structures (LCS). For time independent flow the stable and unstable manifolds are useful for describing separatrices in the flow thus dividing the flow into regions with no exchange of material between the regions. For time dependent flow the asymptotic behaviour for time going to infinity is hard to predict. This had led to the study of finite time Lyapunov exponents when studying LCS.

As noted by Lugt [71] a definition of a vortex in steady flow is *'Any mass of fluid moving around a common axis'*. Then a critical point of center type of the streamlines is indicating a vortex center since then the fluid locally rotates about this point. However, we are considering an unsteady flow which means it may be useful to study the instantaneous streamlines. In loose terms this means we 'take a picture' of the velocity field at a given time, make curves that are tangential to the instantaneous velocity vectors and if closed curves exist, there typically is a critical point of center type indicating a vortex center. The stream function is not a Galilean invariant so the speed of the coordinate system must also be considered. The flow investigated here is sufficiently simple that there are some good candidates. In [34], [33], [101], [78] and [40] the used coordinate system is moving with constant speed corresponding to a point vortex in inviscid flow. We denote this *the patch system*. Thus, in the inviscid case the flow is

steady using this coordinate system. As long as the generating vortex moves close to the inviscid case then the position will be fixed in the comoving frame and closed streamlines around the generating vortex are revealing its presence.

Kudela & Malecha [64] use the coordinate system in which the wall is fixed - we denote this *the wall system*. This is useful since a 'pinch off' mechanism is observed characterising eruption by a sequence of bifurcations in the streamlines. We note that the difference between the two streamline descriptions is adding a small constant to the horizontal velocity component.

A Galilean invariant may be preferable to describe a vortex center. A candidate is the vorticity which Kudela & Malecha [64] also consider. Then an extremum of vorticity can be used to define a vortex center. In general vorticity is large in a shear layer. Hence, fluid moves to the right on the top of the shear layer and to the left below the shear layer but the is no rotation around a common axis. A classical example discussed by Rayleigh is acceleration of a wall from rest to a finite speed. The large velocity gradients in the fluid close to the wall results in extrema of the vorticity along the entire wall despite no obvious vortical structures. We may then restrict our attention to isolated extrema of the vorticity. Jeong & Hussain [58] discuss how this definition can be misleading for a three dimensional flow of a vortex in a shear flow.

It is interesting and quite surprising that vortex centers predicted by the vorticity are also found in the streamline description. Kudela & Malecha [64] observe a bifurcation in the streamlines defining eruption from a streamline point of view which is well aligned with concentrated parcels of vorticity leaving the boundary layer. This was the intriguing motivation for our investigation of comparing streamlines and vorticity contours.

The topology of the stream function has been investigated systematically by Brøns [17] for points close to a wall and for inflow points. We analyse the vorticity by similar means which is an analytical approach to comparing streamlines and vorticity.

Interaction of 'parcels' of concentrated vorticity have been idealised by point vortex models in inviscid flow. However, in point vortex models the streamlines are only considered since the vorticity centers remain at the location of the point vortex that are moving around in the flow but not created nor destroyed. Therefore, a point vortex model is not suitable here. Nevertheless, it is expected that a point vortex model may be qualitatively correct in an intermediate time after vortex formation and eruption and before the vortex has been too diluted by diffusion of vorticity due to the viscosity.

Vorticity and streamlines have been widely used to describe location of vortices.

Therefore, a comparison of the two seems useful. A critical point of center type of the instantaneous streamlines and a local extremum of the vorticity will be considered candidates of a vortex center in our investigations. We investigate the structures in the flow by considering the topology of the level curves of the instantaneous streamlines as well as the level curves of the vorticity. This means that time acts more like a parameter than a variable. We consider the spatial flow pattern for some fixed times, t_0. The stream function is considered in both the wall system and the patch system.

We also analytically investigate bifurcations in the topologies of the vorticity and level curves of the stream function. This is done locally but in a general setting that only uses incompressibility and no slip on the wall. The purpose is to make a catalogue of the possible bifurcations and to compare the topologies of the level curves of the stream lines and the topology of the vorticity. To do this a Taylor expansion is performed and then normal form reduction techniques are used to reduce the number of bifurcation parameters. A challenge here is that the normal form transformations that may be most useful for the level curves of the stream function may not be the most useful for the normal form of the vorticity. However, it is useful to apply the same transformations in both cases to facilitate comparison between the two.

The stream function in the system moving with the vortex can be considered a perturbation (unfolding) to the system where the wall is fixed. We use this in the analytical approach.

3.2 Physical formulation of the problem

Solving the Navier - Stokes equations numerically near a boundary is not an easy task. Professor Mark Thompson and his group at Monash University, Melbourne have developed software suitable for the job. Fortunately, I have been visiting them and used the software.

The incompressible, two-dimensional Navier-Stokes equations, coupled with the continuity equation, provide the starting point for the problem considered here. These need to be supplemented with boundary conditions to complete the problem definition. In particular, the no-slip boundary condition is applied at the solid wall. At the other computational boundaries, which are placed at a considerable distance to avoid adversely affecting the predictions, the velocity is specified from the initial imposed vorticity distribution including the image vortex on the other side of the solid wall, as explained below.

A patch of vorticity placed at some distance above the wall is introduced at time equal to zero. For the current simulations, an initial Gaussian distribution of vorticity is used. One reason to choose a Gaussian distribution is because the associated velocity field can be calculated analytically. Far away from the vorticity patch the velocity field decays inversely with distance from the centre of the vortex. On the other side of the solid boundary an image vortex of opposite sign is placed at the same distance from the wall. This pair of counter-rotating vortices is used to define the velocity field everywhere in the computational domain including on the solid boundary between the vortices and at the outer boundaries of the computational domain. Because the effect of the image vortex is to distort the primary vortex, the velocity field is evolved initially for a short time until initial oscillations are damped and the primary vorticity field readjusts. At that stage the boundary condition at the solid surface is set to no-slip and the main calculation commences.

The physical parameters of the problem are thus the viscosity of the fluid, the strength (circulation) or total vorticity of the vortex patch, the distance between the vortex patch and the wall and the radius of the vortex patch. Non-dimensional variables can be constructed through natural length (L) and velocity (U) scales, which also can be combined to provide a time scale (T).

$$\tilde{\boldsymbol{x}} = \frac{x}{L}\,, \quad \tilde{\boldsymbol{u}} = \frac{u}{U}\,, \quad \tilde{t} = \frac{t}{T} \tag{3.4}$$

with $T = \frac{L}{U}$. At time equal to zero, Γ denotes the circulation of the vortex, a is the core radius (the paramater that enters the exponential in the expression for the Gaussian distribution), d is the distance from the vortex centre to the wall, and ν is the viscosity of the fluid. The length scale and velocity scale are chosen as

$$L = d\,, \quad U = \frac{\Gamma}{2\pi a} \tag{3.5}$$

which means

$$T = \frac{L}{U} = \frac{2\pi a d}{\Gamma}\,. \tag{3.6}$$

The non-dimensional equations thus have d and the ratio between Γ and a scaled out. As a result the vortex always starts with the coordinates $(0, 1)$ with the wall located at $y = 0$.

A Reynolds number can be defined as

$$\mathrm{Re} = \frac{UL}{\nu}\,. \tag{3.7}$$

Thus, the Reynolds number can be considered a re-parametrization of the viscosity. In the scaled equations Re and a are the free parameters. The non-dimensional Navier-Stokes and continuity equations are (dropping the tildes)

$$\frac{\partial \boldsymbol{u}}{\partial t} = -(\boldsymbol{u}\cdot\nabla)\boldsymbol{u} - \frac{1}{\rho}\nabla P + \frac{1}{Re}\nabla^2\boldsymbol{u} \tag{3.8a}$$

$$\nabla\cdot\boldsymbol{u} = 0\,. \tag{3.8b}$$

The value of the parameters are chosen to provide direct comparison with results found in [64]. In that paper, a sum of smoothed point (i.e., potential) vortices are used to model the global vorticity distribution, i.e., it is a 'hard' vortex patch, effectively with constant vorticity dropping suddenly to zero at the circular boundary. Kudela & Malecah [64] use $a = 0.3$ and $\omega_0 = -1.25$ as the total, initial vorticity, where $\Gamma = \omega_0\pi a^2$. We use the same ω_0 and a where a in our case is the characteristic length in the Gaussian distribution. This means that the total vorticity used in [64] match the vorticity within a disc of radius with one standard deviation for our setup. Hence, we use a larger total vorticity. Kudela & Malecha [64] use a numerical approach based on the vortex-in-cell method. We use a different numerical method described in the following.

3.3 Principles of the numerical solution

Some typical steps in finite-element modelling of the fluid flow equations are first described. The problem is how to solve the system of partial differential equations in u (and pressure p) with temporal and spatial derivatives. This differential formulation is called the strong form of the problem. In the weighted-residual approach, the differential equations are first multiplied by a function, called the test function, v, and then integrated over the spatial domain. Performing a partial integration can then typically reduce the order of differentiation by one from the strong form. This is called the weak formulation of the problem.

To proceed using the finite-element method, the spatial domain is discretised, i.e., broken up into a set of discrete elements or finite elements. (The behaviour of the solution accuracy as the number of elements is increased is called 'h-convergence' in the literature.) The functions u and v may belong to two infinite-dimensional function spaces. An approximation to a finite-dimensional function space is then performed. This is typically done by using a finite number of terms from expansions of u and v. In these expansions are a finite number of parameters that have to be chosen in an 'optimal' way to produce a useful solution. Approximating with functions of higher than linear order is characteristic of spectral methods, which are used here. Using increasing higher-order functions to get a better approximation relates to 'p-convergence'.

In the Galerkin method (which we will use for solving the Navier-Stokes equations)

the choice of basis functions for u and v are the same. The measure of 'optimal' is related to the inner product which is a definite integral of the product of functions. Using an approximation to u yields a residual when substituted into the original differential equation. However, we demand this residual must be orthogonal to the space of trial functions given by the finite-dimensional function space approximating u. Thus, once the choice of a spatial discretization and a choice of trial functions with unknown parameters are made, the orthogonality criteria means constraints on the parameters may be formulated. In the best case scenario (which is not the case here) this is a linear problem. Then, the computational work required to obtain a solution is mainly associated with the cost of an inversion (or LU decomposition) of a matrix. This is more expensive when the matrix is large, which in turn is associated with a larger trial function space or a finer discretisation of space. Of course, the problem is that the trial solution becomes better as the matrix becomes larger. However, in addition, the structure of the matrix is of major importance in the computational and storage costs for inverting the matrix. In a finite-element context the bandwidth of the matrix is governed by the way the nodes are numbered. Therefore, much effort in finite-element modelling has been spent on these aspects of the problem.

The computations reported in this thesis are based on a nodal-based two-dimensional spectral-element method. This is effectively a finite-element method, where the emphasis is based on using (increasingly) higher-order weighting (test) and basis functions. A key feature is the use of nodal points within the elements being identical to the evaluation points for Gauss-Legendre-Lobatto numerical integration, which is used to perform the integrations involved with the weighted-residual method. This considerably reduces the computational effort required to perform the required integrations over the standard finite-element approach. Both the weighting functions and the basis functions used to provide a polynomial representation of the solution variables are identical for the current implementation – so it is characterised as a Galerkin method. Indeed these are just tensor-products of Lagrangian polynomials.

In general, the Navier-Stokes equations are hard to solve since there are derivatives in multiple variables, but in particular, because the equations are nonlinear and the continuity equation acts as a constraint on the system. Importantly, it becomes increasingly difficult to obtain accurate solutions at higher Reynolds numbers, as the length-scales (e.g., boundary layer/shear layer thicknesses) reduce, meaning that increasingly more elements or higher resolution within elements are needed to resolve the flows. There is a vast literature on computational fluid dynamics using finite-elements but much of the theory used here follows [63].

First a linear, one-dimensional example is considered to illustrate some important ideas that are also valid for solving the Navier-Stokes equations. Consider the

one-dimensional Poisson equation

$$\frac{\partial^2 u(x)}{\partial x^2} + f(x) = 0\,, \tag{3.9}$$

defined on the standard interval $\Omega = [-1; 1]$. This equation is multiplied by an as yet unspecified function, also called the weight or test function, $v(x)$. Then the resulting equation is integrated over the entire region, which results in the weak formulation of the problem

$$\int_{-1}^{1} v(x) \left(\frac{\partial^2 u}{\partial x^2} + f(x) \right) dx = 0 \tag{3.10}$$

for a set of test functions, v. This can be interpreted as the inner product of the weight function and the differential operator $\frac{\partial^2 u}{\partial x^2} + f(x)$ must vanish. Integration by parts may now be used to reduce the order of the highest derivative by one in equation (3.10).

$$\int_{-1}^{1} \frac{\partial v(x)}{\partial x} \frac{\partial u(x)}{\partial x} dx = v(x) \frac{\partial u(x)}{\partial x} \Big|_{-1}^{1} + \int_{-1}^{1} v(x) f(x) dx\,. \tag{3.11}$$

We have not specified boundary conditions yet. Now, assume there is one Dirichlet and one Neumann boundary condition

$$u(-1) = c_D\,, \quad \frac{\partial u(1)}{\partial x} = c_N\,. \tag{3.12}$$

The weight functions are chosen to vanish on all Dirichlet boundaries, in this case $v(-1) = 0$. Using the boundary conditions in equation (3.11) then one term vanishes due to $v(-1) = 0$, giving

$$\int_{-1}^{1} \frac{\partial v(x)}{\partial x} \frac{\partial u}{\partial x} dx = v(1) c_N + \int_{-1}^{1} v(x) f(x) dx\,. \tag{3.13}$$

Next is the approximation step. In finite-element modelling the domain is divided into non-overlapping elements. In two dimensions these are typically triangles or quadrilaterals, which can also have internal nodes. In the code used later, only quadrilaterals are used. Contributions to the discretised set of equations are then computed separated by integrating over each element and then these are combined to produce the matrix equations. Within each element there are internal nodes at which the solution variables are calculated.

To elaborate a little further, we use a finite dimensional subset of the full function space. The approximated solution is denoted u^δ. Similarly, the weight functions, which are identical for the Galerkin case, are also represented by a

finite-dimensional function space. There is no approximation in this step, since the function $v(x)$ was not in the original statement of the problem. We simply limit the attention to v^δ that are functions that can be constructed from a finite number of functions.

Inserting this into equation (3.13) gives

$$\int_{-1}^{1} \frac{\partial v^\delta(x)}{\partial x} \frac{\partial u^\delta}{\partial x} dx = v^\delta(1) c_N + \int_{-1}^{1} v^\delta(x) f(x) dx \,. \tag{3.14}$$

We want to use the same space of functions to approximate v and u. However, the weight functions vanish at the boundary while which may not be the case for u^δ. Any function u^δ may be decomposed as

$$u^\delta = u^H + u^D \,, \tag{3.15}$$

where u^H vanishes at the boundary and u^D is a known function with value g_D on the boundary. This is similar to finding all solutions to $Ax = b$ by finding one solution $Ax = b$ and all solutions to $Ax = 0$. The decomposition equation (3.15) is inserted in equation (3.14)

$$\int_{-1}^{1} \frac{\partial v^\delta(x)}{\partial x} \frac{\partial u^H}{\partial x} dx = v^\delta(1) c_N + \int_{-1}^{1} v^\delta(x) f(x) dx + \int_{-1}^{1} -\frac{\partial v^\delta(x)}{\partial x} \frac{\partial u^D}{\partial x} dx \,. \tag{3.16}$$

Now the homogenous part, u^H and the test function u^δ both have vanishing values at the boundary and therefore the same function space can be used to express the two functions. The coefficients determining u^δ can then be found from solving a finite, linear algebraic system of equations. The simplest solution space would be piecewise linear functions. However, for better precision a higher-order polynomial basis can be applied. In our case Lagrangian polynomials are used. The node points are chosen to enable Gauss-Lobatto-Legendre (GLL) quadrature, which considerably reduces the computational work required in setting up the matrix system. The Legendre polynomials are a special case of the Jacobi polynomials. The zeros of these do not have an analytic form, but robust algorithms can be used to approximate them to any desired accuracy (see for example [63], appendix A and B). Whilst there is some work in obtaining the internal node points, these only need to be computed once and significantly increase the efficiency of the calculation of the velocity field, which has to be calculated as a sequence of many time steps and for different values of Reynolds number (at least for the cases considered in this thesis).

3.3.1 Spatial integration using Gaussian quadrature

We discuss how to integrate over a single element, since the expansions only have support in one element. The integrations can then be done for all elements and the results are assembled together into a matrix known as the global assembly matrix. Note that the approximation process only enforces continuity in the solution across element boundaries (and not derivatives).

For this quadrature process, an element with $x \in [a, b]$ is first mapped to $\xi \in [-1, 1]$—the standard element. All spatial integration is done using GLL quadrature and Lagrange polynomials. The idea is to approximate the integrand by a polynomial expansion, whose value is known at some node points. By making a polynomial interpolation, $p(x)$ we can get a good approximation to f over the entire element. We take

$$p(x) = \sum_{j=1}^{N} f(x_j) h_j(x)\,, \tag{3.17}$$

where $h_j(x)$ is a Lagrange interpolating polynomial and x_j represents a GLL point within the domain. Then, the integral of p is

$$\int_{-1}^{1} p(x)dx = \int_{-1}^{1} \sum_{j=1}^{N} f(x_j) h_j(x)dx = \sum_{i=1}^{N} \alpha_j f(x_j)\,, \tag{3.18}$$

where

$$\alpha_j = \int_{-1}^{1} h_j(x)dx \tag{3.19}$$

defines a weight on each term $f(x_j)$. Therefore, we get the approximation

$$\int_{-1}^{1} f(x)dx \approx \sum_{i=1}^{N} \alpha_j f(x_j)\,. \tag{3.20}$$

Choosing the points x_j and the polynomial type is crucial for efficient numerics. As indicated, we use the Lagrangian polynomials

$$L_j(x) = \prod_{k=1, k\neq j}^{n} \frac{x - x_k}{x_j - x_k}\,. \tag{3.21}$$

It is worth noticing what happens at the 'special points' $x_1, ..., x_N$. From equation (3.21) it is clear that

$$L_j(x_i) = \delta_{ij}\,, \tag{3.22}$$

with δ_{ij} being the Kronecker delta. Therefore, at the points $x_1, ..., x_N$ the polynomial approximation $p(x)$ is exactly equal to $f(x)$.

GLL quadrature impose the property that equation (3.20) is exact if $f(x)$ is a polynomial of degree $2N-1$ [63]. It may seem surprising that it is possible to get an exact result for higher polynomial order than N. According to Karniadakis et al. [63] the weighting coefficients, α_j can be calculated as

$$\alpha_j = \frac{2}{m\,(m+1)\,(K_m(x_j))^2}\,, \quad j \in \{0,1,...\}\,, \tag{3.23}$$

with

$$K_m = \frac{1}{2^m m!}\frac{d^m}{dz^m}\left(z^2-1\right)^m\,, \quad m \in \{0,1,...\}\,. \tag{3.24}$$

Considering a weak form of a differential equation, terms of the type $\int_{-1}^{1} v(x)f(x)dx$ are present, where $v(x)$ is the weight function. Using a Lagrangian polynomial for the weight function and a Lagrangian interpolation for the function $f(x)$ we get

$$\int_{-1}^{1} L_i(x)f(x)dx \approx \int_{-1}^{1} L_i(x)\sum_{j=1}^{N} f(x_j)L_j(x)dx = \sum_{j=1}^{N} f(x_j)\int_{-1}^{1} L_i(x)L_j(x)dx \tag{3.25}$$

The integral is approximated using GLL quadrature

$$\int_{-1}^{1} L_i(x)L_j(x)dx \approx \sum_{m=1}^{N} \alpha_m L_i(x_m)L_j(x_m) = \sum_{m=1}^{N} \alpha_m \delta_{i,m}\delta_{j,m}\,, \tag{3.26}$$

where the equality follows directly from equation (3.22). Inserting this in equation (3.25) we get

$$\int_{-1}^{1} L_i(x)f(x)dx \approx \sum_{j=1}^{N} f(x_j)\sum_{m=1}^{N} \alpha_m \delta_{i,m}\delta_{j,m} = \alpha_i f(x_i)\,. \tag{3.27}$$

Thus, forming the inner product with the i^{th} Lagrangian polynomial only depend on the i^{th} node point. This diagonal structure is helpful for the numerics. The integrand often involves a derivative. It is possible to approximate the spatial derivatives of a function using the GLL node points. Since there is a mapping to the standard interval $[-1,1]$, differentiation is performed using the chain rule. The derivatives depend on the Lagrange polynomials at the node points [63]. In two dimensions the product space of the one dimensional polynomial space is used. This means that we use Lagrangian polynomials in two directions evaluated at GLL points in both directions. From this construction the two-dimensional Navier-Stokes equations is spatially integrated using GLL quadrature.

3.3.2 Elements of solving the two dimensional Navier-Stokes equations numerically

We will now mention some steps in solving the Navier-Stokes equations which is a much harder problem than the linear problem previously described.

The time integration is performed in three steps, one for each term on the right hand side of equation (3.8a). Formally, we can integrate both sides of equation (3.8a) w.r.t. time over a timestep $\delta\tilde{t}$

$$\int_{\tilde{t}}^{\tilde{t}+\delta\tilde{t}} \frac{\partial \boldsymbol{u}}{\partial t} dt = \int_{\tilde{t}}^{\tilde{t}+\delta\tilde{t}} \left(-(\boldsymbol{u}\cdot\nabla)\boldsymbol{u} - \frac{1}{\rho}\nabla P + \frac{1}{Re}\nabla^2\boldsymbol{u} \right) dt\,. \tag{3.28}$$

In terms of the numerics we identify variables such that $\boldsymbol{u}^{(n)} = \boldsymbol{u}(\tilde{t})$, $\boldsymbol{u}^{(n+1)} = \boldsymbol{u}(\tilde{t}+\delta\tilde{t})$. Thus, using the value $\boldsymbol{u}^{(n)}$ we want to compute the next value $\boldsymbol{u}^{(n+1)}$. The left hand side of equation (3.28) is now written

$$\boldsymbol{u}^{(n+1)} - \boldsymbol{u}^{(n)} = \boldsymbol{u}^{(n+1)} - \boldsymbol{u}^{**} + \boldsymbol{u}^{**} - \boldsymbol{u}^{*} + \boldsymbol{u}^{*} - \boldsymbol{u}^{(n)}\,. \tag{3.29}$$

Here, $\boldsymbol{u}^{*}$ and $\boldsymbol{u}^{**}$ are used to decompose the solution process. The time integration is split in three steps as described in [62]. Terms on the right side of equation (3.28) can then be matched to the right side of equation (3.29) 'term by term'.

$$\boldsymbol{u}^{*} - \boldsymbol{u}^{(n)} = -\int_{\tilde{t}}^{\tilde{t}+\delta\tilde{t}} (\boldsymbol{u}\cdot\nabla)\boldsymbol{u}\, dt \tag{3.30a}$$

$$\boldsymbol{u}^{**} - \boldsymbol{u}^{*} = -\int_{\tilde{t}}^{\tilde{t}+\delta\tilde{t}} \frac{1}{\rho}\nabla P\, dt \tag{3.30b}$$

$$\boldsymbol{u}^{(n+1)} - \boldsymbol{u}^{**} = \int_{\tilde{t}}^{\tilde{t}+\delta\tilde{t}} \frac{1}{Re}\nabla^2\boldsymbol{u}\, dt\,. \tag{3.30c}$$

Of these equations only equation (3.30a) is nonlinear. The goal with this equation is to compute $\boldsymbol{u}^{*}$. This equation is solved by an Adams-Bashforth approximation that uses a weighted extrapolation from past (known) function values, i.e., at n and $n-1$.

$$\int_{\tilde{t}}^{\tilde{t}+\delta\tilde{t}} (\boldsymbol{u}\cdot\nabla)\boldsymbol{u} dt \approx \left(\frac{3}{2}\left((\boldsymbol{u}\cdot\nabla)\boldsymbol{u}\right)^{(n)} - \frac{1}{2}\left((\boldsymbol{u}\cdot\nabla)\,\boldsymbol{u}\right)^{(n-1)} \right) \delta\tilde{t}\,. \tag{3.31}$$

In equation (3.30b) $\boldsymbol{u}^{**}$ and the pressure are the unknowns. This equation is handled by making an intermediate time step $n+\frac{1}{2}$ and making the approximation

$$\boldsymbol{u}^{**} - \boldsymbol{u}^{*} \approx -\left(\frac{1}{\rho}\nabla P\right)^{\left(n+\frac{1}{2}\right)} \delta\tilde{t}\,. \tag{3.32}$$

Taking the divergence of equation (3.32) yields

$$\nabla\cdot\boldsymbol{u}^{**} - \nabla\cdot\boldsymbol{u}^{*} \approx -\left(\frac{1}{\rho}\nabla^2 P\right)^{\left(n+\frac{1}{2}\right)} \delta\tilde{t}\,. \tag{3.33}$$

Now the incompressibility condition equation (3.8b) is used. For a velocity field that is initially divergence free, $\nabla\cdot\boldsymbol{u}^{(n)} = 0$, the condition

$$\nabla\cdot\boldsymbol{u}^{**} = 0 \tag{3.34}$$

is sufficient to make sure it remains divergence free, $\nabla\cdot\boldsymbol{u}^{(n+1)} = 0$, as can be seen by taking the divergence of the equation for the viscous sub-step, discussed below in equation (3.36). Thus, by demanding equation (3.34) to hold then equation (3.33) can be formulated as a Poisson equation for the pressure

$$\frac{1}{\delta\tilde{t}}\nabla\cdot\boldsymbol{u}^{*} \approx \left(\frac{1}{\rho}\nabla^2 P\right)^{\left(n+\frac{1}{2}\right)}\,. \tag{3.35}$$

This is a Poisson equation that can be solved as previously described by making a weak form and using GLL quadrature to evaluate the integrals. This gives a set of linear equations connecting the pressure at each node point, which is solved by LU decomposition. Note that the assembled matrix is not a function of the time step, hence the LU decomposition only has to be done once. The Neumann boundary conditions for the pressure are obtained by taking the dot product of the NS equations with the surface normal vector. These involve the velocity field and Adams-Bashforth projections are used to implement the boundary condition as described in [62]. Typically only a first-order approximation is used (because it is more stable), which leads to a first-order in time approximation to the pressure field. However, the temporal accuracy of the velocity field is one order higher, i.e., formally second-order accurate. Knowing the pressure and $\boldsymbol{u}^{*}$ then $\boldsymbol{u}^{**}$ can be computed from equation (3.30b).

Equation (3.30c) is discretised in time using a second-order accurate theta-modified version of the Crank-Nicholson scheme [19] which enables computation of $\boldsymbol{u}^{(n+1)}$.

$$\boldsymbol{u}^{(n+1)} - \boldsymbol{u}^{**} \approx \frac{1}{2Re}\left((1-\theta)\nabla^2\boldsymbol{u}^{(n+1)} + (1+\theta)\nabla^2\boldsymbol{u}^{(n)}\right)\delta\tilde{t}\,. \tag{3.36}$$

Here, θ is a small constant, which stabilises the scheme against high-frequency oscillations, but does not change the formal second-order temporal accuracy. In the spectral-element context, this leads to a Helmholtz equation, which is treated in a similar way to the Poisson equation for the pressure substep. Further details on the spatial and temporal discretisations can be found in [97].

3.3.3 Further brief computational details

For the main simulations described below, the non-dimensional time step was chosen as 0.005. Halving the time step resulted in negligible changes to the flow evolution (certainly less than 1%). In addition, a spatial resolution study was also performed to verify the spatial resolution was adequate. In a spectral-element context, this can be done by varying the order of the interpolating polynomials used within elements at runtime. Typically tests were done at $Re = 20000$. Eighth-order polynomials were used within elements, i.e., each element consisted of 9×9 internal nodes. This led to better than 1% accuracy in the evolution of the vorticity at the centre of the primary vortex. The mesh incorporated almost 6000 (9×9) elements with mesh compression towards the solid boundary and increased resolution in the neighbourhood of the vortex. The computational domain spanned $-3.63 \leq x \leq 3.63$ and $0 \leq y \leq 5.13$, with the vortex placed at $y = 1$. At the outer computational boundaries the velocity field was fixed from the analytic solution of the initial counter-rotating vortex pair plus the uniform background velocity to keep the vortex initially stationary in the computational domain. (Note that the velocity falls off as $1/r^2$ from the vortex dipole.) At the right boundary, where the flow exits the computational domain, zero-normal and constant pressure boundary conditions are enforced. The macro-element mesh overlaid with the vorticity distribution at a selected time during the calculation is shown in figure 3.4.

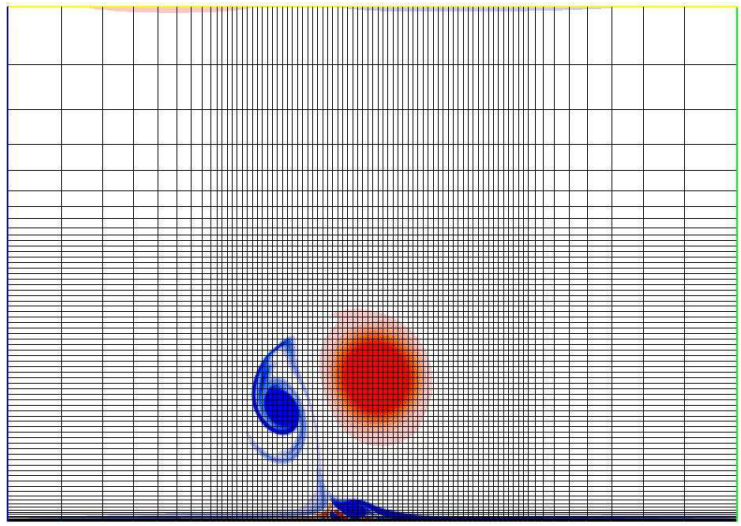

Figure 3.4: Mesh used for the computations. Only the macro-elements are shown. These are further subdivided into 9×9 internal nodes. The vorticity distribution sometime after lift out of the wall vorticity is shown to indicate the evolving vorticity distribution within the mesh system. There is considerable mesh compression towards the boundary to resolve the thin boundary layer at high Reynolds numbers. The Reynolds number in this case is 20000.

3.4 Initial calibration and shifting to a co-moving reference frame

To perform the simulations an initial velocity field is needed. This is done in two steps. First a rotation-symmetric velocity field generated by a Gaussian vortex patch in unbounded space is calculated analytically. This is done from the relation between vorticity and velocity. The calculated velocity field is denoted $\hat{\boldsymbol{u}}$. The vorticity distribution is given by

$$\omega = \omega_0 e^{-\frac{r^2}{a^2}} . \tag{3.37}$$

Since we have a two dimensional flow we get from the curl in cylindrical coordinates

$$\omega = \frac{1}{r}\left(\frac{\partial\left(r\hat{u}_\theta\right)}{\partial r} - \frac{\partial \hat{u}_r}{\partial \theta}\right) . \tag{3.38}$$

Assuming rotational symmetry of the velocity field, the last term vanishes. Combining with equation (3.37) gives

$$\frac{\partial\left(r\hat{u}_\theta\right)}{\partial r} = r\omega_0 e^{-\frac{r^2}{a^2}} . \tag{3.39}$$

Integrating from 0 to r and rearranging yields

$$\hat{u}_\theta = \frac{\omega_0 h^2}{2r}\left(1 - e^{-\frac{r^2}{a^2}}\right) . \tag{3.40}$$

As described previously, the velocity field $\hat{\boldsymbol{u}}$ is then constructed by placing the vortex at the desired distance from the wall together with an image vortex of opposite sign at the same distance below the wall. This combination effectively produces a vortical flow in the physical domain corresponding to a slip condition at the (otherwise) solid surface. Since the pair of counter-rotating vortices self advect due to Biot-Savart induction, a uniform background velocity is added to at least initially maintain the vortices at the same x position. This is effectively equivalent to switching to a moving frame of reference centred on the vortex. This procedure is used to set an initial condition for a first simulation. This does not produce an equilibrium solution to the NS equations; however, after a relatively short time, oscillations of the vortex damp viscously and it readjusts to a new, slightly non-rotationally symmetric, elliptical distribution. That can then be used to form a reasonable starting point for the main computation looking at the secondary vorticity induced at the solid surface and its subsequent behaviour. More information on this settling procedure applied to related problems can be found in [91] and references therein. For Reynolds numbers less than 10000 the settling time was chosen as 1 non-dimensional time unit and for Reynolds number

larger than 10000, twice this value was typically used. Settling the velocity field for too long also leads to viscous spreading of the vortex, increasing its core radius and lowering the effective Reynolds number for the main simulation. This is especially true at lower Reynolds numbers.

After this calibration/settling step, the velocity field at the solid wall is then instantaneously set to zero to commence the main calculation. This process induces an initially infinitely thin vorticity (boundary) layer at the boundary, which diffuses into the domain. Significant advection of this secondary vorticity can then occur leading to the interesting flow physics that forms the basis of the investigations described in this thesis.

3.5 Results of the simulations - topologies for the patch system

First the dynamics is studied in the patch system - the frame that moves with speed of a point vortex with circulation Γ in inviscid flow. The point vortex speed depends linearly on the circulation. The circulation used here corresponds to the vorticity contained in the patch at (0,1) with radius a. This means that only 68 percent of the total, initial vorticity is accounted for. If this was a significant problem the generating vortex patch would move to the left for increasing time. However, the boundary layer response has a much more significant effect and this decreases the speed of the generating vortex patch. The speed of the wall in the patch system is then 0.02812 in dimensionless units.

The dynamics is studied as a time sequence for a fixed Reynolds number. Then the Reynolds number is increased and the time sequence is studied again. In general we observe structures of increasing complexity for increasing Reynolds number. Of course for sufficiently long time the viscosity dampens all motion but we are interested in the transient behaviour where new vortices may be created. The vorticity is marked by coloured regions with twenty colours equally filling the vorticity values -0.3 to 0.3 as default for Re up to 1000. However, to display the vorticity topology optimally the range is often varied but twenty equidistant levels are always used. Plots are often displayed with different span on the axis. When focusing on structures close to the wall, the zoom is often not geometry preserving since the displayed span on the y - axis is smaller than on the x - axis.

The representative cases of Reynolds number 200 is shown in figure 3.5. The blue contours initially centered at $(0, 1)$ is the negative vorticity from the generating vortex patch i.e. the vortex we put to provoke a viscous response from the

boundary layer. At the first time steps vorticity of positive sign is growing close from the wall. This illustrates a problem with the vorticity definition of a vortex; when shear layers are present it may not seem sensible to assign an extremum value of the vorticity 'a vortex centre'. For increasing time a 'tongue' of the boundary layer vorticity is 'drawn' into the surrounding fluid without creating a new vortex off the wall. The black lines are instantaneous streamlines in the patch system. From the very beginning of the simulation a saddle point is present to the right of the vortex center and close to the wall. Since the wall moves from left to right there are no on wall critical points of the streamlines in this coordinate system. Close to the generating vortex the flow is clockwise around the vortex center. Hence, there must be a point of vanishing u between the generating vortex and the wall. Due to the no flux condition v vanishes on the wall. The saddle point in the streamlines in figure 3.5 splits the plane in a region with closed streamlines close to the generating vortex and streamlines extending to infinity in both directions. A local maximum of vorticity is observed on the wall beneath the saddle point in the streamlines. This saddle point and the extremum in the vorticity persist in time and for higher Re.

Increasing the Reynolds number to 500 the first topology observed is similar to lower Re as seen in figure 3.6a and figure 3.6b. Then, a saddle node bifurcation in the streamlines results in a streamline vortex using the closed streamline definition. The vorticity is concentrated in this region but a point of distinct extreme value off the wall is not visible at the time of creation of the streamline center. Such an extreme value has been created in figure 3.6c and here the streamline center and the extreme value of vorticity match fairly well. The region with closed streamlines around the new vortex has grown and is lifted off the wall indicating an eruption event.

In figure 3.6d the streamline center has disappeared through a saddle node bifurcation while the vorticity extreme value is still evident. This suggest that the 'vorticity vortex' is somewhat more robust than the 'streamline vortex'. The generation of the secondary vortex decrease the horizontal motion of the primary vortex compared to the inviscid case. Also, the generating vortex is lifted from its initial position at (1,0) by the presence of the new vortex. For $Re = 1000$ (figure 3.7)the same structures are observed as for $Re = 500$ but also a vorticity minimum is observed on the wall in figure 3.7b.

At $Re = 4000$ the initial time development is similar to lower Reynolds numbers. Again the secondary vortex is first created in the streamline formulation (figure 3.8b and figure 3.8e) but soon after an extreme vorticity value is observed close to the streamline center as can be seen in figure 3.8c and figure 3.8f for the center at y close to 0.3. Here a secondary new streamline center at y close to 0.1 has been created through a saddle node bifurcation. The new center corresponds to a vortex with positive vorticity. Close to the new streamline center there is a

band of large, positive vorticity. This latest created vortex vanish again through a saddle node bifurcation and the vorticity is 'smeared out' which is seen in figure 3.9a near the location of the second generated vortex. The first created vortex is then convected and the vortex vanishes in the streamlines through a saddle node bifurcation while still being visible in the vorticity - see figure 3.9b. A third vortex is created in the 'slipstream' rather far from the wall which is visible in figure 3.9b from the vorticity and also as a streamline center in 3.9c.

At $Re = 5000$ once again the structures at lower Re is observed in figure 3.10a, 3.10b, 3.10c. In figure 3.10d a center in the streamlines has emerged with negative circulation - again through a saddle node bifurcation. The vorticity has a large negative value in a region close to the new streamline center. The latest created vortices are the first to disappear as seen in figure 3.10e and figure 3.10f. The convected vortex vanish in the streamline description in figure 3.11a while being clear as a vorticity extreme value. Also an extreme value of vorticity is visible in the slipstream. In figure 3.11b this is also visible as a streamline center.

For $Re = 10000$ the figures 3.12a -3.12d show the same behaviour as $Re = 5000$. In figure 3.12e a fourth created streamline center is created close to the wall with positive circulation. Here also a local extreme value of the vorticity exists. The two last created vortices then rotate around a common axis and then the second last created vortex vanishes as seen in figure 3.12f where all three vortices have positive circulation. In figure 3.13a the latest created vortex has vanished. In figure 3.13b -d it is clear how the first created vortex convects away from the wall and vanishes as a streamline center in figure 3.13d. Once again it is also observed how a vortex is created in the slipstream rather far from the wall and is visible both in the streamlines and the vorticity in figure 3.13c and figure 3.13d. Though the focus is on vortices it is worth noticing that often the vorticity contours and streamlines are well aligned for example in figure 3.13a.

Summing up the numerical results so far, first vorticity of positive sign builds up over a large region on the wall but no vortices are created. This shear layer makes the definition of a vortex by extremum of vorticity less appealing. Hence, one might want to include more criteria on the eigenvalues of the Hessian of the vorticity for a more clearly defined vortex. Increasing Re , a saddle node bifurcation in the streamlines creates a streamline vortex soon followed by a vorticity vortex with the two vortices being fairly well aligned. For a clear extremum in the vorticity the streamline and vorticity vortices are in general well aligned. For an erupted vortex, the vorticity vortex survives for more time steps than the streamline vortex. Increasing Re , further more vortices appear close to the wall. They often have a short lifetime compared to an erupted vortex but there is often a surprisingly good correspondence between streamlines and the vorticity - up to four streamline centers are observed simultaneously matching regions of concentrated vorticity.

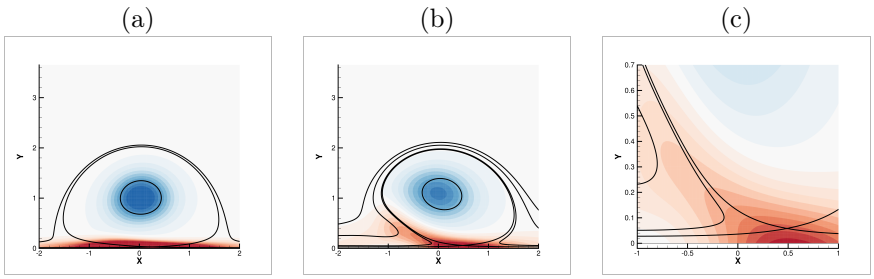

Figure 3.5: Re=200, the patch system.(a) t=5, vorticity contours with values in $[-0.3; 0.3]$. (b) t=30, vorticity contours with values in $[-0.3; 0.3]$. (c) t=30, the zoom is nongeometry preserving since a larger zoom has been used in the y direction. This is often the case when structures in the boundary layer is shown. vorticity contours with values in $[-0.5; 0.5]$

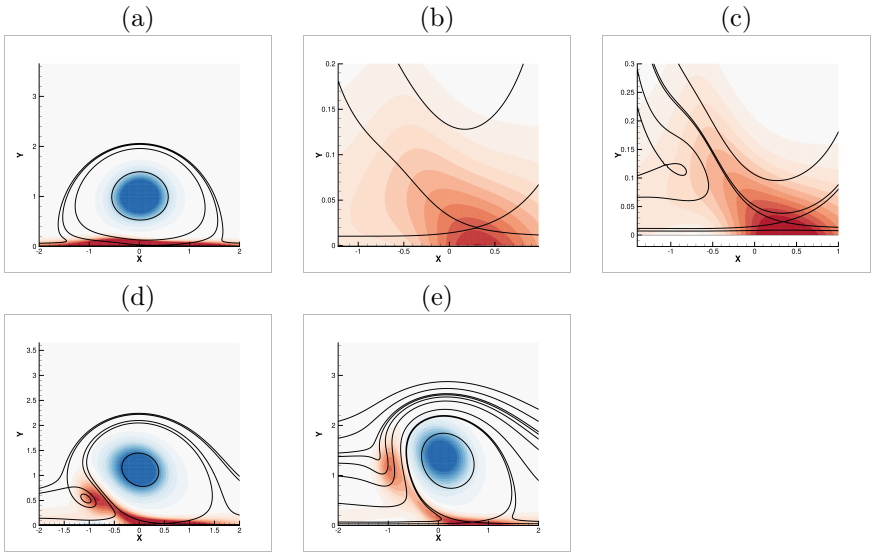

Figure 3.6: Re=500, the patch system.(a) t=8, vorticity contours with values in $[-0.3; 0.3]$. (b) t=8, vorticity contours with values in $[-1.5; 1.5]$. (c) t=14, vorticity contours with values in $[-1; 1]$. (d) t=40, vorticity contours with values in $[-0.3; 0.3]$. (e) t=63, vorticity contours with values in $[-0.3; 0.3]$.

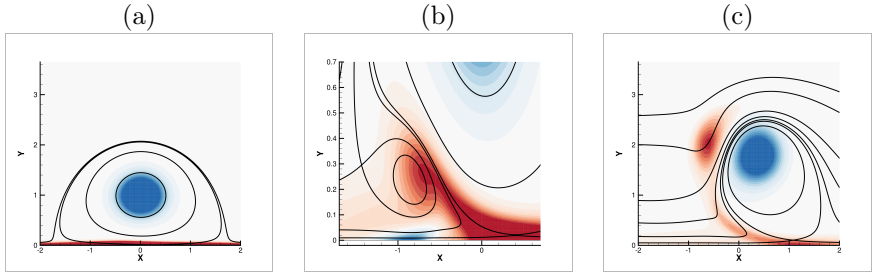

Figure 3.7: Re=1000, the patch system.(a) t=4, vorticity contours with values in $[-0.3; 0.3]$. (b) t=29, vorticity contours with values in $[-0.5; 0.5]$ (c) t=89, vorticity contours with values in $[-0.3; 0.3]$

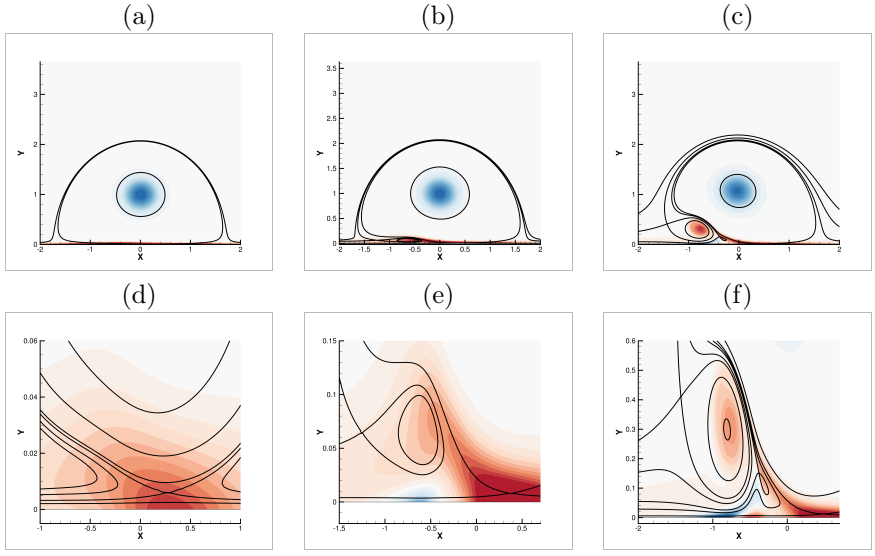

Figure 3.8: Re=4000, the patch system. (a) and (d) t=5, (b) and (e) t=20, (c) and (f) t=45, Vorticity contours with values in $[-1; 1]$ for (a)-(c). Vorticity contours with values in $[-5; 5]$ for (d), $[-2; 2]$ for (e), $[-1.5; 1.5]$ for (e).

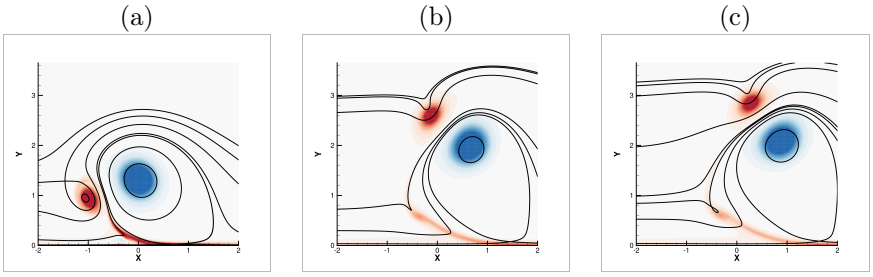

Figure 3.9: Re=4000, the patch system. Vorticity contours with values in $[-0.5; 0.5]$. (a) t=70, (b) t=109, (c) t=116.

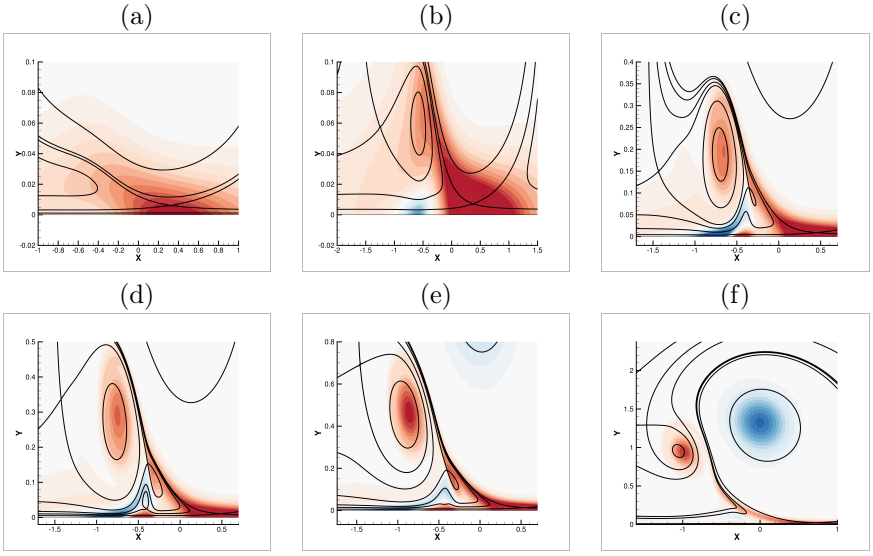

Figure 3.10: Re=5000, the patch system. (a) t=9, vorticity contours with values in $[-4; 4]$. (b) t=20, vorticity contours with values in $[-1.8; 1.8]$. (c) t=38, vorticity contours with values in $[1.5; 1.5]$. (d) t=45, vorticity contours with values in $[-1.4; 1.4]$ (e) t=55, vorticity contours with values in $[-1.0; 1.0]$. (f) t=72, vorticity contours with values in $[-1.0; 1.0]$

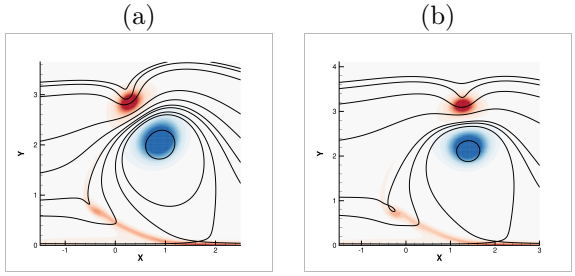

Figure 3.11: Re=5000, the patch system., (a) t=118, vorticity contours with values in $[-0.5; 0.5]$ (b) t=132, vorticity contours with values in $[-0.5; 0.5]$

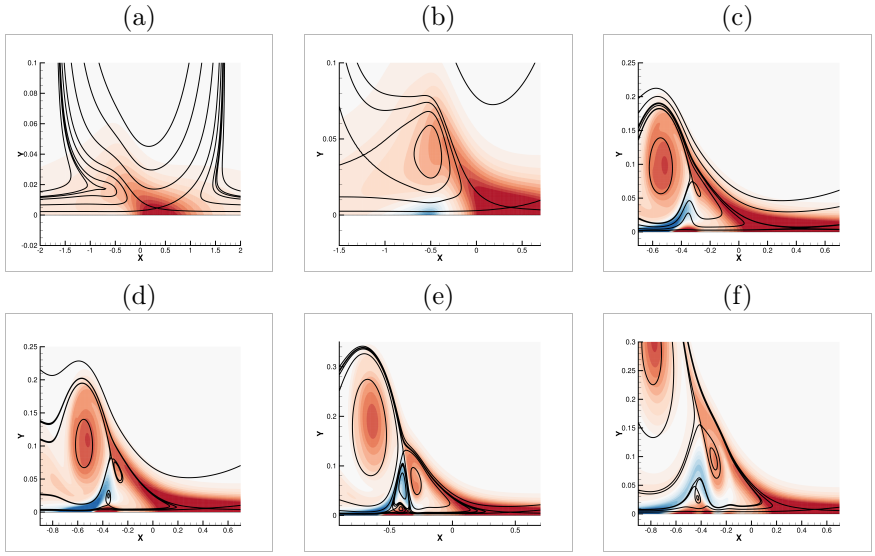

Figure 3.12: Re=10000, the patch system. (a) t=10, vorticity contours with values in $[-5; 5]$. (b) t=20, vorticity contours with values in $[-3; 3]$. (c) t=32, vorticity contours with values in $[-2; 2]$. (d) t=33, vorticity contours with values in $[-2; 2]$. (e) t=42, vorticity contours with values in $[-1.7; 1.7]$ (f) t=51, vorticity contours with values in $[-1.8; 1.8]$

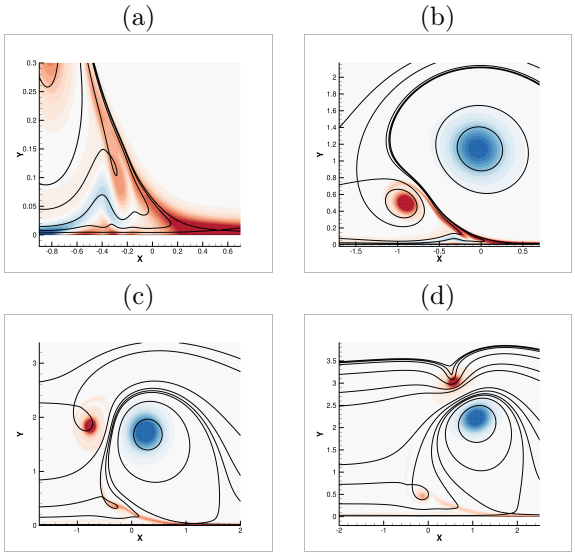

Figure 3.13: Re=10000, the patch system. (a) t=55, vorticity contours with values in $[-1.8; 1.8]$. (b) t=63, vorticity contours with values in $[-1; 1]$. (c) t=101, vorticity contours with values in $[-0.8; 0.8]$. (d) t=130, vorticity contours with values in $[-0.8; 0.8]$.

3.6 Topologies of ψ in the wall system

In the wall system the wall speed is zero and the generating vortex moves initially to the left, parallel to the wall. Since the difference between the wall system and the patch system is merely a constant, horisontal velocity component, the relation between the stream function in the patch system, ψ_p and the stream function in the wall system is simply

$$\psi_w = \psi_p + ky \tag{3.41}$$

where k is -0.02812 given by system parameters. The vorticity contours in this section is kept constant for a given Re. For $Re > 1000$ the contours are in the range -1 to 1 to ease comparison to Kudela & Malecha [64] who use this range. The streamline topologies in the wall system are described as the vorticity is unaltered by the transformation of the coordinate system.

The streamline center corresponding to the generating vortex is slightly shifted in the y direction depending on the sign of the circulation as shown in figure 3.14. This is due to vanishing v along the line parallel to the y axis for a 'perfect' rotational symmetric vortex. A vortex requires a region with both positive and negative u (in a frame moving with the vortex) and the generating vortex initially induces a velocity field from right to left below the vortex center. Of course in the case of a 'weak' vortex it may not be visible in both the patch system and the wall system. Hence, comparing the patch system to the wall system, the free stream has less absolute value in the patch system meaning that regions with positive u is more likely to occur which is needed for a vortex to exist. Therefore, one might expect to see more vortices close to the wall in the patch system than in the wall system. Above the generating vortex the main flow is in the opposite direction. Hence, here the wall system is the more favourable frame for critical points to exists. This is seen in simulation by e.g. comparing figure 3.9b to figure 3.18f.

At $Re = 200$ there are initially no vortices except the generating vortex - see figure 3.15. Then, a streamline vortex is created close to the wall encapsulated by a heteroclinic orbit from two no slip points on the wall. No saddle points are created contrary to the observation in the patch system. Increasing time the vortex disappears again. The same events happen for $Re = 500$ shown in figure 3.16 though also a new streamline vortex is created close to the wall after long time. This vortex is not predicted by the vorticity. At $Re = 1000$ exciting new behaviour reveals itself. First, a center close to the wall is created as seen for lower Re , as well. Then, a saddle- node bifurcation creates a new vortex center inside the preceding recirculation region. This means a 'figure 8' shape

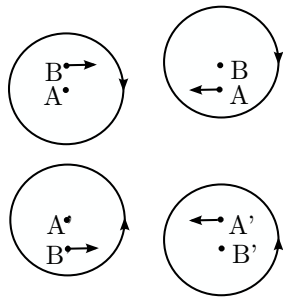

Figure 3.14: A small perturbation of a vortex in the streamline formulation. To the left is the patch system and to the right is the wall system. A and A' are critical points in the patch system and B and B' are critical points in the wall system.

appears in the streamlines encapsulated by a heteroclinic orbit connecting two points on the wall - see 3.16c. The heteroclinic orbit moves closer to the 'figure 8' shape and a bifurcation occurs where the saddle point is connected to two wall points through heteroclinic orbits. Then a new bifurcation occurs such that the heteroclinic orbit only encapsulates the lower center in the streamlines and the upper center and saddle now have no streamline connection to the wall - see 3.16c reproducing the findings in [64]. Then the detached saddle and center convects and rotates around the generating vortex (see figure 3.16d and 3.16e) which is accompanied by a slowdown of the horizontal motion of the generating vortex patch as well as a lift vertically is seen. This is a well known phenomena of aircraft trailing vortices approaching the ground [51]. The streamline center still detached to the wall vanish in 3.16e and a new center appears again in 3.16e. The 'figure 8' bifurcations can be interpreted as the indicator of eruption seen from the streamlines which was found by Kudela & Malecha [64]. The situation with a saddle point connected to the wall through two heteroclinic orbits encapsulating a center will be discussed in the analysis of normal forms.

At $Re = 4000$ and $Re = 5000$ similar behaviour is observed as seen in figure 3.18 and 3.19. At $Re = 10000$ the same characteristic 'figure 8' bifurcation is observed preceeded by an additional creation and elimination of a vortex close to the wall in 3.20c and 3.20d.

Comparing how well the streamlines predicts the vorticity behaviour there is better agreement in the patch system. More vortices are created in the patch system and they align well with extreme values of the vorticity. The streamline vortices in the wall system are only well aligned for vortices with positive circulation - see for example figure 3.20c where in the patch system

also vortices with negative circulation exist figure 3.12e. Also, in the lower center of the 'figure 8' in the wall system no extrema in the vorticity is visible close by. The benefit of the wall system relies on the topological mechanism of eruption through the' figure 8' bifurcation and the erupted vortex is also visible in the wall system. One may be tempted to model the interaction of the erupted vortex and the generating vortex patch by two counter rotating point vortices. For this idealization a saddle point exist on the line connecting the two point vortices. Hence, the 'figure 8' bifucation may be considered necessary for the creation of a saddle point that must exist for this idealisation. Notice, that for increasing time, the alignment of the saddle point and the two streamline centers get better aligned. We return to this discussion when we analyse the topology of the velocity field generated by two Gaussian vortices.

3.7 Conclusion on simulations

For small Re, numbers no new vortices are observed. In a large region on the wall vorticity of positive sign builds up and then a 'tongue' of vorticity may be drawn into the fluid without any vorticity extrema being observed off the wall. Creation of a vortex occurs for sufficiently large Re, whether the contours of ψ_w, ψ_p or vorticity are used as indicators. If streamline centers exist in both the wall system and the patch system there is a small, well understood shift in the direction vertical to the wall. The new vortex alters the generating vortex motion by slowing its horizontal motion and lifting it further from the wall. In the contours of ψ_w eruption happens through a characteristic 'figure 8' bifurcation. Considering ψ_p there is no topological change indicating when a vortex has left the boundary layer. For the vortices with short lifetime not leaving boundary layer there is remarkable good agreement between ψ_p and the vorticity contours while the wall system only seem to reproduce the vortices with positive circulation.

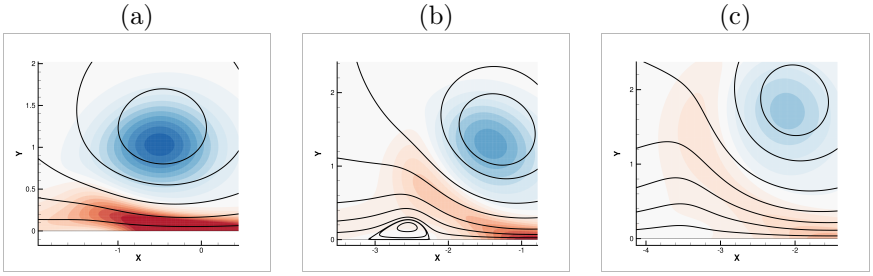

Figure 3.15: *Re*=200, the wall system. The vorticity contours are in the range -0.3 to 0.3. (a) t=18 (b) t=55 (c) t=105.

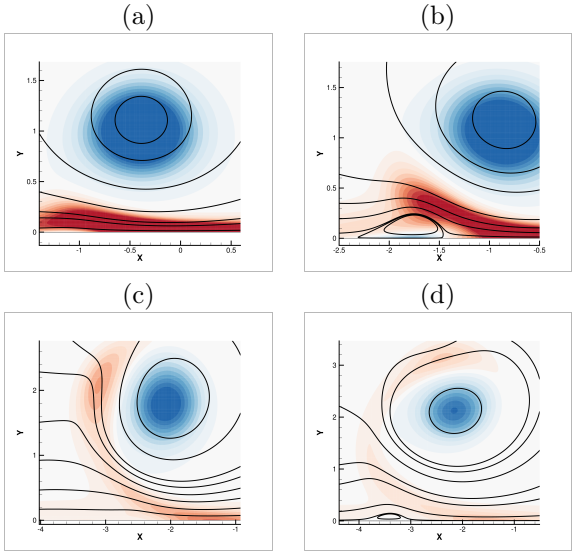

Figure 3.16: *Re*=500, the wall system. The vorticity contours are in the range -0.3 to 0.3. (a) t=14 (b) t=30 (c) t=92 (d) t=134.

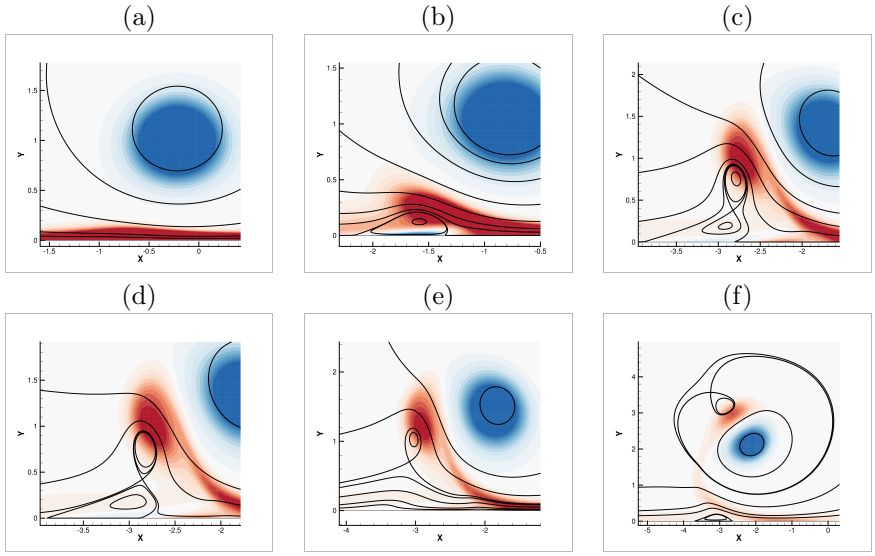

Figure 3.17: Re=1000, the wall system. (a) t=8, (b) t=28, (c) t=61, (d) t=62, (e) t=69, (f) t=115. The vorticity contours are in the range -0.3 to 0.3.

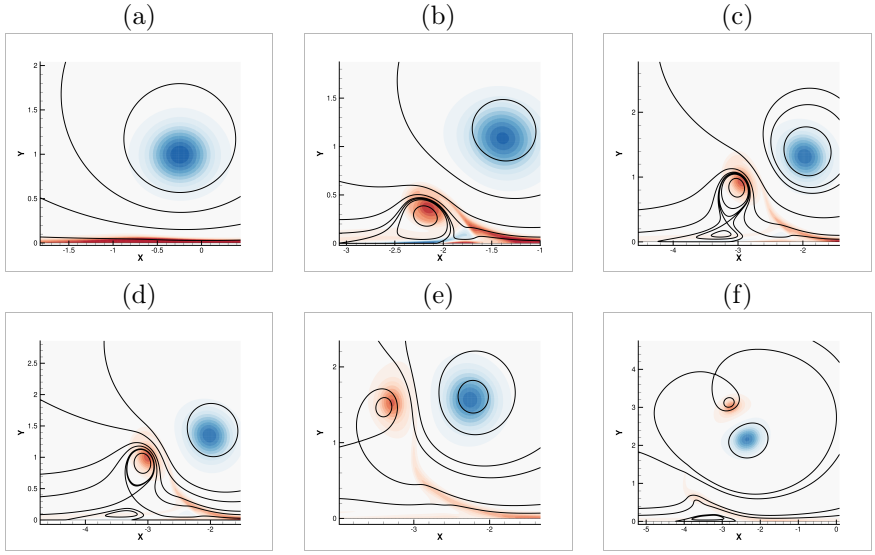

Figure 3.18: Re=4000, the wall system. (a) t=9, (b) t=48, (c) t=70, (d) t=72, (e) t=85, (f) t=122. Vorticity contours from -1 to 1.

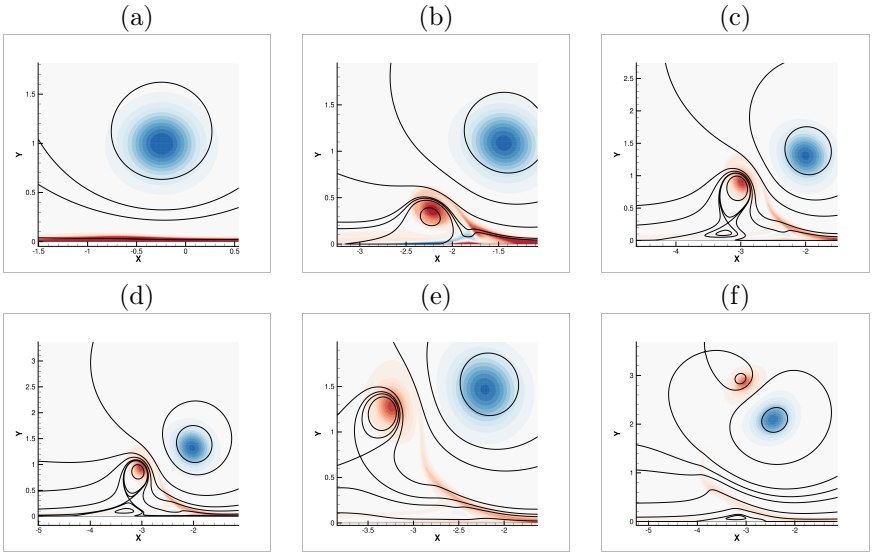

Figure 3.19: Re=5000, the wall system. (a) t=9, (b) t=50, (c) t=71, (d) t=72, (e) t=81, (f) t=118. Vorticity contours from -1 to 1.

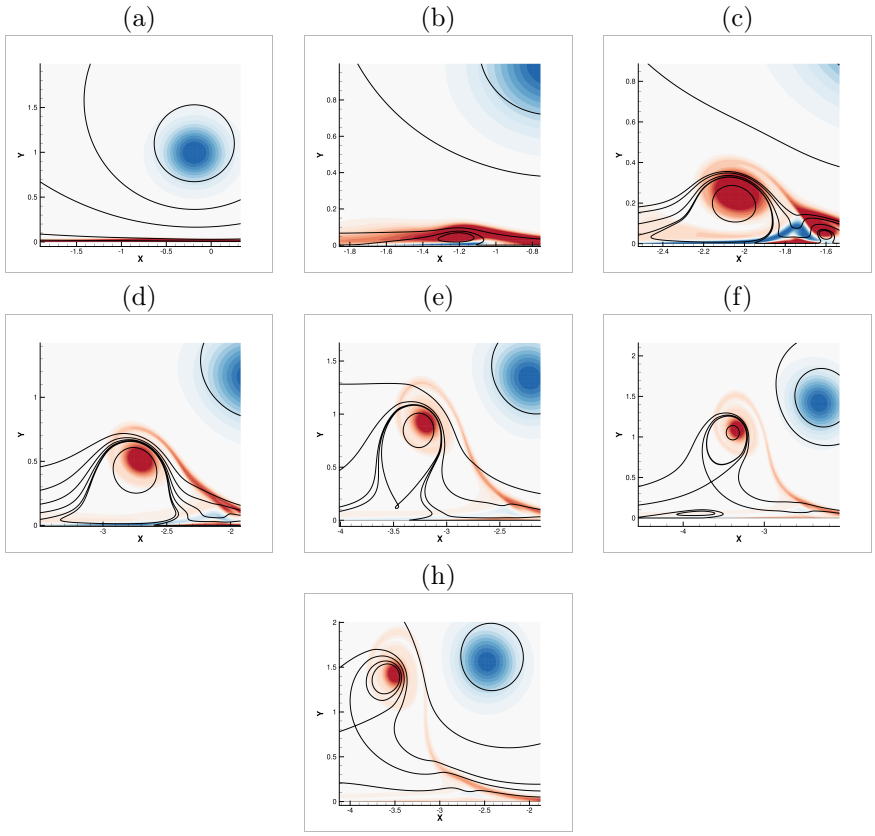

Figure 3.20: Re=10000, the wall system. (a) t=7, (b) t=25, (c) t=47, (d) t=64, (e) t=79, (f) t=84, (g) t=92. Vorticity contours from -1 to 1.

Chapter 4

Analytical approach to stream line and vorticity contour topology

Now the topology of the vorticity contours and streamlines are investigated from a purely theoretical approach using normal form theory.

Normal forms of the stream function have been investigated systematically in [17], [50], [49], [9] where a distinction is made between critical points on a wall and inflow critical points. We will start with constructing normal forms of the stream function where most are well known in literature. The well known examples surves to give an introduction to the methods but are also needed to understand the criteria when considering higher order normal forms. Later we consider normal forms of the vorticity and compare the possible topologies of the vorticity contours and streamlines.

The normal form of the stream function is constructed from a Taylor expansion at a critical point. Then the flow structure is investigated depending on the coefficients in the Taylor expansion. Typically some terms are assumed to be zero (degeneracy condition) and some are assumed non zero (non-degeneracy condition). An unfolding is performed where the degeneracy conditions are relaxed slightly by having small parameters instead of strictly zero. The unfolding

is then put in normal form respecting the boundary conditions. The unfolding leads to bifurcation diagrams with bifurcation parameters depending on the unfolding parameters.

When constructing normal forms nonlinear transformations of the original coefficients are performed in order to obtain fewer terms. The transformations leading to the normal form of the stream function may not lead to the simplest form of the vorticity. However, since we want to compare the vorticity and the stream function it is useful to have the simplest relations between the parameters describing the stream function and the vorticity. Therefore, we apply the same transformations to the vorticity that have been applied to the stream function.

The vorticity is given by minus the Laplacian of the streamfunction. Hence, some terms in the Taylor expansion of the stream function are irrelevant to the vorticity as they disappear by differentiation. Therefore, the level curves of the streamlines may have a more complicated unfolding than the corresponding vorticity unfolding. This supports that one should choose the transformations that simplify the streamfunction the most instead of those that simplify the vorticity the most. Fortunately, it is also these transformations that have already been constructed in [17].

We consider an incompressible, two dimensional flow with no slip boundary conditions. The vorticity is one dimensional and can be analysed by the same means as the stream function. Thus, a local analysis can be implemented identifying critical points and their type depending on certain degeneracy and non degeneracy conditions which are related to the coefficients of a Taylor expansion of the vorticity.

The constraints on the topologies are only due to the no slip wall and incompressibility - not the Navier - Stokes equation. One might expect that including the latter would induce further constraints on the possible topologies. However, [50] showed that for steady flow only in very few cases the Navier - Stokes equations induce further constraints. Thus, since we have simulated the Navier - Stokes equation for unsteady flow even fewer constraints are expected.

The stream function generates a dynamical system from $\frac{\partial \psi}{\partial y}$ and -$\frac{\partial \psi}{\partial x}$ which is related to the velocity field by $u = \frac{\partial \psi}{\partial y}$ and $v = -\frac{\partial \psi}{\partial y}$. Then, ψ is constant along streamlines. Similarly the vorticity generates a dynamical system from $\frac{\partial \omega}{\partial y}$ and -$\frac{\partial \omega}{\partial x}$ thus the methods of analysing the level curves of ψ can be transferred to analyse the vorticity.

The stream function is expanded in a power series so we assume smoothness of

the velocity field to a desired order.

$$\psi = \sum_{i,j=0}^{N} a_{i,j} x^i y^j + \mathcal{O}(2N+1)\,, \tag{4.1}$$

where we can assume $a_{0,0} = 0$ since we are only interested in the topology of the level curves. The streamlines are solutions to the equation

$$\begin{pmatrix} \frac{dx}{dt} \\ \frac{dy}{dt} \end{pmatrix} = \begin{pmatrix} \frac{\partial \psi}{\partial y} \\ -\frac{\partial \psi}{\partial x} \end{pmatrix} = \begin{pmatrix} a_{0,1} \\ -a_{1,0} \end{pmatrix} + \begin{pmatrix} a_{1,1} & 2a_{0,2} \\ -2a_{2,0} & -a_{1,1} \end{pmatrix} \begin{pmatrix} x \\ y \end{pmatrix} + \mathcal{O}(2)\,. \tag{4.2}$$

The streamline topology is affected by the presence of a wall which we assume to be flat. A fixed point at the wall forces a factor of y^2 in the stream function due to the no slip condition which is shown in the following section. The focus is on analytical criteria that can explain some of the observed behaviour in the simulations.

4.0.0.1 Bifurcation of flow away from boundaries

If $a_{1,0} = a_{0,1} = 0$ there is a critical point of the stream lines. If the determinant of the Jacobian $\sqrt{4a_{2,0}a_{0,2} - a_{1,1}^2}$ is nonzero, the Jacobian determines the type of critical point which can either be a saddle or center. In this case there is no information about $d_{0,1}$ or $d_{1,0}$ which is needed for the vorticity. The unfolding of the cusp will be shown now following Brøns [17]. This serves the purpose of showing how 'the method works' in a simple case. Also, since saddles and centers are created and destroyed repeatedly in the streamlines in the patch system it is relevant to know how this connect to theory.

Equation (4.2) is considered assuming $a_{1,0} = a_{0,1} = 0$ to ensure existence of a critical point. The simple linear degeneracy is considered where the Jacobian matrix has two zero eigenvalues but the geometric multiplicity is one. When put in Jordan normal form this means the Jacobian is not the zero matrix but has one off-diagonal entry that is non-zero. Therefore, we assume the degeneracy conditions

$$a_{1,0} = a_{0,1} = a_{1,1} = a_{2,0} = 0\,, \tag{4.3}$$

and the non degeneracy conditions

$$a_{0,2} \neq 0\,, \tag{4.4}$$

This leaves one quadratic term of ψ so it is natural to wonder how the cubic terms affect the topological structure of the streamlines.

$$\psi = a_{0,2}\eta^2 + a_{3,0}\xi^3 + a_{2,1}\xi^2\eta + a_{1,2}\xi\eta^2 + a_{0,3}\eta^3 + \mathcal{O}(4)\,. \tag{4.5}$$

A near -identity quadratic transformation, $(x, y) \to (\xi, \eta)$ is used to simplify the cubic terms as much as possible. A near - identity transformation is characterised by being the identity to first order.

$$x = \xi + r_{2,0}\xi^2 + r_{1,1}\xi\eta + r_{0,2}\eta^2 \tag{4.6a}$$
$$y = \eta + s_{2,0}\xi^2 + s_{1,1}\xi\eta + s_{0,2}\eta^2\,, \tag{4.6b}$$

where $s_{i,j}$ and $r_{i,j}$ are constants to be chosen in a useful way later. Since the determinant of the Jacobian of equation (4.6) is one at the origin, the equation defines a coordinate transformation locally close to the origin. Equation (4.6) is plugged into equation (4.2) and terms of same order are collected

$$\begin{aligned}\psi =& a_{0,2}\eta^2 + a_{3,0}\xi^3 + (2a_{0,2}s_{2,0} + a_{2,1})\,\xi^2\eta + (2a_{0,2}s_{1,1} + a_{1,2})\,\xi\eta^2 \\ &+ (2a_{0,2}s_{0,2} + a_{0,3})\,\eta^3 + \mathcal{O}(4)\,.\end{aligned} \tag{4.7}$$

Since $a_{0,2}$ is assumed to be non zero, only one third order term of ψ is left for the following choice of the coefficients that can be freely chosen

$$s_{2,0} = -\frac{1}{2}\frac{a_{2,1}}{a_{0,2}}\,, \quad s_{1,1} = -\frac{1}{2}\frac{a_{1,2}}{a_{0,2}}\,, \quad s_{0,2} = -\frac{1}{2}\frac{a_{2,1}}{a_{0,2}}\,. \tag{4.8}$$

Then, the stream function is

$$\psi = a_{0,2}\eta^2 + a_{3,0}\xi^3 + \mathcal{O}(4)\,. \tag{4.9}$$

The coefficients $r_{i,j}$ can be set to zero since no other choice facilitate the analysis further. If $a_{3,0} = 0$ one can use a near identity cubic transformation to facilitate the fourth order terms thus sketching a general method. However, we will assume $a_{3,0} \neq 0$ for simplicity. Then, equation (4.9) can be made a little prettier dividing ψ by $2a_{0,2}$ and letting $\xi \to \left(\frac{2a_{0,2}}{3a_{3,0}}\right)^{\frac{1}{3}} \xi$

$$\psi = \frac{1}{2}\eta^2 + \frac{1}{3}\xi^3 + \mathcal{O}(4)\,. \tag{4.10}$$

The truncated normal form is analysed by skipping the terms of fourth or higher order. Notice this is even in η so a reflection symmetry exists. There is one critical point located at $(0, 0)$. Here the determinant of the Hessian vanishes so this does not help to classify the critical point. The stream function is zero at

the origin so any separatrix connected to the critical point must lie on the level curve $\psi = 0$. Renaming the variables back to x and y this happens for

$$y = \pm\sqrt{-\frac{2}{3}x^3}\,, \tag{4.11}$$

which is a *cusp* that can be seen in figure 4.1b.

Unfolding of the cusp

What is then the structure when the degeneracy conditions are replaced by small parameters instead of exactly zero? This is now investigated and is the unfolding part. Therefore, we now have four small unfolding parameters, ϵ_i

$$\epsilon_1 = a_{1,0}\,, \quad \epsilon_2 = a_{0,1}\,, \quad \epsilon_3 = a_{2,0}\,, \quad \epsilon_4 = a_{1,1}\,. \tag{4.12}$$

and the non degeneracy conditions

$$a_{0,2} \neq 0\,, \quad a_{3,0} \neq 0\,, \tag{4.13}$$

leading to ψ on the form

$$\psi = \epsilon_1\xi + \epsilon_2\eta + \epsilon_3\xi^2 + \epsilon_4\xi\eta + a_{0,2}\eta^2 + a_{3,0}\xi^3 + a_{2,1}\xi^2\eta + a_{1,2}\xi\eta^2 + a_{0,3}\eta^3 + \mathcal{O}(4)\,, \tag{4.14}$$

Analysing the problem now may seem much more terrifying with four small parameters. However, a strength of the topological approach using normal forms is that this number can be significantly reduced. Once again a near identity transformation is used - this time with more terms treating the unfolding parameters as variables. Since we got away with just the identity transformation for x in the degenerate case we will try this again to reduce the algebraic work leading to the near identity transformations $x = \xi$ and

$$\begin{aligned} y =& \eta + s_{0,2}\xi^2 + s_{1,1}\xi\eta + s_{0,2}\eta^2 + (s_{1,0,1}\epsilon_1 + s_{1,0,2}\epsilon_2 + s_{1,0,3}\epsilon_3 \\ &+ s_{1,0,4}\epsilon_4)\,\xi + (s_{0,1,1}\epsilon_1 + s_{0,1,2}\epsilon_2 + s_{0,1,3}\epsilon_3 + s_{0,1,4}\epsilon_4)\,\eta\,, \end{aligned} \tag{4.15}$$

where $s_{i,j}$ and $s_{i,j,k}$ are constants to be chosen wisely. Once again the idea is to insert this in the expression for ψ and collect terms of same order to see if some

of the 'free' coefficients can be chosen in a way to simplify ψ. This results in a lenghty expression. However, since the ϵ's are allowed to take any small value, they can specifically take the value zero leading to the choice of $s_{0,2}$, $s_{1,1}$, $s_{0,2}$ that was also used in the degenerate case i.e. equation (4.8). Many of the terms introduced by the transformation equation (4.15) do not help in simplifying the original problem and hence the corresponding coefficients are set to zero. There are three coefficients that can be chosen in a way that simplifies the original problem since the following terms are found in ψ

$$\left(2a_{2,0}s_{1,0,2} - \frac{1}{2}\frac{a_{1,2}}{a_{a_0,2}}\right)\xi\eta\epsilon_2\,,\ (1+2a_{0,2}s_{1,0,4})\,\xi\eta\epsilon_4\,,\ \left(2a_{0,2}s_{0,1,2} - \frac{1}{2}\frac{a_{0,3}}{a_{0,2}}\right)\eta^2\epsilon_2\,. \tag{4.16}$$

which leads to the following choice

$$s_{1,0,2} = \frac{a_{1,2}}{4a_{0,2}^2}\,, \quad s_{1,0,4} = -\frac{1}{2a_{0,2}} \quad s_{0,1,2} = \frac{a_{0,3}}{4a_{0,2}^2}\,. \tag{4.17}$$

This leads to the stream function om the form

$$\psi = \mu_1\xi + \mu_2\eta + \mu_3\xi^2 + a_{0,2}\eta^2 + a_{3,0}\xi^3 + \mathcal{O}(4)\,, \tag{4.18}$$

where $\mathcal{O}(4)$ is fourth order in ξ, η, and ϵ_i and the μ_i are small parameters defined by

$$\mu_1 = \epsilon_1 + \frac{a_{1,2}}{4a_{0,2}^2}\epsilon_2^2 - \frac{1}{2a_{0,2}}\epsilon_2\epsilon_4 \tag{4.19a}$$

$$\mu_2 = \epsilon_2 + \frac{a_{0,3}}{4a_{0,2}^2}\epsilon_2^2 \tag{4.19b}$$

$$\mu_3 = \epsilon_3 - \frac{a_{2,1}}{2a_{0,2}}\epsilon_2\,. \tag{4.19c}$$

Now, the number of parameters has been reduced to three. Additional two can be removed by a coordinate translation along the existing coordinate axis. This freedom allows one to remove the term with second highest degree in a univariate polynomial. The shift from ξ to $\tilde{\xi}$ is given by $\xi = \tilde{\xi} + \xi_0$ with

$$\xi_0 = -\frac{\mu_3}{3a_{3,0}} \tag{4.20}$$

the ξ^2 term is removed and shifting η to $\tilde{\eta}$ by $\eta = \tilde{\eta} + \eta_0$ with

$$\eta_0 = -\frac{\mu_2}{2a_{0,2}} \tag{4.21}$$

the η - term is removed. Notice that the shifts are small for small value of the unfolding parameters hence the local analysis is still applicable for (ξ, η) close to $(0, 0)$. These shifts along the coordinate axis introduce a constant term in the stream function. Since we are only interested in the level curves the value of the constant is unimportant and hence it is omitted (though we still denote the stream function by the same letter, ψ which will often be the case). Skipping the newly invented tilde for aesthetics

$$\psi = \left(\mu_1 - \frac{\mu_3^2}{3a_{3,0}}\right)\xi + a_{2,0}\eta^2 + a_{3,0}\xi^3 + \mathcal{O}(4)\,. \tag{4.22}$$

Finally, we use the freedom in scaling ψ and ξ to get nicer coefficients on η^2 and ξ^3. This is done by dividing ψ with $2a_{0,2}$ and $\xi \to \left(\frac{2a_{0,2}}{3a_{3,0}}\right)^{\frac{1}{3}}\xi$ resulting in the final, neat form of the stream function

$$\psi = c_1\xi + \frac{1}{2}\eta^2 + \frac{1}{3}\xi^3 + \mathcal{O}(4)\,, \tag{4.23}$$

with the bifurcation parameter c_1 being

$$c_1 = \left(\mu_1 - \frac{\mu_3^2}{3a_{3,0}}\right)\left(12a_{0,2}^2 a_{3,0}\right)^{-\frac{1}{3}}\,. \tag{4.24}$$

Only topology preserving transformations have been used from equation (4.14) to equation (4.23) but the latter appears simpler. Notice that changing any of the initial unfolding parameters ϵ_i while fixing the rest causes a change in c_1.

Skipping the terms of fourth order or higher the *truncated normal form* is left. It is easily analysed and for convenience we label (ξ, η) by (x, y).

$$\psi_{trunc} = c_1 x + \frac{1}{2}y^2 + \frac{1}{3}x^3\,. \tag{4.25}$$

Since y only appears squared, the expression is even in y and hence there is a reflectional symmetry in the line $y = 0$. For $c_1 = 0$ the cusp from equation (4.11) reappears. The critical points is determined by vanishing first derivatives giving

$$0 = c_1 + x^2 \tag{4.26a}$$

$$0 = y \tag{4.26b}$$

Hence, all critical points are on the y- axis and there are two critical points for $c_1 < 0$ and none for $c_1 > 0$. The determinant of Hessian of the truncated stream function is $2x$. Hence, in case of two critical points one has negative x-value meaning it is a saddle point and the critical point with negative x-value is a center. The different cases are shown in figure 4.1.

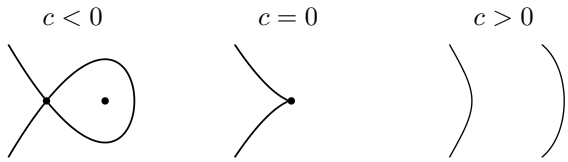

Figure 4.1: Left: Two critical points - a saddle and a center. Middle: One critical point - a cusp. Right: No critical points

4.1 Including investigation of the vorticity

The critical points of the vorticity fulfils

$$\frac{\partial \omega}{\partial x} = 0 \quad \text{and} \quad \frac{\partial \omega}{\partial y} = 0\,, \tag{4.27}$$

which using

$$\omega = -\nabla^2 \psi \tag{4.28}$$

yields

$$-\left(\frac{\partial^3 \psi}{\partial x^3} + \frac{\partial^3 \psi}{\partial x \partial y^2}\right) = 0 \quad \text{and} \quad -\left(\frac{\partial^3 \psi}{\partial y \partial x^2} + \frac{\partial^3 \psi}{\partial y^3}\right) = 0\,. \tag{4.29}$$

This means ψ should be of at least fourth order in x or y to cause bifurcations in ω which excludes interesting behaviour of ω for the simplest bifurcations in ψ.

The vorticity can be expanded in a power series at the same point as ψ

$$\omega = \sum_{i,j=0}^{N} d_{i,j} x^i y^j + \mathcal{O}(2N+1)\,. \tag{4.30}$$

From equation (4.28) the relation between $a_{i,j}$ and $d_{i,j}$ is

$$d_{i,j} = -\left((i+2)\,(i+1)\,a_{i+2,j} + (j+2)\,(j+1)\,a_{i,j+2}\right)\,. \tag{4.31}$$

Some of the lowest order coefficients of the vorticity are given in terms of the coefficients of the stream function in table 4.1. Notice that $a_{i+2,j+2}$ appears in exactly two d's namely $d_{i+2,j}$ and $d_{i,j+2}$.

$d_{0,0}$	$= -2\,(a_{2,0} + a_{0,2})$
$d_{1,0}$	$= -2\,(a_{1,2} + 3a_{3,0})$
$d_{0,1}$	$= -2\,(a_{2,1} + 3a_{0,3})$
$d_{2,0}$	$= -2\,(6a_{4,0} + a_{2,2})$
$d_{0,2}$	$= -2\,(6a_{0,4} + a_{2,2})$
$d_{1,1}$	$= -6\,(a_{3,1} + a_{1,3})$

Table 4.1: Some of the coefficients of the vorticity expressed from the coefficients of the stream function when no further constraints apply

4.1.1 Topologies near a no slip wall

We may Taylor expand the stream function locally at any point in the fluid. Specifically this can be done on a no - slip boundary. This has an impact on the stream function since the velocity field and the stream function are related. The vanishing flow speed on a no - slip wall means that all points on the wall are critical points of the stream function. Some wall points may have a streamline connected to points off the wall. If so it is either a point of attachment or separation depending on the flow direction.

Assuming there is a flat wall at $y = 0$ with fluid in the domain $y \geq 0$ then the no flux condition implies

$$v(x,0) = 0 \quad \Leftrightarrow \quad -\frac{\partial \psi(x,0)}{\partial x} = 0\,, \tag{4.32}$$

which means $\psi(x,0)$ is constant which is chosen to be zero. Taylor expanding at any point on the wall requires equation (4.32) as well as higher order derivatives of x which all vanish. Therefore, only terms with a y derivative survives. Hence, we can write the stream function as a product of a nonsingular $\tilde{\psi}$ and y

$$\psi = y\tilde{\psi} \tag{4.33}$$

Considering the velocity component tangential to the wall

$$u(x,0) = -\frac{\partial \psi(x,0)}{\partial y} = \tilde{\psi}(x,0) + 0\frac{\partial \tilde{\psi}}{\partial y} = \tilde{\psi}(x,0)\,. \tag{4.34}$$

Then, the no slip condition $u(x,0) = 0$ means that y is also a factor in the Taylor expansion of $\tilde{\psi}$. Therefore,

$$\psi = y^2\hat{\psi}\,. \tag{4.35}$$

The velocity field, $u = \frac{\partial \psi}{\partial y}$, $v = -\frac{\partial \psi}{\partial x}$ can then be written as

$$\frac{dx}{dt} = 2y\hat{\psi} + y^2 \frac{\partial \hat{\psi}}{\partial y} \tag{4.36a}$$

$$\frac{dy}{dt} = -y^2 \frac{\partial \hat{\psi}}{\partial x}\,. \tag{4.36b}$$

A common factor of y can be removed by scaling time by y using $s = ty$ with s being the scaled time variable.

$$\frac{dx}{ds} = 2\hat{\psi} + y \frac{\partial \hat{\psi}}{\partial y} \tag{4.37a}$$

$$\frac{dy}{ds} = -y \frac{\partial \hat{\psi}}{\partial x}\,. \tag{4.37b}$$

The streamlines off the wall are identical for equation (4.36) and equation (4.37) - only the speed along a streamline has changed. Any separatrix connected to the wall can then also be found in equation (4.37). While the velocity components (u, v) are given exactly by equation (4.36) we may sometimes denote equation (4.37) by $(\tilde{u}, \tilde{v})$ - the velocity field scaled by y. Even though the scaling is not defined at $y = 0$ there is no singular behaviour in equation (4.37) at $y = 0$. Hence, we may look for critical points on the wall in this system as well (the no-slip critical points) and since this affects the behaviour of the fluid close to the wall, a critical point on the wall in equation (4.37) has implications for the system equation (4.36). Since the flow is incompressible the trace of the Jacobian of the velocity field vanishes. This holds in general and specifically for equation (4.36). However, this does not hold for equation (4.37) that has trace $-\frac{\partial}{\partial x}\hat{\psi}$. This does not open for more types of critical points at points off the wall since here $-\frac{\partial}{\partial x}\hat{\psi}$ vanishes. Since the eigenvalues of a 2x2 matrix are determined by the trace and determinant, the first test for the type of a critical point is to investigate the sign of the determinant of the Jacobian of equation (4.37). Since the two systems equation (4.36) and equation (4.37) are topologically equivalent at in flow points it is not surprising that the type of critical in flow point is determined from the same number of conditions.

Since the eigenvalues are determined from the formula

$$\lambda_{\pm} = \frac{1}{2}\left(\mathrm{tr}J \pm \sqrt{(\mathrm{tr}J)^2 - 4\det J}\right) \tag{4.38}$$

then $\det J < 0$ at a critical point guarantees a positive and a negative λ and hence is sufficient for determining a saddle point for on wall critical points of equation (4.37). Since there has to be a critical point at $y = 0$ in equation (4.37) at an attachment point or separation point this characterised by $\hat{\psi}(x, 0) = 0$.

$d_{0,0}$	$= -2a_{0,2}$
$d_{1,0}$	$= -2a_{1,2}$
$d_{0,1}$	$= -6a_{0,3}$
$d_{2,0}$	$= -2a_{2,2}$
$d_{0,2}$	$= -2\left(6a_{0,4} + a_{2,2}\right)$
$d_{1,1}$	$= -6a_{1,3}$

Table 4.2: Some of the coefficients of the vorticity expressed from the coefficients of the stream function at a point on the wall.

Using $\omega = -\Delta\psi$ we get

$$\omega = -\left(y^2\frac{\partial^2\hat{\psi}}{\partial x^2} + 2\hat{\psi} + 2y\frac{\partial\hat{\psi}}{\partial y} + y^2\frac{\partial^2\hat{\psi}}{\partial y^2}\right). \tag{4.39}$$

Thus, $\omega(x,0) = \hat{\psi}(x,0)$ which means that a separatrix from the flow to the wall is at a point of vanishing vorticity.

An equivalent formulation of Prandtl's separation criterion discussed in section 3.1 is to consider the stream function close to a wall. Due to the no slip condition, y^2 is a factor in the stream function. Demanding $\frac{\partial u(x,0)}{\partial y} = 0$ ensures a critical point on the wall with a separatrix entering the flow (along with the non degeneracy condition $\frac{\partial^2 u}{\partial x \partial y} \neq 0$).

Since the lowest order terms of the stream function near a wall are of order two, there are fewer degeneracy conditions to be met to see interesting behaviour in the vorticity than for an inflow point. Also, the bifurcation diagram of Hartnack [50] for the non simple on wall degeneracy shows resemblance to the 'pinch off' observed in the wall system dynamics. Therefore, the normal forms close to the wall will be considered more thoroughly than the in flow counter parts.

Due to the factor y^2 in the streamfunction close to a wall $a_{i,j}$ vanishes for $j < 2$ which affects the $d_{i,j}$'s as seen in table 4.2.

The vorticity is then

$$\omega = d_{0,0} + d_{1,0}x + d_{0,1}y + d_{1,1}xy + d_{2,0}x^2 + d_{0,2}y^2 + O(||(x,y)||^3), \tag{4.40}$$

with the $d_{i,j}$'s given by table 4.2. It is clear that the $d_{i,j}$'s from table 4.2 form a linear independent set.

4.1.2 Simplifying expressions for the vorticity

So far we have considered various conditions for the stream function and related this to the vorticity. Now we consider the simplest case of a critical point of the vorticity and relates this to the parameters of the stream function.

The critical points of the vorticity fulfils equation (4.27). Then, a critical point at the origin requires

$$d_{1,0} = d_{0,1} = 0\,. \tag{4.41}$$

This can be formulated in terms of the coefficients of the stream function using table 4.1 or table 4.2. Thus, a critical point of the vorticity requires

$$a_{1,2} + 3a_{3,0} = a_{2,1} + 3a_{0,3} = 0\,, \tag{4.42}$$

which near a wall reduce to

$$a_{1,2} = a_{0,3} = 0\,. \tag{4.43}$$

The type of critical point can often be found from the Hessian.

$$H_\omega(0,0) = \begin{pmatrix} 2d_{2,0} & d_{1,1} \\ d_{1,1} & 2d_{0,2} \end{pmatrix}\,, \tag{4.44}$$

with determinant

$$|H_\omega(0,0)| = 4d_{0,2}d_{2,0} - d_{1,1}^2\,. \tag{4.45}$$

If a critical point exists at $(0,0)$ then if $|H_\omega(0,0)| < 0$ then $(0,0)$ is a saddle. If $|H_\omega(0,0)| > 0$ then $(0,0)$ is a local maximum or a local minimum.

Otherwise higher order terms are needed to determine the type of critical point. The simplest way to get vortex defined as an extremum of vorticity is then by having $0 = d_{0,1} = d_{1,0}$, $|H_\omega(0,0)| \neq 0$. This translates to criteria of the coefficients of the stream function by using table 4.1 or table 4.2. In order to observe the mathematically simplest vortex in the streamlines similar criteria apply with a's substituting d's. However, in this case there is no 'overlap' between the coefficients determining the streamline center and the vorticity center, thus quite many conditions have to be simultaneously fulfilled. Nevertheless in the patch system there are parameter regions where we see a rather good agreement between vortices defined in the streamline and vorticity formulation.

4.1.2.1 Topology of the vorticity near a wall

If $d_{0,1} = \epsilon_1$ or $d_{1,0} = \epsilon_2$ are small but not necessarily zero, we may include terms of second order to find critical points. Then, the criteria for critical points is

$$H_\omega(0,0) \begin{pmatrix} x \\ y \end{pmatrix} = - \begin{pmatrix} \epsilon_1 \\ \epsilon_2 \end{pmatrix} . \tag{4.46}$$

Notice that a critical point of ω is close to $(0,0)$ since the ϵ's are small. Assuming $H_\omega(0,0)$ is invertible the y - coordinate of equation (4.46) is then

$$y = \frac{1}{|H_\omega(0,0)|} \left(d_{1,1}\epsilon_1 - 2d_{2,0}\epsilon_2 \right) . \tag{4.47}$$

If this changes sign as the ϵ's are varied a critical point of ω emerges close to the wall. Since $\epsilon_1 = d_{0,1} = -6a_{0,3}$ the unfolding happens close to $a_{0,3} = 0$. However, when analysing the streamline topology close to a wall, $a_{0,3} \neq 0$ is the criteria for a nonzero Jacobian i.e. a simple linear degeneracy which is needed in theorem 6 and 7 by Brøns [17]. Thus, we have to consider a non simple degeneracy of the streamline topology to consider bifurcations in the streamlines for the same parameters where bifurcations in the vorticity is observed. A simple linear degeneracy in the stream function near a wall then means there is no critical point of the vorticity.

4.2 Comparison of the streamline topologies in the patch system and the wall system

Since two stream functions are used in the simulations it is relevant to study analytically how structures in the streamlines of the two systems are related.

The wall system is connected to the patch system by adding a constant velocity in the x - direction. Denoting the velocity in the patch system by (u_p, v_p) and the velocity in the wall system by (u_w, v_w) then $v_w = v_p$ and

$$u_w = u_p + C . \tag{4.48}$$

Using the stream function this means

$$\frac{\partial \psi_w}{\partial y} = \frac{\partial \psi_p}{\partial y} + C \quad \Rightarrow \psi_w = \psi_p + Cy . \tag{4.49}$$

C may be considered small in the simulations. We may therefore consider the normal forms of ψ_w and perturb the $a_{0,1}$ term in order to analyse ψ_p. Therefore, the analysis of ψ_p may be considered an unfolding of ψ_w. The wall velocity is now nonzero and therefore there are no longer critical points along the entire wall.

First, the least degenerate case is considered. From $(u_p, v_p) = (\partial_y \psi_p, -\partial_x \psi_p)$ a Taylor expansion is made for small wall speed

$$\begin{pmatrix} u_p \\ v_p \end{pmatrix} = \begin{pmatrix} -C \\ 0 \end{pmatrix} + \begin{pmatrix} 2a_{0,2} \\ 0 \end{pmatrix} y + y \begin{pmatrix} 2a_{1,2} & 3a_{0,3} \\ 0 & -a_{1,2} \end{pmatrix} \begin{pmatrix} x \\ y \end{pmatrix} + O(3) \quad (4.50)$$

In the case of vanishing wall speed $C = 0$, a factor y is present in all terms and hence the system can be scaled by y resulting in the condition of a critical point at (0,0) as $a_{0,2} = 0$. Then the type of critical point is determined by the 2 by 2 matrix in equation (4.50) which is non singular for $a_{1,2} \neq 0$. This means the matrix has real eigenvalues, one positive and one negative and hence the critical point is a saddle. Therefore, a non degenerate critical wall point is a saddle point. Still keeping $C = 0$ and using $a_{0,2}$ as unfolding parameter merely causes the critical point to move slightly along the wall keeping the type for $a_{1,2} \neq 0$. Allowing C as a small parameter the condition for a critical point is then

$$-C + 2a_{0,2}y = 0\,, \quad (4.51)$$

which is solvable for $a_{0,2} \neq 0$. However, we want $C, a_{0,2}$ and y to all be small and still equation (4.51) to be fulfilled. This is possible if C is not independent on the first unfolding parameter $a_{0,2}$ but instead

$$C = k a_{0,2}^2\,, \quad (4.52)$$

for some constant k. Keeping in mind this constraint, a critical point then has to fulfill

$$y = \frac{1}{2} k a_{0,2}. \quad (4.53)$$

This has to be a positive number for a critical point to exist since there is only flow above the wall. In case the critical point is within the physical domain it is a saddle, still implied by non zero $a_{1,2}$ in the higher order term Hence, changing the wall speed slightly from zero may either move the saddle point off the wall and into the fluid or remove the critical point completely.

This is observed e.g. initially for the generating vortex patch. In the wall system there are two attachment points of the streamlines one on either side of the vortex. In the patch system there is a saddle point slightly above the wall to

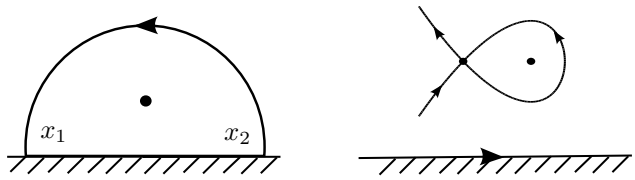

Figure 4.2: A center in the wall system (left) and in the patch system (right)

right of the vortex center. Also the later response in the boundary layer show this behaviour when comparing the patch system and the wall system.

A heuristic explanation is also given by considering figure 4.2. In the wall system there is a center and two critical points on the wall connected by a heteroclinic orbit through the flow confining a region where closed streamlines exist and a critical point of center type. Considering figure 4.2(a) the critical point on the no slip wall at x_1 is characterised by the flow streaming to the left just above the wall i.e. $\frac{\partial u(x_1,0)}{\partial y} < 0$. Adding a small, constant positive velocity u_0 removes critical points on the wall as seen in figure 4.2(b) - the patch system. However, since $\frac{\partial u(x_1,0)}{\partial y} < 0$ still applies this means $u(x_1, y)$ increases from positive to negative value thus passing through zero. At x_2 where the flow in the wall system is an attachment point the effect of going to the patch system is to 'lift' off the saddle point into the fluid. At the detachment point x_2 in the wall system, there is also created an inflow point with vanishing u in the patch system but here the v component is positive so a 'turning point' of the streamline is observed where the streamline has vertical tangent. The center in the wall system is not a center in the patch system. Close to the center, strictly above and below it the flow is tangential to the wall. Hence, adding a small constant velocity moves the center slightly in the vertical direction. In case of clockwise rotating vortex the y- value is increased when going to the patch system by adding a positive, constant velocity.

4.2.0.2 Unfolding of a simple degenerate critical point on the wall with wall speed as unfolding parameter

The unfolding of the simple degenerate critical point where the wall is stationary leads to the simplest bifurcation where a center is created on the wall and then can be 'lifted' into the fluid as the bifurcation parameter is varied. We now perform the unfolding where also the wall speed is an unfolding parameter to see how a vortex generated on the wall in the patch system may appear in the patch system. To ease the understanding we start by analysing the wall system and

proceed to the full unfolding corresponding to the patch system As previously shown the stream function has a factor of y^2 in every term for a point on a stationary no slip wall leading to the velocity field

$$\begin{pmatrix} \frac{\partial \psi}{\partial y} \\ -\frac{\partial \psi}{\partial x} \end{pmatrix} = y \left(\begin{pmatrix} 2a_{0,2} \\ 0 \end{pmatrix} + \begin{pmatrix} 2a_{1,2} & 3a_{0,3} \\ 0 & -a_{1,2} \end{pmatrix} \begin{pmatrix} x \\ y \end{pmatrix} \right) + \mathcal{O}(3) \tag{4.54}$$

It is clear that all wall points are critical points. Scaling time by y does not change the streamlines off the wall, only the speed along each streamline. Therefore an inflow separatrix connected to a wall point in equation (4.54) must correspond to a critical point with the same separatrix in the following times-scaled system

$$\begin{pmatrix} \frac{\partial \psi}{\partial y} \\ -\frac{\partial \psi}{\partial x} \end{pmatrix} = \begin{pmatrix} 2a_{0,2} \\ 0 \end{pmatrix} + \begin{pmatrix} 2a_{1,2} & 3a_{0,3} \\ 0 & -a_{1,2} \end{pmatrix} \begin{pmatrix} x \\ y \end{pmatrix} + \mathcal{O}(2) \tag{4.55}$$

A critical point on the wall of equation (4.55) occurs for $a_{0,2} = 0$. Then, assuming $a_{1,2} \neq 0$ it is immediately clear from the linear term in equation (4.55) that the critical point is a saddle. The eigenvalue $2a_{1,2}$ has eigenvector along the wall and the eigenvector $-2a_{1,2}$ has eigenvector in the direction $(a_{0,3}, a_{1,2})$ which is the tangent of the inflow separatrix connected to the critical point. Hence, if $a_{1,2} < 0$ the critical point is a separation point and if $a_{1,2} > 0$ it is an attachment point. From table 4.2 it is clear that for $a_{1,2} \neq 0$ there is no critical point in the vorticity since $d_{1,0}$ has to vanish.

4.2.0.3 Simple, linear degeneracy on the wall

If $a_{1,2} = 0$ higher order terms have to be taken into consideration. We assume $a_{3,0} \neq 0$ which means we consider the simple linear degeneracy since the Jacobian has zero as double eigenvalue, but the geometric multiplicity is one. Since $a_{3,0}$ has to vanish for a critical point in the vorticity (see table 4.2). However, we include the analysis since it is a useful for the comparison between the patch system and the wall system. The stream function now has the form

$$\psi = y^2 \left(a_{0,3} y + a_{2,2} x^2 + a_{1,3} xy + a_{0,4} y^2 + \mathcal{O}(3) \right) . \tag{4.56}$$

As for the in flow we try with the identity transformation in x. For the y transformation it is important to keep track of the wall. By using the transformation

$$x = \xi \tag{4.57a}$$

$$y = \eta + s_{1,1} \xi \eta + s_{0,2} \eta^2 \tag{4.57b}$$

the wall is mapped from $y = 0$ to $\eta = 0$ where as usually $s_{1,1}$ and $s_{0,2}$ are constants to be determined conveniently shortly. Equation (4.57) is inserted in the stream function equation (4.56).

$$\psi = \eta^2 \left(a_{0,3}\eta + a_{2,2}\xi^2 + (3s_{1,1}a_{0,3} + a_{1,3})\,\xi\eta + (3s_{0,2}a_{0,3} + a_{0,4})\,\eta^2 + \mathcal{O}(3) \right) . \tag{4.58}$$

Two terms can be removed by choosing the constants to be

$$s_{1,1} = -\frac{a_{1,3}}{3a_{0,3}}\,, \quad s_{0,2} = -\frac{a_{0,4}}{3a_{0,3}} \tag{4.59}$$

leading to the stream function

$$\psi = \eta^2 \left(a_{0,3}\eta + a_{2,2}\xi^2 + \mathcal{O}(3) \right) . \tag{4.60}$$

If $a_{2,2} = 0$ higher order terms have to be considered. For simplicity assume $a_{2,2} \neq 0$. Since $a_{3,0} \neq 0$ equation (4.60) is divided with $a_{3,0}$ to get a neater coefficient on the η^3 term. Then, to get a neat coefficient on the $\xi^2\eta^2$ term ξ is scaled by a factor $\sqrt{\left|\frac{a_{0,3}}{2a_{2,2}}\right|}$ resulting in the stream function

$$\psi = \eta^2 \left(\eta + \frac{1}{2}\sigma\xi^2 + \mathcal{O}(3) \right) . \tag{4.61}$$

where σ is a sign coming from the scaling of ξ

$$\sigma = \operatorname{sign}\left(\frac{a_{2,2}}{a_{0,3}} \right) . \tag{4.62}$$

Multiplying ψ by σ, making the truncated normal form and relabelling back to x and y

$$\psi = y^2 \left(\sigma y + \frac{1}{2}x^2 \right) . \tag{4.63}$$

As always the entire wall consists of critical points. After scaling time with y the velocity equations are

$$\tilde{u} = 3\sigma y + x^2 \tag{4.64a}$$

$$\tilde{v} = -xy \tag{4.64b}$$

$$\tag{4.64c}$$

There is one critical point at $(0, 0)$. Since the stream function has value 0 at the origin the equation to be fulfilled for a separatrix connected to the critical point is $y^2\left(\sigma y + \frac{1}{2}x^2\right) = 0$. Looking for inflow separatrices $y > 0$ so the separatrix must fulfil

$$y = -\frac{1}{2}\sigma x^2\,, \tag{4.65}$$

which give a positive y for $\sigma = -1$. Hence, for $\sigma = -1$ there is a degenerate saddle and for $\sigma = 1$ there is a degenerate center.

4.2.0.4 Unfolding of simple degenerate critical point on the wall

An unfolding is now performed. We still assume a no slip wall at $y = 0$ and two small parameters, ϵ_1 and ϵ_2 are introduced.

$$\epsilon_1 = a_{0,2}\,, \quad \epsilon_2 = a_{1,2} \tag{4.66}$$

We then study the streamlines of the stream function given by

$$\psi = y^2 \left(\epsilon_1 + \epsilon_2 x + a_{0,3} y + a_{2,2} x^2 + a_{1,3} xy + a_{0,4} y^2 + \mathcal{O}(3)\right)\,, \tag{4.67}$$

still assuming a simple degeneracy $a_{0,3} \neq 0$. A near identity transformation is defined respecting the wall at $y = 0$ and including terms in the unfolding parameters

$$x = \xi \tag{4.68a}$$
$$y = \eta + s_{1,1}\xi\eta + s_{0,2}\eta^2 + \left(s_{0,1,1}\epsilon_1 + s_{0,1,2}\epsilon_2\right)\eta\,. \tag{4.68b}$$

Equation (4.68) is inserted in equation (4.67) and using the values of $s_{1,1}$ and $s_{0,2}$ that proved useful for vanishing unfolding parameters defined in equation (4.59)

$$\begin{aligned}\psi =& y^2 \left(\epsilon_1 + 2s_{0,1,1}\epsilon_1^2 + s_{0,1,2}\epsilon_1\epsilon_2 - \left(\frac{2a_{1,3}}{3a_{0,3}}\epsilon_1 - \epsilon_2\right)\xi \right.\\ &+ \left(a_{0,3} + \left(3a_{0,3}s_{0,1,1} - \frac{2a_{0,4}}{3a_{0,3}}\right)\epsilon_1 + 3a_{0,3}s_{0,1,2}\right)\eta \\ &\left. + a_{2,2}\xi^2 + \mathcal{O}(3)\right)\,.\end{aligned} \tag{4.69}$$

An obvious choice of the remaining constants is then

$$s_{0,1,1} = \frac{2a_{0,4}}{9a_{0,3}^2}\,, \quad s_{0,1,2} = 0 \tag{4.70}$$

giving ψ the appearance

$$\psi = y^2 \left(\epsilon_1 + \frac{4a_{0,4}}{9a_{0,3}^2}\epsilon_1^2 - \left(\frac{2a_{1,3}}{3a_{0,3}}\epsilon_1 - \epsilon_2\right)\xi + a_{0,3}\eta + a_{2,2}\xi^2 + \mathcal{O}(3)\right)\,. \tag{4.71}$$

We still assume that $a_{2,2} \neq 0$. A translation of ξ then can be used to remove the second highest order term in ξ. This is accomplished by writing $\xi = \xi_{\text{new}} + \xi_0$

with ξ_0 being a constant chosen to make the linear term in ξ_{new} vanish when inserted in equation (4.71). This gives the value of ξ_0

$$\xi_0 = \frac{a_{1,3}}{3a_{0,3}a_{2,2}}\epsilon_1 - \frac{1}{2a_{2,2}}\epsilon_2\,, \tag{4.72}$$

This is a small number which is important since the analysis is performed close to $(\xi, \eta) = (0, 0)$. Then the stream function has the form

$$\psi = y^2\left(\mu + a_{0,3}\eta + a_{2,2}\xi^2 + \mathcal{O}(3)\right)\,, \tag{4.73}$$

where μ is a small parameter depending on ϵ_1 and ϵ_2. Now, all that is left is to get rid of $a_{0,3}$ and $a_{2,2}$ by using the same scaling of ψ and ξ as was performed without unfolding parameters resulting in the stream function

$$\psi = y^2\left(c_0 + \sigma y + \frac{1}{2}x^2 + \mathcal{O}(3)\right)\,, \tag{4.74}$$

where c_0 is a small parameter depending on the initial unfolding parameters ϵ_1 and ϵ_2 and for vanishing c_0 the normal form with strict degeneracy conditions is retrieved.

Now the topology of the truncated normal form of equation (4.74) is investigated and the results are summarised in figure 4.3. The truncated normal form is even in x so there is an even number of critical points off the line $x = 0$. The velocity field with time scaled by y is then

$$\tilde{u} = 2c_0 + 3\sigma y + x^2 \tag{4.75a}$$

$$\tilde{v} = -xy \tag{4.75b}$$

The no - slip critical points are found at $y = 0$ meaning that $2c_0 + x^2 = 0$ must be fulfilled which is possible for $c_0 \leq 0$ in which case $x = \pm\sqrt{c_0}$. Thus, this is independent of σ. The determinant of the Jacobian is $-2x^2 + 3\sigma y$ hence negative at any wall point guaranteeing that at on wall critical point is a saddle. There is at most one inflow critical point which is located at $(0, -\frac{2}{3}c_0\sigma)$ existing in the relevant domain for $\frac{c_0}{\sigma} < 0$. At this point the determinant of the Jacob $-2c_0$ hence a being a saddle for $c_0 > 0$ and a center for $c_0 < 0$. Hence, for $c_0 > 0$ and $\sigma = -1$ an inflow saddle exists and for $c_0 < 0$ and $\sigma = 1$ an inflow center exists. At the wall the stream function has vanishing value but at a possible inflow critical point the value is nonzero. Therefore, the inflow saddle existing for $c_0 > 0$, $\sigma = -1$ is not connected to a heteroclinic separatrix. The curve $y = \sigma\left(c_0 + \frac{1}{2}x^2\right)$ has vanishing value of ψ. In case of two no slip critical points they fulfill this equations. The physical domain shows that for $\sigma < 0$, $c_0 > 0$ there is a heteroclinic connection between the two wall saddle points

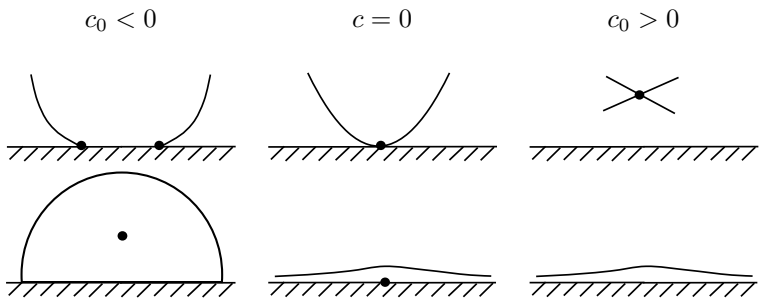

Figure 4.3: Unfolding of a simple degenerate critical point on a wall. Top row $\sigma = -1$, bottom row $\sigma = 1$. c_0 increases from negative to positive values going from left coloumn to the right with the center column denoting the degenerate case $c_0 = 0$. Thus perturbing c_0 close to 0 can lead to the birth of a vortex as seen in the bottom row.

going through inner points of the fluid. In this case the heteroclinic orbit and the wall encapsulates a center since the center is at heteroclinic orbit goes through the point σc_0. The case $\sigma > 0$ and varying c_0 from positive to negative values then creates a center on the wall which is lifted into the flow encapsulated by a streamline connected to the wall defining a rotation dominated region. This is an example of a 'a birth of a vortex' close to a wall seen from normal form perspective.

4.2.0.5 Unfolding of simple degenerate critical point with non zero wall speed

We consider the unfolding of a simple degenerate critical point on a wall i.e. $\epsilon_1 = a_{0,2}$ (critical point condition), $\epsilon_2 = a_{1,2}$ (degenerate critical point), $a_{0,3} \neq 0$ (simple degeneracy) and then add the new unfolding parameter $\epsilon_0 = a_{0,1}$.

This means the stream function is on the form

$$\psi = \epsilon_0 y + \epsilon_1 y^2 + \epsilon_2 x y^2 + a_{0,3} y^3 + a_{0,4} y^4 + a_{2,2} x^2 y^2 + a_{1,3} x y^3 + \mathcal{O}(5)\,, \quad (4.76)$$

where $\mathcal{O}(5)$ are terms of at least fifth order in combinations of x and y. The task is now to get a simpler form of the stream function using coordinate transformations. We strive to make coordinate transformations that ease comparison to the well known case where $\epsilon_0 = 0$. A near identity transformation to new coordinates (ξ, η) is constructed where coefficients r_i and s_j are determined later to simplify

the first terms of the stream function as much as possible.

$$x = \xi + r_0\epsilon_0 + r_1\epsilon_1 + r_2\epsilon_2 \tag{4.77a}$$

$$\begin{aligned} y = \eta &+ (s_{0,1,0}\epsilon_0 + s_{0,1,1}\epsilon_1 + s_{0,1,2}\epsilon_2)\,\eta \\ &+ (s_{1,1} + s_{1,1,0}\epsilon_0 + s_{1,1,1}\epsilon_1 + s_{1,1,2}\epsilon_2)\,\xi\eta \\ &+ (s_{0,2} + s_{0,2,0}\epsilon_0 + s_{0,2,1}\epsilon_1 + s_{0,2,2}\epsilon_2)\,\eta^2\,. \end{aligned} \tag{4.77b}$$

While it previously have been sufficient with $r_i = 0$ we now need the freedom to chose the r_i less trivially. In the degenerate case $\epsilon_0 = \epsilon_1 = \epsilon_2 = 0$. Here it is useful with

$$s_{0,2} = -\frac{1}{3}\frac{a_{0,4}}{a_{0,3}}\,, \quad s_{1,1} = -\frac{1}{3}\frac{a_{1,3}}{a_{0,3}} \tag{4.78}$$

to remove the terms with xy^3 and y^4. We want to remove these terms for any small value of the ϵ's. Thus, we use equation (4.78) and equation (4.77) in equation (4.76). We only include first order terms in the ϵ's since we only include this order in equation (4.76). Consider the coefficient to the η^4 term

$$\left(2a_{0,4}s_{0,1,0} + a_{1,4}r_0 + 3a_{0,3}s_{0,2,0} - \frac{a_{1,3}a_{0,4}r_0}{a_{0,3}}\right)\epsilon_0 \tag{4.79a}$$

$$+\left(2a_{0,4}s_{0,1,1} + a_{1,4}r_1 + 3a_{0,3}s_{0,2,1} - \frac{a_{1,3}a_{0,4}r_1}{a_{0,3}} + \frac{1}{9}\frac{a_{0,4}^2}{a_{0,3}^2}\right)\epsilon_1 \tag{4.79b}$$

$$+\left(2a_{0,4}s_{0,1,2} + a_{1,4}r_2 + 3a_{0,3}s_{0,2,2} - \frac{a_{1,3}a_{0,4}r_2}{a_{0,3}}\right)\epsilon_2\,. \tag{4.79c}$$

Each of the ϵ terms can be removed by the following choice of some of the free parameters

$$s_{0,2,0} = -\frac{1}{3a_{0,3}^2}\left(2a_{0,4}a_{0,3}s_{0,1,0} - a_{1,3}a_{0,4}r_0\right) \tag{4.80a}$$

$$s_{0,2,1} = -\frac{1}{27a_{0,3}^3}\left(18a_{0,4}a_{0,3}^2 s_{0,1,1} + 9a_{1,4}a_{0,3}^2 r_1 - 9a_{1,3}a_{0,3}a_{0,4}r_1 + a_{0,4}^2\right) \tag{4.80b}$$

$$s_{0,2,2} = -\frac{1}{3a_{0,3}^2}\left(2a_{0,4}a_{0,3}s_{0,1,2} - a_{1,3}a_{0,4}r_2\right)\,. \tag{4.80c}$$

By similar considerations more terms can be removed, for example the $\xi\eta^3$ term

by choosing

$$s_{1,1,0} = -\frac{1}{9a_{0,3}^2}\left(3a_{1,3}a_{0,3}s_{0,1,0} - 3a_{1,3}^2 r_0 - 4a_{2,2}a_{0,4}r_0\right) \tag{4.81a}$$

$$s_{1,1,1} = -\frac{1}{27a_{0,3}^3}\left(2a_{0,4}a_{1,3} - 9a_{1,3}^2 a_{0,3}r_1 - 12a_{2,2}a_{0,4}a_{0,3}r_1 + 9a_{0,3}^2 a_{1,3}s_{0,1,1}\right) \tag{4.81b}$$

$$s_{1,1,2} = -\frac{1}{9a_{0,3}^2}\left(-3a_{1,3}^2 r_2 - 2a_{0,4} + 3a_{1,3}a_{0,3}s_{0,1,2} - 4a_{2,2}a_{0,4}r_2\right) . \tag{4.81c}$$

In the case $\epsilon_0 = 0$ the η^3 term is independent of ϵ_1 and ϵ_2 to linear order by the right choice of the remaining free parameters. This is still possible for $\epsilon_0 \neq 0$ by choosing

$$s_{0,1,0} = -\frac{1}{3a_{0,3}}a_{1,3}r_0 \tag{4.82a}$$

$$s_{0,1,1} = -\frac{1}{9a_{0,3}^2}\left(-2a_{0,4} + 3a_{1,3}a_{0,3}r_1\right) \tag{4.82b}$$

$$s_{0,1,2} = -\frac{1}{3a_{0,3}}a_{1,3}r_2 . \tag{4.82c}$$

Notice that equation (4.82) appears in equation (4.80) and equation (4.81).

Also, for $\epsilon_0 = 0$ the term with the second highest power in ξ can be removed. This is still the case if we choose

$$r_0 = 0 \tag{4.83a}$$

$$r_1 = \frac{1}{3a_{2,2}a_{0,3}}a_{1,3} \tag{4.83b}$$

$$r_2 = -\frac{1}{2a_{2,2}} . \tag{4.83c}$$

Now all the free parameters in equation (4.77) have been assigned.

We still have the option of scaling ξ, η and ψ to normalize some coefficients. We can normalise the $\xi^2\eta^2$ coefficient to $\frac{1}{2}$ and the η^3 coefficient to ± 1. Denoting the current coefficient to $\xi^i y^j$ by $\tilde{a}_{i,j}$ this is done by defining new variables X and Y by

$$X = \frac{\sqrt{2}}{2}\xi \tag{4.84a}$$

$$Y = \frac{|\tilde{a}_{0,3}|}{|\tilde{a}_{2,2}|}\eta . \tag{4.84b}$$

Scaling ψ absorbs a common factor

$$\Psi = \frac{\tilde{a}_{0,3}^2}{\tilde{a}_{2,2}^3}\psi\,. \tag{4.85}$$

The coefficient to Y^3 is now σ given by equation (4.62)

Renaming X and Y to x and y, the stream function is now written

$$\Psi = y\left(c_1\,(1+\alpha x) + c_0 y + \sigma y^2 + \frac{1}{2}x^2 y\right) + \mathcal{O}(5)\,, \tag{4.86}$$

where

$$c_1 = \frac{|a_{0,3}|}{|a_{2,2}|a_{2,2}}\epsilon_0 \tag{4.87a}$$

$$c_0 = -\frac{1}{3}\frac{a_{0,4}}{a_{2,2}a_{0,3}}\epsilon_0 + \frac{1}{a_{2,2}}\epsilon_1\,, \tag{4.87b}$$

are small parameters and

$$\alpha = -\frac{\sqrt{2}}{6}\frac{a_{1,3}}{a_{0,3}}\,. \tag{4.88}$$

Thus, including the new unfolding parameter ϵ_0 results in an extra parameter, c_1, in the normal form.

4.2.1 Topology of normal form

We disregard the $\mathcal{O}(5)$ terms in equation (4.86), and name the remaining part ψ.

$$\psi = y\left(c_1\,(1+\alpha x) + c_0 y + \sigma y^2 + \frac{1}{2}x^2 y\right)\,. \tag{4.89}$$

We note first that for $c_1 = 0$ equation (4.89) reduces to the truncated form of equation (4.74). Differentiation is performed to prepare for critical point investigation.

$$\frac{\partial\psi}{\partial x} = y\,(c_1\alpha + xy) \tag{4.90a}$$

$$\frac{\partial\psi}{\partial y} = c_1\,(1+\alpha x) + 2c_0 y + 3\sigma y^2 + x^2 y\,. \tag{4.90b}$$

Due to the extra unfolding parameter there is a term with that is linear in y. Hence, a time scaling with y in the velocity field cannot be performed.

From equation (4.90a) a critical point must fulfil

$$\frac{\partial \psi}{\partial x} = 0 \quad \Leftrightarrow \quad y = 0 \quad \vee \quad x = -\frac{c_1 \alpha}{y} \,. \tag{4.91}$$

Inserting $y = 0$ in $\frac{\partial}{\partial y}\psi = 0$

$$0 = c_1 \left(1 + \alpha x\right) \,. \tag{4.92}$$

This means that for nonzero α then for any value of c_1 and c_0 there is a fixed point on the wall at $(x, y) = (-\frac{1}{\alpha}, 0)$. However, since the analysis is only valid for (x, y) close to $(0, 0)$ we disregard this critical point. For $\alpha = 0$ and c_1 nonzero there are no critical points on the wall. Notice that for $c_1 = 0$ then the entire wall consists of critical points.

We use $x = -\frac{c_1 \alpha}{y}$ in $\frac{\partial}{\partial y}\psi = 0$ to investigate more possibilities of critical points.

$$\frac{3}{2}\sigma y^2 + c_0 y + \frac{1}{2} c_1 = 0 \,, \tag{4.93}$$

which has 2 solutions if

$$d = c_0^2 - 3\sigma c_1 > 0 \,, \tag{4.94}$$

which are

$$y_\pm = \frac{-c_0 \pm \sqrt{d}}{3\sigma} \,. \tag{4.95}$$

This means $d = 0$ is a parabola in (c_0, c_1) space defining regions with zero or two solutions of equation (4.93). In case of two solutions it is necessary that they occur for $y > 0$. For $\sigma = 1$ then $y_+ > y_1$ and for $\sigma < 0$ then $y_+ < y_1$. For $\sigma = 1$ and $c_1 > 0$ then $d = c_0^2 - 3\sigma c_1 > c_0^2$ thus considering equation (4.95) $y_+ > 0$ and $y_- < 0$. Similarly for $\sigma > 0$ and $c_1 < 0$ then $d = c_0^2 - 3\sigma c_1 < c_0^2$ - when two solutions exist they have same sign which opposite of c_0. The constraint of positive y at the critical point includes the c_0 axis a bifurcation curve and makes half the parabola $d = 0$ redundant. Similar arguments apply to the case $\sigma = -1$

Since the unfolding is local the critical points must be located close to $(x, y) = (0, 0)$. From equation (4.95) and equation (4.94) y is guaranteed small. From equation (4.95) and the critical point criteria for x being $x = -\frac{c_1 \alpha}{y}$ we get

$$x = \frac{-3\sigma\alpha c_1}{-c_0 \pm \sqrt{c_0^2 - 3\sigma c_1}} = \alpha \left(c_0 \pm \sqrt{c_0^2 - 3\sigma c_1} \right) \,. \tag{4.96}$$

Then the critical point value of x is small for small unfolding parameters so no further restrictions are needed.

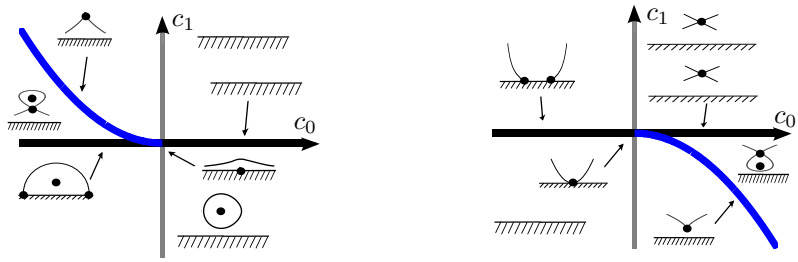

Figure 4.4: Sketch of the bifurcation diagram with wall speed as new unfolding parameter. Left $\sigma = 1$, right $\sigma = -1$. Blue and black curves are bifurcation curves. For $c_1 \neq 0$ the wall is moving in horizontal direction.

The determinant of the Hessian of the stream function is

$$D(x,y) = -3x^2y^2 + 6\sigma y^3 + 2c_0y^2 - 4c_1\alpha xy - c_1^2\alpha^2\,, \tag{4.97}$$

Investigating the type of critical point if $d > 0$ we first insert the x - value

$$D\left(-\frac{c_1\alpha}{y_\pm}, y_\pm\right) = 2y_\pm^2\left(c_0 + 3\sigma y_\pm\right)\,. \tag{4.98}$$

Inserting equation (4.95) in D

$$D\left(-\frac{c_1\alpha}{y_\pm}, y_\pm\right) = 2y_\pm^2\left(\pm\sqrt{d}\right)\,. \tag{4.99}$$

Therefore, if $d > 0$ then y_+ is a center and y_- is a saddle. Thus, a saddle node bifurcation happens for d crossing zero. This bifurcation is off the wall.

The bifurcation diagram is shown in figure 4.4 for $\sigma = \pm 1$. The diagram with $\sigma = 1$ has also been constructed by Bakker [9] using different transformations. Along the parabolic bifurcation curve the inflow cusp is seen as the transition between a saddle and center and no critical points. The behaviour going from positive to zero wall speed is more exotic. Consider for example $\sigma = 1$ and $c_0 < 0$. Decreasing the wall speed from positive c_1 the saddle point approaches the y axis. In the limit $c_1 \to 0$ the saddle point tends to y-axis (see equation (4.93)) with x - value tending to $-\frac{2}{3}c_0$ as seen from equation (4.96) . However, at $c_1 = 0$ the entire y - axis consists of critical points but only the no slip critical points at $x = \pm\sqrt{c_0}$ have inflow separatrix connections. Decreasing the c_0 from zero there is only an inflow center present which is simply due to the saddle point being located at negative y - values. It is not surprising that the c_0 axis constitutes a bifurcation curve since c_1 is proportional to the wall speed. At zero

wall speed the entire c_0 axis consist of critical points while there are none for non zero wall speed.

Interpreting to the simulations especially the case of a vortex is interesting. Considering the wall system we see vortices on the form prescribed by $c_0 < 0, c_1 = 0$ and when going to the patch system they are often visible along with a saddle as prescribed by $c_0 < 0, c_1 > 0$. This behaviour is seen for vortices with positive circulation.

Hence, there is good agreement between the theory and the observed simulated Navier - Stokes equations. The bifurcation diagram predicts not too surprisingly that if the wall speed is increased enough then no critical points can be observed as seen by crossing the parabola in figure 4.4a.

4.2.2 Topology of stream function and vorticity for unfolding of non-simple degenerate on-wall critical points of ψ

We consider the wall system looking for a situation where interesting dynamics occur in both the streamlines and vorticity contours. For the streamlines $a_{0,2} = 0$ guarantees a critical point and $a_{1,2} = 0$ means it is degenerate. The simple, degenerate critical points are characterised by having nonzero linear part of equation (4.55) which means $a_{0,3} \neq 0$. However, since $a_{0,3} = 0$ is needed for a critical point of the vorticity this means a non-simple, degenerate critical point on the wall has to be considered for interesting behaviour of the vorticity to occur simultaneously. Unfortunately, normal form theory is based on a non zero linear part. However, Hartnack [50] managed to get a useful normal form of the stream function despite this.

The stream function is on the form

$$\psi(x, y) = y^2 \left(\epsilon_1 + \epsilon_2 x + \epsilon_3 y + a_{2,2}x^2 + a_{1,3}xy + a_{0,4}y^2\right) , \tag{4.100}$$

where ϵ_i are small parameters and we assume $a_{2,2} \neq 0$, $4a_{0,4}a_{2,2} - a_{1,3}^2 \neq 0$. The vorticity $\omega = -\nabla^2\psi$ is then

$$\omega(x, y) = -2\,\epsilon_1 - 2\,\epsilon_2 x - 6\,\epsilon_3 y - 2\,a_{2,2}x^2 - 6\,a_{1,3}xy - (12\,a_{0,4} + 2a_{2,2})\,y^2 . \tag{4.101}$$

The stream function topology has been investigated in [50] after some topology preserving transformations. The same transformations will be applied to the vorticity to ease comparison. Since ω is a second order polynomial in x and y it

is immediately clear that the critical points of ω are given by a linear (affine) equation.

Defining the coordinate transformation

$$\begin{pmatrix} x \\ y \end{pmatrix} = \begin{pmatrix} -\frac{\epsilon_2}{2a_{2,2}} \\ 0 \end{pmatrix} + \begin{pmatrix} -\frac{\sqrt{|4a_{0,4}a_{2,2}-a_{1,3}^2|}}{2|a_{2,2}|} & -\frac{a_{1,3}}{2a_{2,2}} \\ 0 & 1 \end{pmatrix} \begin{pmatrix} X \\ Y \end{pmatrix} \tag{4.102}$$

the stream function may be written in a simpler form

$$\begin{aligned} \tilde{\psi}(X,Y) = \left(\frac{4a_{2,2}a_{0,4} - a_{1,3}^2}{4a_{2,2}}\right) y^2 \left(\frac{4\,\epsilon_1 a_{2,2} - {\epsilon_2}^2}{4\,a_{0,4}a_{2,2} - {a_{1,3}}^2} - 2\,\epsilon_2 a_{1,3}\right. \\ \left. +4\,\frac{\epsilon_3 a_{2,2}}{4\,a_{0,4}a_{2,2} - {a_{1,3}}^2} Y + Y^2 + \sigma X^2\right) \end{aligned} \tag{4.103}$$

where $\sigma = \text{sign}(4a_{0,4}a_{2,2} - a_{1,3}^2)$. Defining parameters $c_{0,2}$ and $c_{0,3}$ by

$$c_{0,2} = \frac{4\,\epsilon_1 a_{2,2} - {\epsilon_2}^2}{4\,a_{0,4}a_{2,2} - {a_{1,3}}^2} \tag{4.104}$$

$$c_{0,3} = \frac{-2\,\epsilon_2 a_{1,3} + 4\,\epsilon_3 a_{2,2}}{4\,a_{0,4}a_{2,2} - {a_{1,3}}^2} \tag{4.105}$$

then the topology of equation (4.100) is equivalent to the topology of $\hat{\psi}(X,Y)$

$$\hat{\psi}(X,Y) = y^2\left(c_{0,2} + c_{0,3}y + y^2 + \sigma X^2\right)\,. \tag{4.106}$$

A bifurcation diagram has been constructed in [50].

Using the same transformations for the vorticity does not make it prettier, but it is nevertheless still quadratic in X and Y.

$$\omega(X,Y) = -2\epsilon_1 + \frac{\epsilon_2^2}{2a_{2,2}} + 3\left(\frac{\epsilon_2 a_{1,3}}{a_{2,2}} - 2\epsilon_3\right) Y - \frac{|4a_{0,4}a_{2,2} - a_{1,3}^2|}{2a_{2,2}} X^2 \tag{4.107}$$

$$- 2\sqrt{|4a_{0,4}a_{2,2} - a_{1,3}^2|}\,\frac{a_{1,3}}{|a_{2,2}|} XY + \left(\frac{5a_{1,3}^2}{2a_{2,2}} - 12a_{0,4}\right) Y^2\,. \tag{4.108}$$

The critical points fulfil $\frac{\partial}{\partial X}\omega = \frac{\partial}{\partial Y}\omega = 0$ and can be written as $A\boldsymbol{x} = \boldsymbol{b}$ with

$$A = \begin{bmatrix} -4\,a_{2,2}\left|\frac{a_{0,4}}{a_{2,2}} - \frac{1}{4}\frac{{a_{1,3}}^2}{{a_{2,2}}^2}\right| & -4\,a_{1,3}\sqrt{\left|\frac{a_{0,4}}{a_{2,2}} - \frac{1}{4}\frac{{a_{1,3}}^2}{{a_{2,2}}^2}\right|} \\ -4\,a_{1,3}\sqrt{\left|\frac{a_{0,4}}{a_{2,2}} - \frac{1}{4}\frac{{a_{1,3}}^2}{{a_{2,2}}^2}\right|} & -4\,a_{2,2} + 5\,\frac{{a_{1,3}}^2}{a_{2,2}} - 24\,a_{0,4} \end{bmatrix} \tag{4.109}$$

$$\boldsymbol{b} = \begin{pmatrix} 0 \\ -3\frac{a_{1,3}}{a_{2,2}}\epsilon_2 + 6\epsilon_3 \end{pmatrix} \tag{4.110}$$

Notice that the unfolding parameters ϵ_2 and ϵ_3 only appear in $\boldsymbol{b}$ and that ϵ_1 does not appear at all. The determinant of A determines if the equation is always solvable

$$\det(A) = \left|\frac{4\,a_{0,4}a_{2,2} - {a_{1,3}}^2}{{a_{2,2}}^2}\right|\left(4\,{a_{2,2}}^2 - 9\,{a_{1,3}}^2 + 24\,a_{0,4}a_{2,2}\right)\,. \tag{4.111}$$

Thus, for a unique solution we need $4\,{a_{2,2}}^2 - 9\,{a_{1,3}}^2 + 24\,a_{0,4}a_{2,2} \neq 0$ which is a 'new' condition. In case a critical point exists it has only physical meaning if the y - coordinate is non negative. Assuming $|A| \neq 0$ the y - coordinate can be calculated.

$$y_{\text{critical}} = \frac{3a_{1,3}\epsilon_2 - 6\epsilon_3 a_{2,2}}{4\,{a_{2,2}}^2 - 9\,{a_{1,3}}^2 + 24\,a_{0,4}a_{2,2}}\,. \tag{4.112}$$

The Hessian of ω equals A so if a critical point exists we can immediately use the second derivative test to conclude on the type of critical point. If $a_{2,2} > 0$ and $4\,{a_{2,2}}^2 - 9\,{a_{1,3}}^2 + 24\,a_{0,4}a_{2,2} < 0$ then the critical point is a maximum. If $a_{2,2} < 0$ and $4\,{a_{2,2}}^2 - 9\,{a_{1,3}}^2 + 24\,a_{0,4}a_{2,2} < 0$ then the critical point is a minimum. If $4\,{a_{2,2}}^2 - 9\,{a_{1,3}}^2 + 24\,a_{0,4}a_{2,2} > 0$ the critical point is a saddle. The only topological importance of the unfolding parameters is in equation (4.112).

A bifurcation in ω occurs if y_{critical} crosses the y - axis. This is independent on σ which was not the case for the streamline topology.

With $\beta = y_{\text{critical}}$ we have the parameters $c_{0,2}$, $c_{0,3}$, and β that determines the topology of ψ and ω. If $a_{1,3} \neq 0$ there is a unique correspondence between ϵ_1, ϵ_2, and ϵ_3 and $c_{0,2}$, $c_{0,3}$, and β. This means we can add an orthogonal β - axis to the bifurcation diagram in [50]. A critical point of ω is created for β going from negative to positive values and the curves in the bifurcation diagram in [50] are extended to surfaces in the $c_{0,2}$, $c_{0,3}$, β space. Therefore, this is a case where a creation of a vortex in the vorticity formulation may be related to a bifurcation in the streamlines for a curve in a three dimensional parameter space that are not parallel to the one of the axis. The bifurcation diagram for the streamlines

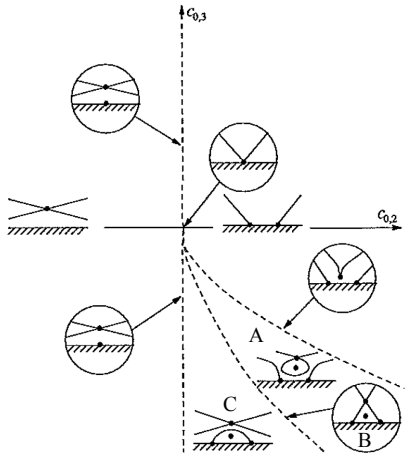

Figure 4.5: The bifurcation diagram from Bakker [50] (reprinted with permission, A, B, C not in the original diagram) for the non simple on wall degeneracy, $\sigma = -1$. Including an orthogonal β - axis corresponds to including the vorticity. Here the behaviour is simple - crossing $\beta = 0$ means creation/destruction of a critical point of the vorticity.

for $\sigma = -1$ is shown in figure **??**. The bifurcation A,B,C are interesting to relate to the numerics. They are the lower part of the 'figure 8' bifurcation seen in the wall system e.g. figure 3.19c, 3.19d.

4.3 Conditions for exactly overlapping contours of ψ and ω

For some of the simulations a good agreement between the instantaneous streamlines and the vorticity contours is observed. Now analytical conditions are sought to ensure the two sets of contours are identical.

The contours of the stream function fulfill the equation

$$\psi(x, y) = c_1 \,, \tag{4.113}$$

where c_1 is some constant. At a point where $\frac{\partial \psi}{\partial y} \neq 0$ the curve given by equation

(4.113) is locally represented as a function of x such that

$$\psi(x,y) = \psi(x,f(x)) = c_1\,, \tag{4.114}$$

where the curve $(x, f(x))$ is a part of the contour curve. Differentiating equation (4.114) yields an expression for f':

$$f'(x) = -\frac{\frac{\partial\psi(x,f(x))}{\partial x}}{\frac{\partial\psi(x,f(x))}{\partial y}}\,. \tag{4.115}$$

Similarly the contours of the vorticity fulfil

$$\omega(x,y) = c_2\,, \tag{4.116}$$

where a part of the curve is only depending on x if $\frac{\partial\omega}{\partial y} \neq 0$ in which case

$$\omega(x,g(x)) = c_2\,. \tag{4.117}$$

After differentiation one gets

$$g'(x) = -\frac{\frac{\partial\omega(x,f(x))}{\partial x}}{\frac{\partial\omega(x,f(x))}{\partial y}}\,. \tag{4.118}$$

We pick some arbitrary point in the plane where $\frac{\partial\psi}{\partial y} \neq 0$ and $\frac{\partial\omega}{\partial y} \neq 0$. Then for ω and ψ to have the same contour through this point the slopes of the curves must match i.e. $f'(x) = g'(x)$. From equation (4.118) and equation (4.115) this means

$$\frac{\partial\omega}{\partial x}\frac{\partial\psi}{\partial y} - \frac{\partial\psi}{\partial x}\frac{\partial\omega}{\partial y} = 0\,. \tag{4.119}$$

If $\frac{\partial\psi}{\partial x} \neq 0$ and $\frac{\partial\omega}{\partial x} \neq 0$ the argument may be repeated with x being a function of y. Therefore, the only restriction is for both partial derivatives vanishing i.e. at a critical point. We may then the demand that the critical points of ψ must match the critical points of ω.

Conversely, if equation (4.119) holds then

$$-\frac{\frac{\partial\omega}{\partial x}}{\frac{\partial\omega}{\partial y}} = -\frac{\frac{\partial\psi}{\partial x}}{\frac{\partial\psi}{\partial y}} \tag{4.120}$$

for nonvanishing denominators. Therefore, equation (4.119) ensures the same slope of the vorticity contour and the streamline at the common point $(x, y) = (x, g(x)) = (x, f(x))$ which means that the two curves are identical due to existence and uniqueness of solutions to an initial value problem [73]. Thus, at typical points the level curves of ψ and ω are identital if and only if equation (4.119) holds.

So far the special relation $\omega = -\Delta\psi$ has not been used i.e. equation (4.119) is the criterion for overlapping contours for any two real valued functions of two variables. Inserting the relation between ψ and ω a criterion is formulated only from derivatives of the stream function equivalent to equation (4.119)

$$-\left(\frac{\partial^3\psi}{\partial x^3}+\frac{\partial^3\psi}{\partial x\partial y^2}\right)\frac{\partial\psi}{\partial y}+\frac{\partial\psi}{\partial x}\left(\frac{\partial^3\psi}{\partial y^3}+\frac{\partial^3\psi}{\partial y\partial x^2}\right)=0\,. \tag{4.121}$$

In the context of normal forms where a Taylor expansion is used, equation (4.121) gives a constraint on the coefficients.

Testing whether equation (4.119) holds for parts of the simulations is most easily done using the velocity coordinates instead of derivatives of the stream function. However, the derivatives of the vorticity makes a lot of 'noise' especially in regions with low absolute value of the vorticity. Since we already have the streamlines and vorticity contours available we will not pursue implementation of equation (4.119) further in the simulations.

The evolution of the vorticity in two dimensions is described by the well known vorticity equation

$$\frac{\partial\omega}{\partial t}+\boldsymbol{u}\cdot\nabla\omega=\frac{1}{Re}\Delta\omega \tag{4.122}$$

where the second term is exactly the left side of equation (4.119). Using $u=\frac{\partial\psi}{\partial y}$, $v=-\frac{\partial\psi}{\partial x}$ equation (4.119) may be formulated in coordinate free form as

$$\boldsymbol{u}\cdot\nabla\omega=0\,. \tag{4.123}$$

A simple condition on the stream function guarantees equation (4.123) holds. Consider the stream function in polar coordinates $\psi(r,\theta)$ with

$$\boldsymbol{u}=\frac{1}{r}\frac{\partial\psi}{\partial\theta}\boldsymbol{e}_r-\frac{\partial\psi}{\partial r}\boldsymbol{e}_\theta \tag{4.124}$$

If ψ is rotational symmetric i.e. independent of θ then $\boldsymbol{u}$ only has a component in the $\boldsymbol{e}_\theta$ direction. For ψ only depending on r so does ω by $\omega = -\Delta\psi$. This

means $\nabla\omega$ is in the $\boldsymbol{e}_r$ direction meaning equation (4.123) is fulfilled. If the vorticity is proportional to the stream function the contours are matching. An example is the inner part of the Lamb - Chaplygin vortex pair studied by Billant et al. [11].

From equation (4.123), restricting the attention to flow with overlapping streamlines and vorticity contours globally means that we seek solutions to the Navier - Stokes equation which also solves the 'heat equation'

$$\frac{\partial\omega}{\partial t} = \frac{1}{Re}\Delta\omega \tag{4.125}$$

which is well studied and similar to diffusion problems with Re^{-1} acting like the diffusion constant.

Conversely, from equation (4.122) if $\frac{\partial\omega}{\partial t}$ and $\frac{1}{Re}\Delta\omega$ are vanishing - for example for large Re, far from walls, and during a suitable time frame (these conditions should be specified for a proper investigation), then $D = 0$ which means the vorticity and streamline contours are identical. This may explain why there is a better match between the streamlines and vorticity for increasing Re in the simulations.

There is still the question of which coordinate system to use when studying the streamlines. Demanding also the 'singular' contours to match i.e. the critical points then the most dominant critical points are best matched in the patch system. Here the critical point of the streamlines at the center of the generating vortex match the extreme value of the vorticity at least before an eruption event.

4.4 Conclusion on analysis

The normal form approach does not reveal simple connections between the streamline topology and the vorticity contour topology. Only for a non simple degenerate on wall critical point may a bifurcation occur in both the streamlines and the vorticity contours. However, a bifurcation in the streamlines happens for a change in other parameters than for the vorticity. The streamline bifurcations contain the lower part of the 'figure 8' bifurcation observed in numerics.

The streamline topology in the patch system and in the wall system are investigated from normal forms and structures are found which are also seen in the simulations.

A criterion for exactly matching contours of the vorticity contours and streamlines

are derived. These occur when the Navier - Stokes equations and the heat equation have identical solutions. It is argued that the patch system should then be chosen for best alignment of streamlines and vorticity contours since this means the contours at least match locally close to the generating vortex patch.

Chapter 5

Streamline and vorticity contour topology of two perfect vortices

In the past two chapters we have mainly focused on the creation and destruction of secondary vortices.

The interaction of the generating vortex with a long living erupted vortex is also of interest. For this we will consider an idealised model of two interacting vortices in two dimensions. In many aspects the analysis resembles the case of two point vortices. However, viscous effects mean that one vortex can 'disappear'. This was observed for low Re in chapter 3.1.

To understand the observed topology for an erupted vortex interacting with the generating vortex some simple models may be considered. The first choice may be to use point vortices. However, point vortices cannot account for diffusion of vorticity leading to vanishing of the vortices for increasing time. Streamlines and dynamics of point vortices have been extensively studied analytically. Hence, a model including viscous effects that can be investigated analytically may be a useful supplement. For point vortices the vorticity remains infinite at the vortex centers as they are moving in the fluid. For a fluid with viscous forces this is not the case. We will investigate the streamline and vorticity contour topology of

two 'perfect' vortices soon to be defined in unbounded fluid.

There is no wall present so the relation to chapter 3.1 relies on the assumption that the interaction of an erupted vortex and a the generating vortex is not too affected by the wall. As we will see some conclusions from the idealised two - vortex interaction match the observed behaviour from chapter 3.1.

First we discuss properties of one perfect vortex. Then, we will consider a combination of such two vortices.

We want to consider a streamline vortex and a vorticity vortex both possessing rotational symmetry. This can be obtained through the following assumptions using polar coordinates.

For the vorticity we assume

(I) $\omega = \omega(r)$, (rotational symmetry)

(II) $\omega'(r) \to 0$ for $r \to 0$ (critical point at origo)

(III) $\omega'(r) \neq 0$ for $r \neq 0$ (only one vorticity extrema)

(IV) $\omega \to 0$ for $r \to \infty$.

For the velocity field we assume

(a) $\boldsymbol{u} = u_\theta(r)\boldsymbol{e}_\theta$, (rotational symmetry with closed streamlines around origo)

(b) $u_\theta(r) \to 0$ for $r \to 0$ (critical point and necessary for a smooth velocity field at origo),

(c) $u_\theta(r) \neq 0$ for $r \neq 0$ (only one streamline center.)

(d) $u_\theta(r) \to 0$ for $r \to \infty$ (this defines a unique coordinate system)

Furthermore, the velocity field is assumed to be sufficiently smooth.

The list of assumptions may seem extensive. A canonical example fulfilling the assumptions is a Lamb - Oseen vortex (to appear in equation (5.11)). We will dwell on this case later. One reason for this more general setting, is that some arguments become clearer and shorter from this approach.

From the curl in cylindrical coordinates we get

$$\omega = \frac{1}{r}\frac{\mathrm{d}\,(ru_\theta)}{\mathrm{d}r}\,, \tag{5.1}$$

or equivalently

$$u_\theta = \frac{1}{r}\int_0^r r'\omega(r')dr'\,. \tag{5.2}$$

By property III and IV ω has constant sign throughout space. This then implies that u_θ same sign by 5.2 (consistent with 'the right hand rule' for the curl).

From the stream function in polar coordinates equation (4.124) and property equation (a) we get that $\psi = \psi(r)$. Hence, we may use $u_\theta = \frac{\mathrm{d}\psi}{\mathrm{d}r}$. If this inserted in the assumptions for $\boldsymbol{u}$ we get equivalent criteria for ψ that was assumed for $\boldsymbol{u}$

(A) $\psi = \psi(r)$, (rotational symmetry with closed streamlines around origo)

(B) $\frac{\mathrm{d}\psi}{\mathrm{d}r} \to 0$ for $r \to 0$ (smooth velocity field at origo),

(C) $\frac{\mathrm{d}\psi}{\mathrm{d}r} \neq 0$ for $r \neq 0$ (only one streamline center.)

(D) $\frac{\mathrm{d}\psi}{\mathrm{d}r} \to 0$ for $r \to \infty$ (this defines a unique coordinate system)

The criteria for ψ and ω are identical. From the analysis in the previous chapter, the vorticity contours and streamlines are exactly overlapping since ψ is independent of θ and the critical points match.

We now consider a model with *two* rotational invariant vortices a distance $2d$ apart in unbounded flow where the above assumptions hold for each. Hence, one rotationally invariant vortex is at $(x, y) = (-d, 0)$ and one at $(x, y) = (d, 0)$. The resulting velocity field is assumed to be the superposition of the two velocity field contributions (see figure 5.2). Since the curl is a linear operation, the vorticity field is also the superposition of the two vorticity contributions and similarly we the new stream function is a sum of the two stream functions.

First, we consider the topology of the instantaneous streamlines and vorticity contours. Strong results can be obtained, summarised in the following lemma.

Lemma 5.1 *Properties of streamlines and vorticity contours of superposition of two perfect vortices.*

All critical points occur on the x-axis and at least one exists. Critical points are zeros of $\frac{\partial}{\partial x}\omega(x, 0)$ *and* $\frac{\partial}{\partial x}\psi(x, 0)$ *respectively. For vortices of same sign critical points only occur for* $|x| < d$ *and for vortices of opposite sign critical points only*

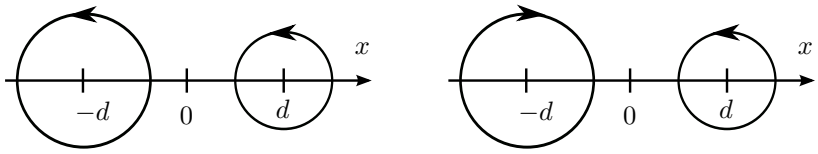

Figure 5.1: For two counter rotating vortices there are no critical points between the vortex centers. For two corotating vortices there can only be critical points on the line between the vortex centers.

occur for $|x| > d$. The type of critical points are known. Increasing distance from $x = d$ the first occurring critical point is a center and then of alternating type. Similar conclusion applies for increasing distance from $x = -d$.

The remaining part of this section is dedicated to prove the lemma. Then, we use lemma 5.1 in the study of the instantaneous streamlines and vorticity contours of two Gaussian vortices. We then investigate a dynamical model assuming the center of a vortex moves in the velocity field dictated by the other vortex.

Proof. Proof of lemma 5.1. At the center of one vortex there will only be a velocity field component from the other vortex from the assumption $u_\theta(r) \to 0$ as $r \to 0$. Since the velocity field contribution from the other vortex is nonzero this means that there are no critical points of the streamlines at the center of the two vortices. Similarly, $\frac{\partial \omega}{\partial x}$ and $\frac{\partial \omega}{\partial y}$ are linear in the contribution from the two vortices and the contribution from one vortex at its center vanishes. Therefore there are no critical points of the vorticity at the $(-d, 0)$ and $(d, 0)$.

Obviously the new, total velocity and vorticity fields do not possess rotational symmetry. Therefore, it is useful to use Cartesian coordinates.

The vorticity is given by the two contributions ω_1 and ω_2

$$\omega = \omega_1(r_1) + \omega_2(r_2)\,. \tag{5.3}$$

with (see figure 5.2)

$$r_1^2 = (x + d)^2 + y^2 \tag{5.4a}$$
$$r_2^2 = (x - d)^2 + y^2 \tag{5.4b}$$

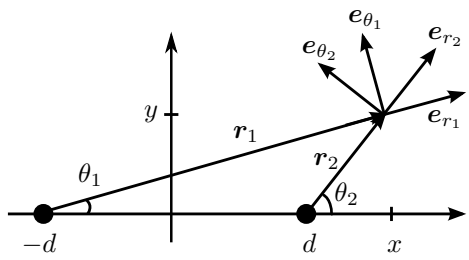

Figure 5.2: The coordinate system of two rotational invariant vortices. Each have a velocity field contribution $\boldsymbol{u}_i = u_{\theta_i}\boldsymbol{e}_{\theta_i}$.

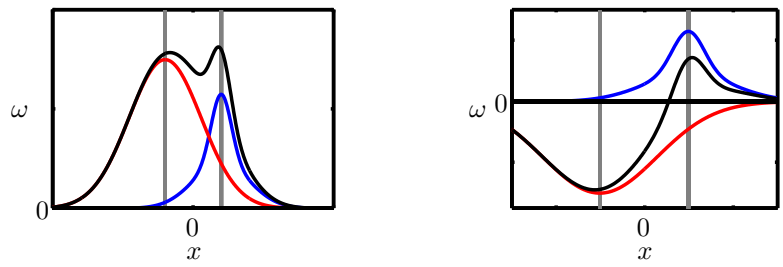

Figure 5.3: The vorticity contributions from the two vortices with blue and red and the sum in black, and with grey lines at $x = \pm d$. Some regions can be excluded to have critical points due to same sign of the derivative of the $\omega_1(r)$ and $\omega_2(r)$. (a) For two corotating vortices there can only be critical points of the vorticity on the line segment between the vortex centers - the black curve has nonzero derivative for $|x| > 1$. (b) For two counter rotating vortices there are no critical points of the vorticity between the vortex centers.

The critical points are computed from the partial derivatives using equation (5.4)

$$\frac{\partial \omega}{\partial x} = (x+d)\,\frac{\omega_1'(r_1)}{r_1} + (x-d)\,\frac{\omega_2'(r_2)}{r_2} \tag{5.5a}$$

$$\frac{\partial \omega}{\partial y} = y\left(\frac{\omega_1'(r_1)}{r_1} + \frac{\omega_2'(r_2)}{r_2}\right) \tag{5.5b}$$

It is clear that $y = 0$ solves $\frac{\partial \omega}{\partial y} = 0$. Other solutions require $0 = \frac{\omega_1'(r_1)}{r_1} + \frac{\omega_2'(r_2)}{r_2}$. Using this in equation (5.5a) gives $2\omega_1'(r_1)r_1^{-1}$ which is nonzero. Therefore, $y = 0$ is required for a critical point. The critical points are zeroes of

$$\frac{\partial \omega(x,0)}{\partial x} = \operatorname{sgn}(x+d)\;\omega_1'(r_1(x,0)) + \operatorname{sgn}(x-d)\;\omega_2'(r_2(x,0))\,. \tag{5.6}$$

If the two, initial rotational invariant vortices have the same sign of rotation, say a maximum, then $\omega_1' < 0$ for $x > -d$ and $\omega_2' < 0$ for $x > d$. This means according to equation (5.6) that there are no critical points for $x \geq d$. By similar reasoning there are no critical points for $x \leq -d$. See figure 5.3.

If the two, initial rotational invariant vortices have opposite sign of circulation, say that the initial vortex centred at $-d$ corresponds to a minimum and the initial vortex at $x = d$ corresponding to a maximum then $\frac{\partial \omega(x,0)}{\partial x} > 0$ for $|x| < d$ since both terms of equation (5.6) are positive in this region. This means there can only be critical points for $|x| \geq d$.

Since the vorticity is non zero at e.g. $x = d$ there must exist a critical point of ω to satisfy the vanishing vorticity (and hence vanishing derivative) at $\pm\infty$.

We compute the second order derivatives to determine the type of a critical point

$$\frac{\partial^2 \omega(x,0)}{\partial x \partial y} = 0 \tag{5.7a}$$

$$\frac{\partial^2 \omega(x,0)}{\partial y^2} = \frac{\omega_1'(r_1)}{r_1} + \frac{\omega_2'(r_2)}{r_2} \tag{5.7b}$$

Using the critical point criteria $\frac{\partial \omega}{\partial x} = 0$ in equation (5.7b) we obtain

$$\frac{\partial^2 \omega(x_{cp},0)}{\partial y^2} = 2d\frac{w_2'(r_2)}{(x_{cp}+d)r_2} \tag{5.8}$$

which has constant sign for $|x_{cp}| < d$ and $|x_{cp}| > d$.

Notice that by equation (5.6)

$$\operatorname{sgn}\left(\frac{\partial\omega(d,0)}{\partial x}\right) = \operatorname{sgn}\left(\omega_1'(r_1(x,0))\right) \tag{5.9a}$$

$$\operatorname{sgn}\left(\frac{\partial\omega(-d,0)}{\partial x}\right) = -\operatorname{sgn}\left(\omega_2'(r_1(x,0))\right) \tag{5.9b}$$

which is useful for determining the sign of $\frac{\partial^2\omega(x,0)}{\partial x^2}$.

First we consider the case $\omega_1' > 0$, $\omega_2' > 0$. Then, $\frac{\partial\omega(x,0)}{\partial x}$ goes from negative to positive value as x is increased from $-d$ to d. Hence, an odd number of critical points exists. The first critical point will then have $\frac{\partial^2\omega(x,0)}{\partial x^2} > 0$ and if more exist the sign will alternate. The determinant of the Hessian of the vorticity is then from equation (5.7b) and equation (5.8) positive at the first critical point and then with alternating sign. Hence, the first critical point is a local extremum and then of alternating type.

In the case of $\omega_1' < 0$, $\omega_2' > 0$ if critical points exists for $x > d$ the first will have $\frac{\partial^2\omega(x,0)}{\partial x^2} < 0$ by equation (5.9a) and $\frac{\partial^2\omega(x,0)}{\partial y^2} < 0$ by equation (5.8) hence the product again being positive. Since only $\frac{\partial^2\omega(x,0)}{\partial x^2}$ alternates sign the first appearing critical point for $x > d$ is an extremum and then of alternating type. Simililarly for $x < -d$ where if a critical point exists the first has $\frac{\partial^2\omega(x,0)}{\partial x^2} < 0$ by equation (5.9b) and $\frac{\partial^2\omega(x,0)}{\partial y^2} < 0$ for all $x < -d$. Hence, decreasing x from $-d$ the first appearing critical point (if it exists) is an extremum and then of alternating type.

The critical points of the stream lines are computed as well

$$\frac{\partial\psi}{\partial x} = (x+d)\,\frac{\psi_1'(r_1)}{r_1} + (x-d)\,\frac{\psi_2'(r_2)}{r_2} \tag{5.10a}$$

$$\frac{\partial\psi}{\partial y} = y\left(\frac{\psi_1'(r_1)}{r_1} + \frac{\psi_2'(r_2)}{r_2}\right) \tag{5.10b}$$

Since the equations have similar structure as equations 5.5 and the same assumptions apply to the stream function as to the vorticity by A-D and I-IV, similar conclusions apply about location, existence and type of critical points. □

5.1 Topology of two Gaussian vortices

With one point vortex as initial condition, $\omega_0 = \Gamma_0 \delta(\boldsymbol{x})$ the Navier - Stokes equation can be solved analytically relying on rotational symmetry yielding [92] the Lamb - Oseen vortex

$$\omega(r,t) = \frac{\Gamma_0}{\pi\sigma^2} e^{-\frac{r^2}{\sigma^2}}, \qquad u_\theta = \frac{\Gamma_0}{2\pi r}\left(1 - e^{-\frac{r^2}{\sigma^2}}\right), \quad u_r = 0, \tag{5.11}$$

with

$$\sigma = \sqrt{4\nu t}. \tag{5.12}$$

This means that 'far away' i.e. for $\frac{r^2}{\sigma^2} >> 1$ then $u_\theta \approx \frac{\Gamma_0}{2\pi r}$ which is the velocity generated by a corresponding point vortex. The Lamb - Oseen vortex is stable for any Γ as proved by Gallay & Wayne [39].

The streamfunction can then be computed from equation (5.11) using $\omega = -\Delta\psi$ or $\frac{\partial}{\partial r}\psi = -u_\theta$

$$\psi(r) = -\frac{\Gamma_0}{2\pi}\left(\ln(r) - \int_r^\infty \frac{e^{-\frac{\hat{r}^2}{\sigma^2}}}{\hat{r}} d\hat{r}\right). \tag{5.13}$$

The integral does not have a closed form solution. The analysis is carried out considering the velocity field which does have a closed form. However, for numerics a formula of the stream function is still useful. To implement in Matlab the substitution $t(r) = \frac{r^2}{\sigma^2}$ is performed leading to

$$\psi(r) = -\frac{\Gamma_0}{2\pi}\left(\ln(r) - \frac{1}{2}\int_{\frac{r^2}{\sigma^2}}^\infty \frac{e^{-t}}{t} dt\right). \tag{5.14}$$

where the integral now can be evaluated in Matlab using expint($\frac{r^2}{\sigma^2}$). Notice, that

$$\frac{\mathrm{d}}{\mathrm{d}r}\left(-\frac{1}{2}\mathrm{expint}\left(\frac{r^2}{\sigma^2}\right)\right) = -\frac{e^{-\frac{r^2}{\sigma^2}}}{r}. \tag{5.15}$$

It can be easily verified that a Gaussian vortex fulfills the properties *(A)-(D)* and *(I)-(IV)*.

If the initial vorticity consists of a weighted sum of delta functions no closed form solution can be expected.

Gallay [38] proved that (under certain conditions) a sum of point vortices as initial conditions the Navier - Stokes equations the solution converge to a sum

of Lamb - Oseen vortices for viscosity going to zero and for some finite time. A related result was obtained by Marchioro [72].

A model that takes into account diffusion of vorticity of point vortices is the multi Gaussian model also known as the core-growth model. Core-growth model with few vortices have been investigated in [60, 61, 59]. Here, the center of the Gaussian vortices move in a field prescribed by the other vortices (similar to inviscid point vortex dynamics) and the 'core' of the vortices diffuse as predicted by the Lamb- Oseen solution of a single vortex. In the multi Gaussian model the vorticity and velocity are calculated from a superposition of Gaussian terms. This is not an exact solution of the Navier - Stokes equations but we will here regard it as a simple model allowing some viscous effects. A multi Gaussian model with a few number of vortices can be analysed in detail and may show qualitative information that is valuable also for more realistic flow.

In [60, 59] the instantaneous streamlines and vorticity contours of three Gaussian vortices are investigated with some constraints on the choice of the circulation. The three circulations are chosen such that the three vortices stay aligned and the whole configuration rotates with time dependent rotation rate. Interestingly the vortices configuration does not move in inviscid flow, hence the observed rotation is viscously induced. The multi Gaussian model is compared to numerical solution of the two - dimensional Navier - Stokes equations and they have similar behaviour in many aspects. However, the flow of the Navier - Stokes equations seem more 'distorted' and 'entangled'.

Vortex merging is a complicated process and the literature on the subject is huge. Cerretelli & Williamson [23] describe vortex merging through four stages, where diffusive growth is the first. Brandt & Nomura [12] also discuss four vortex merging stages in two - dimensional flow for symmetric vortex merging depending on the vorticity gradient and rate of strain. In [13] the situation with asymmetric vortices is investigated. A merging criteria for two-dimensional co-rotating vortices has been proposed by Meunier et al. [74]. For the experimental part the early stage vortices are found to agree well with Gaussian vortices. In [75] two point vortices and two Gaussian vortices are discussed in relation to vortices behind an aircraft, which is also discussed by Jacquin et al. [57]. Even when restricting the attention to inviscid flow, vortex merging is a complicated phenomena as seen in the experiments of Amoretti et al. [7].

We consider two Gaussian vortices. Vortex 1 is situated at $(-d, 0)$ and vortex 2 is situated at $(d, 0)$. We allow two different σ 's corresponding to the vortices being created at different times. We assume $\Gamma_2 > 0$ which does not exclude any case - we can still investigate opposite signed circulations of the two vortices as well as circulations with the same sign. The vorticity is follwing the core -

growth model

$$\tilde{\omega} = \frac{\Gamma_1}{\pi\sigma_1^2} e^{-\frac{(X+d)^2+Y^2}{\sigma_1^2}} + \frac{\Gamma_2}{\pi\sigma_2^2} e^{-\frac{(X-d)^2+Y^2}{\sigma_2^2}} . \tag{5.16}$$

Making the scaling $x = dX$, $y = dY$, $\omega = \frac{\sigma_2^2}{\pi\Gamma_2}\tilde{\omega}$, $u = \frac{2\pi}{d\Gamma_2}U$, $v = \frac{2\pi}{d\Gamma_2}V$ and defining the parameters

$$\alpha = \frac{\Gamma_1}{\Gamma_2}, \quad \beta = \frac{d^2}{\sigma_2^2}, \quad \delta = \frac{d^2}{\sigma_1^2} \tag{5.17}$$

the vorticity becomes

$$\omega = \alpha\frac{\delta}{\beta} e^{-\delta\left((x+1)^2+y^2\right)} + e^{-\beta\left((x-1)^2+y^2\right)}, \tag{5.18}$$

In a similar way the stream function consistent of two terms of the form of equation (5.14) becomes

$$\begin{aligned}\psi =& \alpha \ln\left((x+1)^2+y^2\right) + \ln\left((x-1)^2+y^2\right) \\ & - \alpha\,\mathrm{expint}\left(\delta\left((x+1)^2+y^2\right)\right) - \mathrm{expint}\left(\beta\left((x-1)^2+y^2\right)\right) .\end{aligned} \tag{5.19}$$

Notice that the stream function and the vorticity is invariant to $y \to -y$ so there is mirror symmetry in the line $y = 0$ when considering the contours of ψ and ω.

The vorticity field and the stream function then depend on the three independent parameters α, β and δ where the two latter are always positive and $\alpha \neq 0$. A three parameter dynamical system can in general contain very exotic behaviour. Our goal is to study the topology of the instantaneous streamlines and the vorticity of this system. We perform the analysis at $t = 0$ but for all possible parameter combinations. Later, we revisit the dynamical model with moving vortex centers and use the topologies at $t = 0$ for instantaneous streamlines and vorticity contours at subsequent times.

5.1.1 Topology of the streamlines of two Gaussian vortices

We now analyse the streamline topology of two Gaussian vortices, equation (5.19) which is facilitated by the analysis of lemma 5.1. Hence, the critical points are

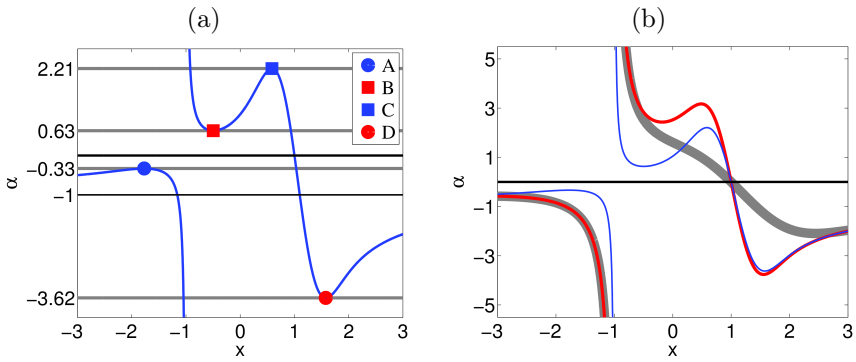

Figure 5.4: Example of $f(x, \beta, \delta)$ for different values of parameters. (a) $(\beta, \delta) = (5, 3)$ and the different regimes of α leading to the same topology bounded by bifurcation lines (grey). (b) Some typical graphs of $f(x, \beta, \delta)$. Grey curve corresponds to $(\beta, \delta) = \left(1, \frac{1}{2}\right)$, blue curve corresponds to $(\beta, \delta) = (5, 3)$, red curve corresponds to $(\beta, \delta) = \left(5, \frac{1}{2}\right)$

computed by solving $\frac{\partial}{\partial x}\psi = 0$. Fortunately, the derivative of ψ can be written in closed form - a consequence of equation (5.15).

$$-\frac{\partial \psi}{\partial x} = \alpha \frac{1}{x+1}\left(1 - e^{-\delta\left((x+1)^2\right)}\right) + \frac{1}{x-1}\left(1 - e^{-\beta\left((x-1)^2\right)}\right). \tag{5.20}$$

Despite the simplification described in the previous section it is still a three parameter problem to determine the topology of the streamlines of two Gaussian vortices. A kind of 'decoupling' of the parameters can be obtained by rewriting $\frac{\partial \psi(x_{cp},0)}{\partial x} = 0$ as

$$\alpha = f(x_{cp}, \beta, \delta), \tag{5.21}$$

with

$$f(x, \beta, \delta) = -\frac{(x+1)\left(1 - e^{-\beta(x-1)^2}\right)}{(x-1)\left(1 - e^{-\delta(x+1)^2}\right)}, \tag{5.22}$$

which is valid since $x = -1$ is not a critical point. See figure 5.4 for typical graphs of f. The interpretation is the following; for a given, fixed (β, δ) there is a unique graph of $y = f(x, \beta, \delta)$ for varying x through $\mathbb{R} \setminus \{-1, 1\}$. A value of α corresponds to a line $y = \alpha$. Hence, an intersection between the two graphs corresponds to a critical point. This means we only need to study local minima, local maxima and behaviour at the limits $\pm\infty$ of f as β and δ is varied. Then, we know the bifurcation points of (α, β, δ). Typical streamlines are seen in figure 5.5.

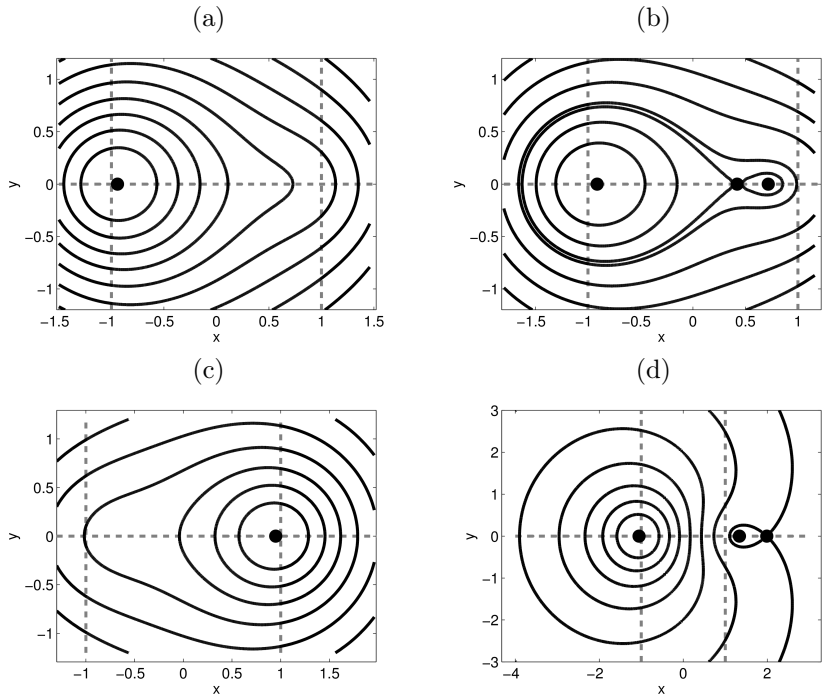

Figure 5.5: Streamlines for $(\beta, \delta) = (5, 3)$ and varying α. Critical point determined from figure 5.4 are marked by a dot. (a) $\alpha = 3$. (b) $\alpha = 2$.(c) $\alpha = \frac{1}{2}$, (d) $\alpha = -3$.

In figure 5.4a the graph of $f(x, \beta, \delta)$ is shown for $(\beta, \delta) = (5, 3)$. Four local extrema of exist denoted by A, B, C and D. For $\alpha > 2.21$ one critical point exist. It is of center type and with $-1 < x_{cp} < 1$. For large α the critical point approaches $(x, y) = (-1, 0)$. This streamline topology is shown in figure 5.5a. $\alpha = 2.21$ is the bifurcation value where a cusp appears. At $2.21 > \alpha > 0.63$ three critical points exist on the line $y = 0$ in the strip $-1 < x < 1$ with two centers and a saddle in between. See also figure 5.5b. For $0 < \alpha < 0.63$ the vortex strength of the vortex at -1 dominates sufficiently such that only a critical exist which approaches $x = 1$ as α goes to 0 - see figure 5.5c. Hence, for fixed (β, δ) and large α and for α approaching zero, one vortex dominates. For negative α close to 0 there is still only one center, the manifestation of one vortex having dominant strength. However, now the center is located at $x > 1$. At $\alpha = -0.33$ a bifurcation happens such that for $-0.33 > \alpha > -1$ three critical points exist. A center and a saddle appear for $x < -1$ with the center being closest to $x = -1$ As $\alpha \to -1^+$ the saddle point moves $-\infty$ and for $\alpha < -1$ it has disappeared to reappear on the positive x-axis for large x-value. See figure 5.5d. At $\alpha = -3.62$ the saddle and center on the positive x-axis annihilates such that for $\alpha < -3.62$ a center at $x < -1$ is the only critical point. Hence, this is again a region of one vortex dominating the flow. As $\alpha \to -\infty$ the center approaches $(x, y) = (-1, 0)$. Hence the case $-\Gamma_1 >> \Gamma_2$ resembles the case with only one vortex.

Some properties in the lemma below prove that the graphs really are typical.

Lemma 5.2 *Analytical results about topology of the streamlines.*

(P1) *For $|\alpha|$ large and $|\alpha|$ small there is exactly one critical point of the streamlines. For $\alpha \to 0$ there is a critical point approaching $(x, y) = (1, 0)$ and for $\alpha \to \pm\infty$ there is a critical point approaching $(x, y) = (-1, 0)$ for any fixed (β, δ).*

(P2) *At least three critical points of the streamlines are guaranteed for α close to but not equal to -1, $\forall \beta, \delta > 0$.*

(P3) *For large (β, δ) there are at least three critical points of the streamlines for α close to 1.*

(P4) $f(-x, \delta, \beta) = \frac{1}{f(x, \beta, \delta)}$.

(P5) *$A(\beta, \delta)$ and $D(\beta, \delta)$ exist $\forall \beta, \delta > 0$ and $-1 < A(\beta, \delta) < 0$, $D(\beta, \delta) < -1$.*

(P6) $\lim_{x \to \pm\infty} f(x, \beta, \delta) = -1$.

(P7) $f(x, \beta, \delta) \gtrless 0$, $\frac{\partial}{\partial \beta} f(x, \beta, \delta) \gtrless 0$, $\frac{\partial}{\partial \delta} f(x, \beta, \delta) \lesseqgtr 0$ *for* $|x| \lesseqgtr 1$.

We postpone the proof of lemma 5.2 to the end of the section and first discuss some consequences.

Property $(P1)$ means, that if one vortex strength is much larger than the other, then there is only one critical point. However, 'much larger' may depend on (β, δ). Then the critical point is located close to the position of the original 'strong vortex' and it is of center type. This is not seen in the point vortex model having singularities at the point vortices. For Gaussian vortices, the bounded value at the vortex centers means the global velocity field can be completely dominated by one vortex.

Property $(P2)$ means that near $\alpha = -1$ more exotic behaviour is guaranteed with at least three critical points. In case of exactly three critical points, they are all aligned with a center for $x_1 < -1$, $x_2 > 1$ and a saddle for $x_3 < x_1$ if $\alpha > -1$ and $x_3 > x_1$ for $\alpha < -1$. This is related to property $(P6)$ - see also figure 5.4.

By equation (5.17) β, δ growing means the point vortex case is approached since the Gaussian distribution is then more concentrated like a point vortex. By property $(P3)$ the guarantee of at least three critical point for large β, δ and comparable vortex strengths is similar to the point vortex case, interpreting the vortex centers as critical points.

Property $(P4)$ means a local maximum at $f(x_0, \beta, \delta)$ corresponds to a local minimum $f(-x_0, \delta, \beta)$. Relating to figure 5.4 this means $B(\beta, \delta) = \frac{1}{C(\delta,\beta)}$ and $A(\beta, \delta) = \frac{1}{D(\delta,\beta)}$ Hence, there is no need to study the behaviour in the quadrant $\beta > 0$, $\delta > 0$ but merely the triangle $\beta > \delta > 0$. The physical interpretation is that for a given $\Gamma_1, \Gamma_2, \sigma_1, \sigma_2$ then interchanging circulation and variances, $\tilde{\Gamma_1} = \Gamma_2, \tilde{\Gamma_2} = \Gamma_1, \tilde{\sigma_1} = \sigma_2, \tilde{\sigma_2} = \sigma_1$ the same physical situation occurs which is counted twice letting the parameters vary unconstrained.

Properties $(P5)$ - $(P7)$ are useful for getting an overview on numerics as parameters are varied.

We now proceed with more numerical results. Tracking the local extrema of f for varying (β, δ) simplifies finding the bifurcation points significantly. An important numerical result is that at most three critical points are observed for any set of parameters (α, β, δ).

In figure 5.4b three graphs of f are shown for varying (β, δ). Consider the grey curve. Numerics show there are no local extrema for positive f and analysis guarantees that f attain any value in $\mathbb{R}^+$. Hence, for any $\alpha > 0$ there is one critical point of center type. Its location approaches $x = -1$ for large α and

$x = -1$ for small α. Increasing β to 5 gives the red curve. Now a region with three critical points exist. It is worth noticing that the red curve is above the grey curve for $|x| < 1$ and the red curve is below the grey curve for $|x| > 1$ representing the sign of $\frac{\partial f}{\partial \beta}$. The blue curve corresponds to $(\beta, \delta) = (1, \frac{1}{2})$, hence a decrease in δ compared to the red curve. Still a region of three critical points exist for $\alpha > 0$. For $|x| < 1$ the blue curve is below the red curve and for $|x| > 1$ the blue curve is above the red curve illustrating the sign of $\frac{\partial f}{\partial \delta}$. From the sign of the derivatives of f one can see that if A is the only extremum for $x < -1$, and if D is the only extremum for $x > 1$ then $\frac{\partial A(\beta,\delta)}{\partial \beta} < 0$, $\frac{\partial A(\beta,\delta)}{\partial \delta} > 0$, $\frac{\partial D(\beta,\delta)}{\partial \beta} < 0$, $\frac{\partial D(\beta,\delta)}{\partial \delta} > 0$. This means that for $0 > \alpha > -1$ the region of three critical points increases by increasing δ or decreasing β while for $\alpha < -1$ the region of three critical points increases for decreasing δ or increasing β.

The bifurcation points in (α, β, δ) - space are surfaces. We need to keep track of four such surfaces corresponding to A, B, C, D. Since each of the four surfaces can be formulated as a function of only (β, δ), we show slices of (α, β, δ) - space with constant α. In figure 5.6a we consider the behaviour for $\alpha > 0$ exemplified by $\alpha_{\text{crit}} = 1.9$. The blue curves is the level curve of $C(\beta, \delta) = 1.9$ and the red curve is the level curve for $B(\beta, \delta) = 1.9$. The two curves meet at the annihilation/creation point of B and C. Hence, there is one curve dividing (β, δ) in two regions with different topologies. In figure 5.6b we show level curves of B and C for varying values of α_{crit}. The creation/annihilation of B and C form a line. Below this line there are exactly one critical point of the streamlines regardless the value of α. Notice, that the grey curve in figure 5.4b has (β, δ) - values from this region.

For A and D there is no annihilation curve - they live robustly in different parts of parameter space by property $(P5)$ of lemma 5.2. In figure 5.7a the level curve corresponding to $\alpha_{\text{crit}} = -0.3$ is displayed, and in 5.7b the level curves are shown for various α_{crit}. It is clear that the value of A increases as δ increases consistent with property $(P7)$ of lemma 5.2. A seems 'invariant' to changes in β. However, this is also observed on figure 5.4b comparing the grey and red curve. The behaviour of D is shown in figure 5.8 for changing parameters.

A common characteristic of figures 5.6, 5.7, 5.8 is that for a fixed α_{crit}, for small (β, δ) the topology with only one critical point of the streamlines dominates and for large (β, δ) three critical points exist matching the point vortex case if the singular points are interpreted as centers.

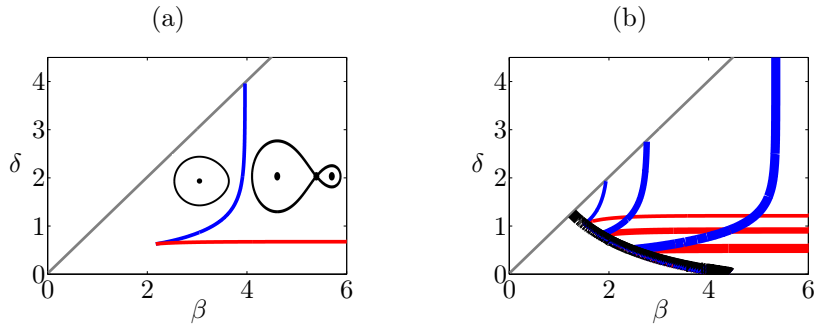

Figure 5.6: Investigation of streamlines for $\alpha > 0$. In (a) the blue curve shows $C(\beta, \delta) = \alpha_{\text{crit}}$ and the red curve shows $B(\beta, \delta) = \alpha_{\text{crit}}$ with $\alpha_{\text{crit}} = 1.9$ - compare to figure 5.4. In (b) similar curves are shown with thicker curves corresponding to larger value of α_{crit} along with the black curve showing where B and C vanish. For (β, δ) below the black curve exists exactly one critical point for any $\alpha > 0$.

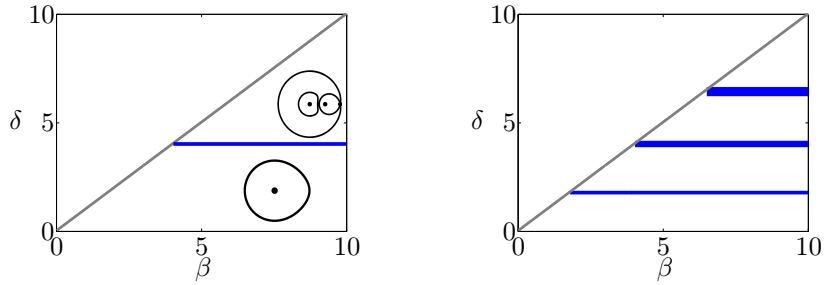

Figure 5.7: Investigation of streamlines for $-1 < \alpha < 0$. With $\alpha_{\text{crit}} = -0.3$, $D(\beta, \delta) = \alpha_{\text{krit}}$ is shown. To the right are increasing α_{crit} corresponding to increasing curve width.

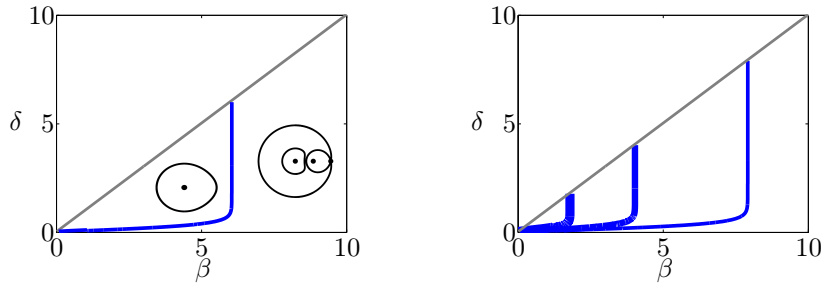

Figure 5.8: Investigation of streamlines for $\alpha < -1$. $\alpha_{\text{crit}} = -3.8$. Increasing thickness correspond to increasing value of α_{crit}.

PROOF. We now prove lemma 5.2.

First considering equation (5.22) notice that $f < 0$ for $|x| > 1$, and $f > 0$ for $|x| < 1$. By direct computation, observe f has the property

$$f(-x, \delta, \beta) = \frac{1}{f(x, \beta, \delta)}\,, \tag{5.23}$$

Notice

$$\lim_{x \to \pm\infty} f(x, \beta, \delta) = -1\,. \tag{5.24}$$

Using L'Hospital's rule

$$\lim_{x \to 0^{\pm}} \frac{1 - e^{-kx^2}}{x} = 0 \tag{5.25}$$

for constant, positive k. Then,

$$\lim_{x \to 1} f(x, \beta, \delta) = 0 \tag{5.26a}$$

$$\lim_{x \to -1^{\pm}} f(x, \beta, \delta) = \pm\infty\,. \tag{5.26b}$$

This means that for $\alpha \to 0$ there is a critical point approaching $(x, y) = (1, 0)$ and for $\alpha \to \pm\infty$ there is a critical point approaching $(x, y) = (-1, 0)$ for fixed (β, δ).

Since f is surjective on $\mathbb{R} \setminus \{0\}$ then at least one critical point exist for any allowed α. Except for the divergence at $x = -1$ f is bounded. This means that for fixed (β, δ) and for sufficiently large $|\alpha|$ there is only one critical point with location close to $x = -1$. Since f is continuous for $|x| < 1$ where $f > 0$ and for $|x| > 1$ where $f < 0$, and considering equation (5.26) then for $\alpha \to 0$ only one critical point exists and it is located close to $x = 1$.

Analytical statements about local maxima and minima of f are not easily obtained from the complicated expression for $\frac{\partial f}{\partial x}$. However, we may obtain information about existence of local extrema depending on how f approaches

-1 at $\pm\infty$. First consider $x > 2$ to investigate the behaviour at large x

$$\begin{aligned} -f(x,\beta,\delta) &= \frac{(x+1)\left(1-e^{-\beta(x-1)^2}\right)}{(x-1)\left(1-e^{-\delta(x+1)^2}\right)} \\ &> \frac{x+1}{x-1}\left(1-e^{-\beta(x-1)^2}\right) \\ &= 1+\frac{2}{x-1}-e^{-\beta(x-1)^2}-\frac{2}{x-1}e^{-\beta(x-1)^2} \\ &> 1+\frac{2}{x-1}-3e^{-\beta(x-1)^2} \\ &= 1+\frac{1}{x-1}\left(2-3\frac{x-1}{e^{\beta(x-1)^2}}\right) \end{aligned} \tag{5.27}$$

(5.28)

Since

$$\lim_{x\to\infty}\frac{x-1}{e^{\beta(x-1)^2}} = 0 \tag{5.29}$$

$-f(x) > 1$ for large x. Since f is larger than -1 as $x \to 1$ and f approaches -1 from below for increasing x this means at least one local minimum of f exists with function value less than -1.

Similarly we investigate the behaviour for x negative with large absolute value. The easiest argument for existence of a local maximum is then using equation (5.23) since inequality (5.28) holds for any positive β and δ. This means that for any (β,δ) then for α close to -1 three critical points are guaranteed.

One could wonder if a similar conclusion applies to some $\alpha > 0$. It seems at least likely in the limit where a point vortex model is approached i.e. for the vortices being 'far apart'. A region with at least three critical points for $\alpha > 0$ is guaranteed if there exists a region with positive slope of f for $-1 < x < 1$. By straightforward calculation

$$\frac{\partial f(0,\beta,\delta)}{\partial x} = \beta e^{-\beta}\left(e^{-\delta}-1\right)+\delta e^{-\delta}\left(e^{-\beta}-1\right)+e^{-\beta-\delta}-e^{-\delta}-e^{-\beta}+1 \tag{5.30}$$

which is positive for large (β,δ). Since

$$f(0,\beta,\delta) = \frac{1-e^{-\beta}}{1-e^{-\delta}} \tag{5.31}$$

which approaches 1 for large (β,δ) this means that for large (β,δ) there are at least three critical points for α close to 1.

To analyse the behaviour of f as parameters are varied the following derivatives are calculated

$$\frac{\partial f(x,\beta,\delta)}{\partial \beta} = -\left(x+1\right)\left(x-1\right)\frac{e^{-\beta(x-1)^2}}{1-e^{-\delta(x+1)^2}} \tag{5.32}$$

$$\frac{\partial f(x,\beta,\delta)}{\partial \delta} = \frac{\left(x+1\right)^3\left(1-e^{-\beta(x-1)^2}\right)e^{-\delta(x+1)^2}}{\left(x-1\right)\left(1-e^{-\delta(x+1)^2}\right)}\,. \tag{5.33}$$

Hence, the sign of $\frac{\partial f}{\partial \beta}$ and f are identical while $\frac{\partial f}{\partial \delta}$ has opposite sign. □

5.2 Topology of the vorticity contours

Now the topology of the vorticity contours of two Gaussian vortices are investigated by same means as the streamline topology.

From equation (5.18) the x - derivative of ω is computed.

$$\frac{\partial \omega}{\partial x} = -2\left(\alpha\frac{\delta^2}{\beta}\left(x+1\right)e^{-\delta\left((x+1)^2+y^2\right)} + \beta\left(x-1\right)e^{-\beta\left((x-1)^2+y^2\right)}\right) \tag{5.34}$$

From lemma 5.1 the critical points are determined from the zeros of $\frac{\partial \omega(x,0)}{\partial x}$

$$0 = -2\left(\alpha\frac{\delta^2}{\beta}\left(x+1\right)e^{-\delta(x+1)^2} + \beta\left(x-1\right)e^{-\beta(x-1)^2}\right)\,. \tag{5.35}$$

Since we want to compare the vorticity and streamline topology, it seems useful to isolate α, using $x=-1$ is not a critical point.

$$\alpha = g(x,\beta,\delta)\,, \tag{5.36}$$

with g being

$$g(x,\beta,\delta) = -\frac{\beta^2\left(x-1\right)}{\delta^2\left(x+1\right)}e^{-\beta(x-1)^2+\delta(x+1)^2}\,. \tag{5.37}$$

Now, the limiting behaviour of g a long with knowledge of local extrema completely determines the topology similar to f in the streamline case. The conclusions for the vorticity are similar in many aspects. Graphs of g and typical

vorticity conturs are shown in figure 5.9. It turns out the analysis is particularly simple for $\beta = \delta$. We will treat this case separately in section 5.2.0.1. First, we will highlight some useful analytical results relating to the vorticity contour topology.

Lemma 5.3 *Analytical results about topology of the vorticity contours.*

(W1) *For $|\alpha|$ large and small $\alpha > 0$ there is only one critical point of the vorticity contours. For $\alpha \to 0^+$ there is a critical point approaching $(x, y) = (1, 0)$ and for $\alpha \to \pm\infty$ there is a critical point approaching $(x, y) = (-1, 0)$ for any fixed (β, δ).*

(W1) *For $x > 1$ exists exactly one local extremum, D', being a local minimum. Hence, for $D' < \alpha < 0$ exists three critical points of the vorticity contours, with centers at $x_1 < -1$, $x_2 > 1$ and a saddle at $x_3 > x_2$. For $\alpha < D'$ exists exactly one critical point. It is of center type and is located at $x_1 < -1$.*

(W3) *For $\beta + \delta > 1$ exists a region of $\alpha > 0$ containing $\frac{\beta^2}{\delta^2} e^{-\beta+\delta}$ where exactly three critical points of the vorticity contours are guaranteed. All critical points occur for $|x| < 1$ with a saddle point surrounded by two centers.*

(W4) *Exactly three critical points of the vorticity contours are guaranteed for $\alpha \to 0^-$, $\forall$ fixed $\beta, \delta > 0$.*

(W5) $\lim_{x\to\pm\infty} g(x, \beta, \delta) = 0$ *for $\beta \leq \delta$.*

(W6) *For $x < -1$ g is monotonically increasing and surjective on $(0, -\infty)$ for $\beta > \delta$.*

(W7) $g(-x, \delta, \beta) = \frac{1}{g(x,\beta,\delta)}$.

(W8) $\frac{\partial D'}{\partial \delta} < 0$ *for* $\delta > \frac{1}{2}$.

We save the proof to the end of the section. The results in lemma 5.3 are often stronger than in 5.2. A reason for this is the zeroes of $\frac{\partial g}{\partial x}$ are the zeroes of a third order polynomial. One zero correspond to D' and there may exist two more. If they exist they are located at $|x| < 1$ and corresponds to B' and C' in figure 5.9.

We have a good understanding of the vorticity contour topology from lemma 5.3. Many of the properties have an analogue in lemma 5.2. As for the streamlines we only need to study $\beta \geq \delta$ due to property $(W7)$.

One may wonder, why no A' exists corresponding to A in the streamline case. A' does not exist for $\beta > \delta$ and D' does not exist for $\beta < \delta$. Hence, in case of

three critical points of the vorticity contours for $\alpha < 0$ the saddle point always occur for $x > 1$ for $\beta > \delta$ while for the streamlines this depends on whether α is smaller or larger than -1.

In figure 5.12 graphs of f and g are shown for the same parameter values. The region with three critical points are much larger for the vorticity than for the streamlines. The local maximum of the blue curve for $|x| < 1$ and the local minimum for $|x| > 1$ cannot be seen in figure 5.12a.

In figure 5.10a contour of $B' = C' = 8$ is shown dividing (β, δ)- plane in two regions with different topologies for $\alpha_{\text{crit}} = 8$. In 5.10b the behaviour is shown for varying value of α. As for the streamlines, a region exists with no critical points of the vorticity contours for any $\alpha > 0$ bounded by the black curve and the axes in 5.10b. In figure 5.11 the behaviour of D' is shown.

It is clear that the streamline and vorticity contours share much behaviour. However, the topologies with three critical points cover a much larger part of parameter space for the vorticity contours than for the streamlines which is illustrated in figure 5.12, figure 5.13 and figure 5.19.

Proof. We now prove lemma 5.3. By direct computation on equation (5.37)

$$g(-x, \delta, \beta) = \frac{1}{g(x, \beta, \delta)}\,, \tag{5.38}$$

so only $\delta < \beta$ need to be considered. Notice $g > 0$ for $|x| < 1$ and $g < 0$ for $|x| > 1$ and

$$\lim_{x \to 1} g(x, \beta, \delta) = 0 \tag{5.39a}$$

$$\lim_{x \to -1^{\pm}} g(x, \beta, \delta) = \pm\infty\,. \tag{5.39b}$$

The limiting behaviour depends on the value of the parameters as can be seen from writing g as

$$g(x, \beta, \delta) = -\left(\frac{\beta}{\delta}\right)^2 \frac{(x-1)}{(x+1)} e^{-\delta\left(\left(\frac{\beta}{\delta}-1\right)x^2 - 2\left(\frac{\beta}{\delta}+1\right)x + \frac{\beta}{\delta} - 1\right)} \tag{5.40}$$

where the sign of the leading term, $\left(\frac{\beta}{\delta} - 1\right) x^2$, in the exponential determines the behaviour for large $|x|$. Hence,

$$\lim_{x \to \pm\infty} g(x, \beta, \delta) = -\infty\,, \quad \text{for } \frac{\beta}{\delta} < 1\,. \tag{5.41}$$

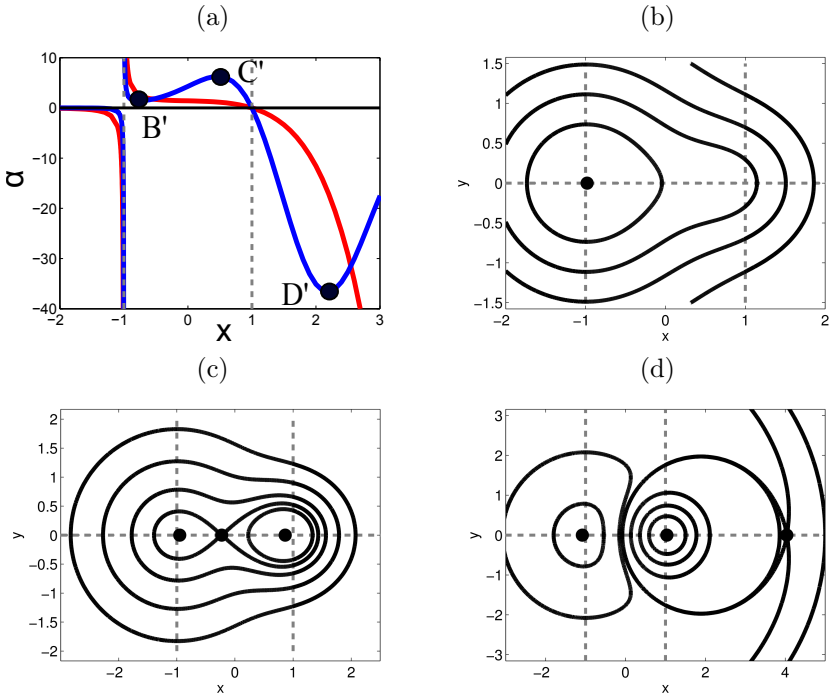

Figure 5.9: (a) $y = g(x, \beta, \delta)$ with $(\beta, \delta) = (0.5, 0.4)$ for the red curve and $(\beta, \delta) = (1.3, 0.4)$ for the blue curve. The blue curve has three local extrema - two of them are for $|x| < 1$ and one for $x > 1$. The red curve only has a local extrema, located at $x > 1$ and not visible on the figure. (b) - (d) shows the possible topology of the contours of ω for $\beta > \delta$. $(\beta, \delta) = (1.3, 0.4)$ and for (b) $\alpha = 7$, for (c) $\alpha = 3$ and for (d) $\alpha = -1$.

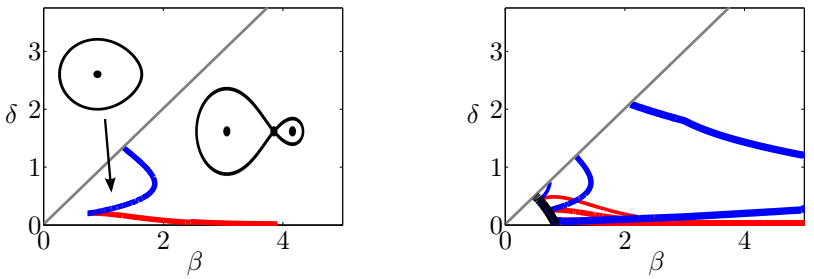

Figure 5.10: Investigation of vorticity contours for $\alpha > 0$. $\alpha_{\text{crit}} = 8$ left. Right $\alpha_{\text{crit}} = 1.5, 5, 100$ with increasing value for increasing line width.

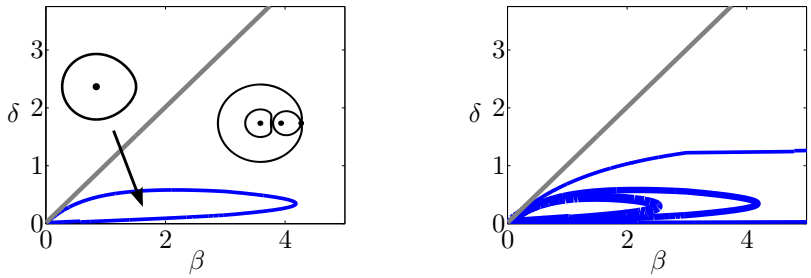

Figure 5.11: Investigation of vorticity contours for $\alpha < 0$. $\alpha = -100$ left. and $\alpha = -50, -100, -10000$ right.

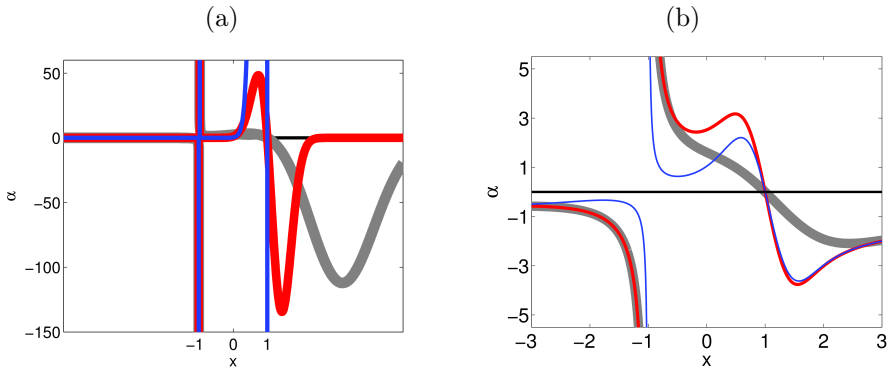

Figure 5.12: Graphs of g in (a) and f in (b) for the same parameter values. Grey curve corresponds to $(\beta, \delta) = \left(1, \frac{1}{2}\right)$, blue curve corresponds to $(\beta, \delta) = (5, 3)$, red curve corresponds to $(\beta, \delta) = \left(5, \frac{1}{2}\right)$. The region with three critical points fills more of parameter space for the vorticity contours than the streamlines.

For $\frac{\beta}{\delta} = 1$ the leading term vanishes so a simpler case arise. We will treat this case separately in section 5.2.0.1.

The derivative of g is simple enough to analyse

$$g'_x(x,\delta,\beta) = -2\frac{\beta^2 e^{-\beta(x-1)^2+\delta(x+1)^2}}{\delta\,(x+1)^2}p(x,\beta,\delta) \tag{5.42}$$

with $p(x,\beta,\delta)$ being a third order polynomial. This means that closed form solutions of the local extrema of g exists relying on the closed form solutions of a third order polynomial. However, these are not easy to analyse.

One or three local extrema of g exists since we are looking for real solutions of a third order polynomial.

$$p(x,\beta,\delta) = \left(\frac{\beta}{\delta}-1\right)x^3 - \left(\frac{\beta}{\delta}+1\right)x^2 + \left(1-\frac{\beta}{\delta}\right)x - \frac{1}{\delta} + \frac{\beta}{\delta} + 1\,. \tag{5.43}$$

It is convenient to use Descartes' rule of sign when considering the number of real solutions. The rule states that the positive, real roots of a polynomial is the number of sign changes in the ordered sequence of coefficients in the polynomial or lower than this number by a multiple of two. Investigating the number of solutions for $x > 1$ can then be done by a shift $w = x - 1$, which leads to

$$p(w+1,\beta,\delta) = \left(\frac{\beta}{\delta}-1\right)w^3 + 2\left(\frac{\beta}{\delta}-2\right)w^2 - 4w - \frac{1}{\delta}\,. \tag{5.44}$$

which has one sign change since $\frac{\beta}{\delta} > 1$ and the number of sign changes in this sequence is then independent of the sign of $\left(\frac{\beta}{\delta}-2\right)$. Therefore, there is exactly one local extremum of g for $x > 1$. By studying g directly we could easily have seen that a local minimum exists, However, we have now proven that there is exactly one extremum for $x > 1$. For $x < -1$ we consider $z = -(x+1)$.

$$p(-(z+1),\beta,\delta) = -\left(\frac{\beta}{\delta}-1\right)w^3 - 2\left(\frac{\beta}{\delta}-2\right)w^2 - 4\gamma w - \frac{1}{\delta}\,. \tag{5.45}$$

Here, there are no sign changes so there are no local extremum for $x < -1$. g increases monotonically from a limit value at 0 for $x \to -\infty$ to $-\infty$ for $x \to -1$. Therefore, there is always exactly one minimum for g for $x > 1$, g spans $\mathbb{R}^-$ for $x < -1$ monotonically, and there may be zero or two critical points of g for $|x| < 1$.

The derivatives of g with respect to the parameters are

$$\frac{\partial g(x,\beta,\delta)}{\partial \beta} = \frac{\beta^2}{\delta^2}\frac{x-1}{x+1}e^{-\beta(x-1)^2+\delta(x+1)^2}p_1(x,\beta) \tag{5.46a}$$

$$\frac{\partial g(x,\beta,\delta)}{\partial \delta} = -\frac{\beta^2}{\delta^2}\frac{x-1}{x+1}e^{-\beta(x-1)^2+\delta(x+1)^2}p_2(x,\delta)\,. \tag{5.46b}$$

with

$$p_1(x,\beta) = x^2 - 2x + 1 - \frac{2}{\beta} = \left(x - \left(1+\sqrt{\frac{2}{\beta}}\right)\right)\left(x - \left(1-\sqrt{\frac{2}{\beta}}\right)\right) \tag{5.47}$$

and

$$p_2(x,\delta) = x^2+2x+1-\frac{2}{\delta} = \left(x - \left(-1+\sqrt{\frac{2}{\delta}}\right)\right)\left(x - \left(-1-\sqrt{\frac{2}{\delta}}\right)\right)\,. \tag{5.48}$$

Recall that $\frac{\partial f}{\partial \beta}$ and $\frac{\partial f}{\partial \delta}$ has constant sign for $|x|<1$ and $|x|>1$. In contrast, $\frac{\partial g}{\partial \beta}$ and $\frac{\partial g}{\partial \delta}$ also change sign as p_1 or p_2 change sign. However, increasing δ from a value larger than $\frac{1}{2}$ means that p_2 is positive for $x>1$. Therefore, $\frac{\partial g}{\partial \delta}<0$ for $\delta > \frac{1}{2}$ and $x>1$. Hence, the local minimum of g for $x>1$ decreases its value as δ is increased from values larger than $\frac{1}{2}$.

Similarly for $\beta < \frac{1}{2}$ then $p_1<0$ for $|x|<1$ meaning that g increases value for $|x|<1$ as β is increased to a value below $\frac{1}{2}$. For $|x|<1$ there can be zero or two local extrema. A sufficient criteria for two extrema is a point $|x|<1$ where $g'_x(x,\beta,\delta)>0$. Since

$$g'_x(0,\delta,\beta) = 2\frac{\beta^2}{\delta^2}e^{-\beta+\delta}\left(\beta+\delta-1\right)\,. \tag{5.49}$$

A sufficient criteria for two extrema for $|x|<1$ is $\beta+\delta>1$. Comparing to equation (5.30) we may suspect two extrema in a larger parameter domain for the vorticity than for the streamlines. This is validated by the numerics. Also, for the vorticity three critical points are guaranteed if either δ or β is larger than one. For the streamlines both β and δ has to be large. □

5.2.0.1 Vorticity contour topology for $\beta = \delta$

Now we consider $\beta = \delta$. Denote

$$h(x, \beta) = g(x, \beta, \beta) = -\frac{x-1}{x+1} e^{4\beta x} . \tag{5.50}$$

We notice the implication from equation (5.38)

$$h(-x, \beta) = \frac{1}{h(x, \beta)} . \tag{5.51}$$

Hence, a local maximum of h at x means a local minimum of h at $-x$ and vice versa.

$$\lim_{x \to \infty} h(x, \beta) = -\infty \tag{5.52a}$$

$$\lim_{x \to -\infty} h(x, \beta) = 0 \tag{5.52b}$$

$$\lim_{x \to -1^{\pm}} h(x, \beta) = \pm\infty . \tag{5.52c}$$

The derivative of h is

$$\frac{2}{(x+1)^2} e^{4\beta x} \left(-2\beta x^2 + 2\beta - 1\right) \tag{5.53}$$

which has two zeros for $\beta > \frac{1}{2}$

$$x_{\pm} = \pm\sqrt{1 - \frac{1}{2\beta}} \tag{5.54}$$

appearing for $|x| < 1$. $x_+ = -x_-$ was also expected from equation (5.51). The extrema are denoted B' and C' - see figure 5.14

At the bifurcation value $\beta = \frac{1}{2}$ the critical value of x is 0 and $h(0, \frac{1}{2}) = 1$. In case of two local extrema their product is 1 by equation (5.51) which means that the region for two critical points grows from $\alpha = 1$ as β is increased.

Two graphs of h can be seen in figure 5.14. By computing the local minimum B' and the local maximum, C' we get the bifurcation diagram in 5.15a where crossing of the blue or black curve corresponds to a change in topology by a saddle node bifurcation. For any given $\beta = \delta$ then for sufficiently large or small, positive α then only one critical point of the vorticity contour exists which is of center type.

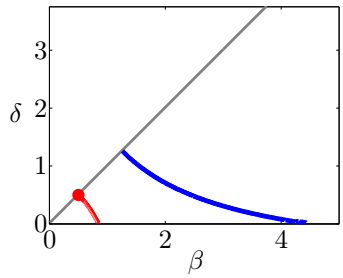

Figure 5.13: The blue curve is the bifurcation $B = C$ and the red curve is the corresponding curve $B' = C'$. The red dot is $\left(\frac{1}{2}, \frac{1}{2}\right)$ which is the creation of local extrema for $\beta = \delta$. This point is neatly on the red curve.

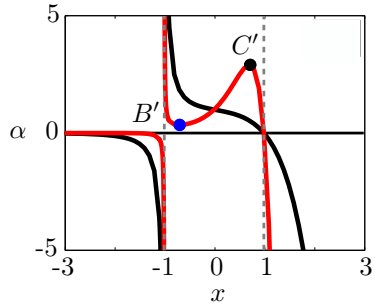

Figure 5.14: $\delta = \beta$. The red curve is the graph of $y = h(x, 1)$ and the black curve is the graph of $y = h(x, 0.4)$. The two local extrema appear for $|x| < 1$ and are symmetric around $x = 0$.

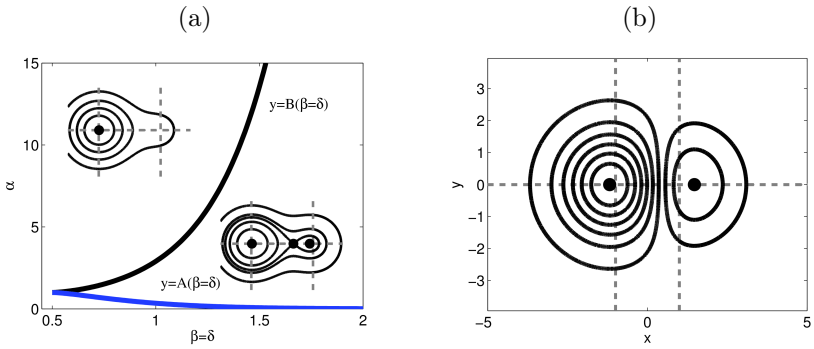

Figure 5.15: (a) The bifurcation diagram for $\delta = \beta$ corresponding to figure 5.5. The black curve corresponds to the local maximum of g as δ is varied and the blue curve corresponds to the local minimum. (b) For $\beta = \delta$ and $\alpha < 0$ two centers are the only critical points. Here $\beta = \delta = 0.4$, $\alpha = -2$.

There are no singularities in g as $\delta \to \beta$. However, there is significant change in g at this limit. For $\beta > \delta$ g has one critical point for $x > 1$ giving a lower bound on g in this region. Hence, for negative values of α larger than this local minimum there are three critical points of the vorticity contours and for α smaller than this value there is one critical point. However, as $\delta \to \beta^-$ x has to be very large before the second order term is dominant in the exponential of g, equation (5.43). Before this happens the linear term dominates forcing the value of g to be very low. Hence, the local minimum gets very low in this limit. This means the saddle point of the vorticity contour moves very far from $x = 0$. At $\beta = \delta$ there are exactly two critical points of g for any $\alpha > 0$ which may be interpreted as the saddle has moved to infinity as the local minimum moves to negative infinity. Hence, restricting the parameters to $\beta = \delta$ gives a radically different behaviour when considering $\alpha < 0$.

5.3 Conlusion on topology of streamlines and vorticity of two Gaussian vortices

The streamline topology and the vorticity contour are very alike in many aspects. At least one critical point and at most three critical point exist. For $\alpha > 0$ critical points only occur for $|x| < 1$ and for $\alpha < 0$ critical points only occur for $|x| > 1$. For $\alpha < 0$ increasing $|x|$ from 1 the first occurring critical point is a center and then of alternating type. For $\alpha > 0$ the same holds for decreasing $|x|$ from 1. For sufficiently large $|\alpha|$ and for $\alpha \to 0^+$ there is only one critical point which is the manifestation of one vortex globally dominating the flow regardless of the variances of the Gaussian distributions and the distance between the vortices. However, 'large' depends on the value of (β, δ). For $\alpha \to 0^-$ the conclusion still applies to the streamlines but for the vorticity there are two centers and a saddle. The case $\alpha < 0$, $\beta = \delta$ has special character for the vorticity where two centers and no saddles exist. The topology shown in figure 5.9d is not obtainable, whereas the streamlines have no special topology restricted to this parameter range. For large β and δ there exists a range of α close to 1 such that there are three critical points of the streamlines. Hence, for 'distant' vortices with comparable vortex strength the streamlines look like those for two point vortices.

For α close to -1 there is always three critical points of the streamlines for any value of β and δ. The parameter region where three critical points exist of the streamlines constitute a small subset of the parameter region where three critical points exist of the vorticity contours. Topologies with three critical points dominate for large β and δ corresponding to the point vortex case when the singularities are interpreted as centers, while exactly one critical point dominates for β and δ small.

5.4 Two moving, rotational invariant vortices

So far we only consider instantaneous streamlines at $t = 0$ but for any values of the parameters (α, β, δ). One might want to be more ambitious and study the instantaneous streamlines at any $t \geq 0$. For point vortex models as well as multi-Gaussian models the center of a vortex moves in the field described by the remaining vortices. We will use the same assumption here reconsidering two rotational invariant vortices not necessarily Gaussian. In case of viscous flow this means the viscous effect is included separately for each vortex and this has to fulfil rotational symmetry.

Let the center of vortex 1 at (x_1, y_1) be advected in the field of vortex 2 at (x_2, y_2) and vice versa - see figure 5.16. Each vortex induce a velocity contribution of the form $\boldsymbol{u}_i = u_{\theta_i} \boldsymbol{e}_{\theta_i}$ - see figure 5.2.

We allow u_{θ_1} and u_{θ_2} to depend on time and on parameters to take into account viscous effects. The functional form of u_{θ_1} and u_{θ_2} may be different. However, the assumption on initial rotational invariant fields can not be relaxed. This guarantees that the force on a vortex is orthogonal to the distance vector connecting the vortices. Since $|r_1| = |r_2|$ the common value is denoted r. With

$$\boldsymbol{e}_{\theta_1} = \frac{y_1 - y_2}{r} \boldsymbol{e}_1 + \frac{x_2 - x_1}{r} \boldsymbol{e}_2 \,, \tag{5.55}$$

and $\boldsymbol{e}_{\theta_2} = -\boldsymbol{e}_{\theta_1}$ we get using the contribution from vortex i on vortex j being $u_{\theta_i}(r)\boldsymbol{e}_{\theta_i}$ that

$$\frac{\mathrm{d}x_1}{\mathrm{d}t} = \frac{y_2 - y_1}{r} u_{\theta_2} \,, \qquad \frac{\mathrm{d}y_1}{\mathrm{d}t} = \frac{x_1 - x_2}{r} u_{\theta_2} \tag{5.56a}$$

$$\frac{\mathrm{d}x_2}{\mathrm{d}t} = \frac{y_1 - y_2}{r} u_{\theta_1} \,, \qquad \frac{\mathrm{d}y_2}{\mathrm{d}t} = \frac{x_2 - x_1}{r} u_{\theta_1} \tag{5.56b}$$

One may consider the time derivative of $r^2 = (x_2 - x_1)^2 + (y_2 - y_1)^2$ to demonstrate that $\frac{\mathrm{d}r}{\mathrm{d}t} = 0$ using equation (5.56). Hence, the distance between the two vortices is a time constant. However, we will use complex coordinates to simplify the derivation of the rotation rate of the vector connecting the two vortices. Also, complex coordinates have been the preferred set up for point vortex dynamics and hence a complex formulation may facilitate the comparison to this. Defining

$$z = x + iy \tag{5.57}$$

the equations of motion equation (5.56) can be formulated (using a bar for complex conjugate)

$$\frac{\mathrm{d}\bar{z}_1}{\mathrm{d}t} = \frac{\mathrm{d}x_1}{\mathrm{d}t} - i\frac{\mathrm{d}y_1}{\mathrm{d}t} \tag{5.58}$$

$$= \frac{y_2 - y_1}{r} u_{\theta_2} - i\frac{x_1 - x_2}{r} u_{\theta_2} \tag{5.59}$$

$$= \frac{\bar{z}_2 - \bar{z}_1}{r} i u_{\theta_2} \tag{5.60}$$

and similarly

$$\frac{\mathrm{d}\bar{z}_2}{\mathrm{d}t} = \frac{\bar{z}_1 - \bar{z}_2}{r} i u_{\theta_1} . \tag{5.61}$$

Defining

$$Z = z_1 - z_2 \tag{5.62}$$

the vector Z has length r and is the vector from $x_1 + iy_1$ to $x_2 + iy_2$. An evolution equation for Z is then constructed directly from equation (5.60) and equation (5.61)

$$\frac{\mathrm{d}\bar{Z}}{\mathrm{d}t} = -\frac{\bar{Z}}{|Z|} i \left(u_{\theta_1} + u_{\theta_2}\right) \tag{5.63}$$

and forming the complex conjugate we get

$$\frac{\mathrm{d}Z}{\mathrm{d}t} = \frac{Z}{|Z|} i \left(u_{\theta_1} + u_{\theta_2}\right) . \tag{5.64}$$

Considering the time derivative of the squared length, of Z and using equation (5.63) and equation (5.64)

$$\frac{\mathrm{d}|Z|^2}{\mathrm{d}t} = \frac{\mathrm{d}}{\mathrm{d}t}\left(Z\bar{Z}\right) = \frac{\mathrm{d}Z}{\mathrm{d}t}\bar{Z} + Z\frac{\mathrm{d}\bar{Z}}{\mathrm{d}t} = 0 . \tag{5.65}$$

This proves the distance between the center of the two initial vortices is conserved. Writing Z in complex form

$$Z = re^{i\phi} \tag{5.66}$$

with r being constant in time, the rotation rate of Z can easily be computed by inserting equation (5.66) in equation (5.64)

$$\frac{\mathrm{d}\phi}{\mathrm{d}t} = \frac{u_{\theta_1} + u_{\theta_2}}{r} . \tag{5.67}$$

For time independent u_{θ_1} and u_{θ_2} the rotation rate is constant as for the case of point vortices. However, for a diffusing vortex core u_{θ_1} and u_{θ_2} are time dependent so the rotation rate is time dependent. Nevertheless, even for time dependent $u_{\theta_1} = -u_{\theta_2}$ the vector Z has a constant angle. For point vortex flow with two point vortices the flow is further simplified by a constant of the flow being $\Gamma_1 z_1 + \Gamma_2 z_2$. Divided by $\Gamma_1 + \Gamma_2$ this is called the center of vorticity and it is the rotation center for circular motion of each of the two vortices. For arbitrary, $u_\theta(r, t)$ one cannot expect this invariant to exists. This means the vector Z may translate as well as rotate.

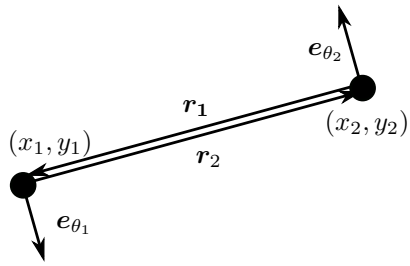

Figure 5.16: The motion of one vortex center is prescribed by the field of the other vortex.

5.4.1 Implications for the multi Gaussian model

In the multi Gaussian model with two Gaussian vortices the distance between the vortices is conserved. Therefore, a comoving frame exists in which the location of the Gaussian vortex centers are fixed. The time dependence in this frame is only visible through the diffusing vortex cores. This means the thorough analysis performed for the instantanous streamlines at $t = 0$ in previous sections also applies to $t > 0$ restricting the paths through the bifurcation diagrams to match diffusing cores. This means that the time evolution induces α is fixed while β and δ goes to zero. If the initial topology consists of three critical points then as β and δ approach zero, only one critical point remains.

The meaning of different β and δ is seen from equation (5.12); the vortices are created at different times. Considering the case $\sigma_1 > \sigma_2$ this means we can use $\sigma_1^2 = 4\nu(t + t_0)$, $\sigma_2^2 = 4\nu t$ for $t_0 \geq$. Using equation (5.12) this means a curve of increasing time is given by the parametrized curve

$$(\beta(t), \delta(t)) = \frac{d^2}{4\nu}\left(\frac{1}{t}, \frac{1}{t + t_0}\right). \tag{5.68}$$

The time evolution are then curves with constant α and (β, δ) following the curves in figure 5.17

We can apply the formula for the rotation rate equation (5.67) on two Gaussian vortices which in unscaled variables is

$$\frac{\mathrm{d}\phi}{\mathrm{d}t} = \frac{\Gamma_1\left(1 - e^{-\frac{(2d)^2}{\sigma_1^2}}\right) + \Gamma_2\left(1 - e^{-\frac{(2d)^2}{\sigma_2^2}}\right)}{2\pi(2d)^2} \tag{5.69}$$

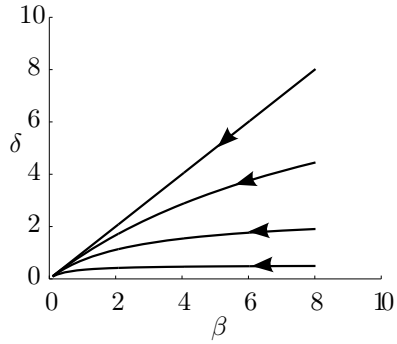

Figure 5.17: Black curves showing $(\beta(t), \delta(t))$ corresponding to equation (5.68).

which for σ_1 and σ_2 tending to zero tends to the constant rate $\frac{\Gamma_1+\Gamma_2}{2\pi(2d)^2}$ well known for two point vortices. Hence, sharply defined Gaussian vortices rotate like point vortices.

For diffusing vortex cores σ_1 and σ_2 tend to infinity. Then $\frac{\mathrm{d}\phi}{\mathrm{d}t}$ goes to zero, and for $\Gamma_1\Gamma_2 > 0$, or $\sigma_1 = \sigma_2$ it is clear from inspection of $\frac{d^2\phi}{dt}$ that this happens monotonically implying that the vorticity simply dampens the rotation. This is also found in [61] in the special case $\Gamma_1 = \Gamma_2$ and $\Gamma_1 = 2\Gamma_2$.

A case with three vortices being stationary in the inviscid case is studied by Jing et al. [60]. Here, inclusion of viscous effects using the multi Gaussian model cause rotation of the configuration that ultimately dies out - i.e. a viscously induced rotation which is also seen in direct simulation of the Navier - Stokes equation.

A very special case occurs for $\Gamma_1 = -\Gamma_2$ and $\sigma_1 = \sigma_2$. Then the rotation rate is 0 for any time which is also well known from the point vortex case.

The existence of a time invariant center of vorticity is used for the point vortex case to deduce that each vortex moves on a circle. This relies on a certain linear combination of the position of the vortices being a time invariant. We investigate if a linear combination of the vortex postions is conserved in the model considered here similar to the center of vorticity. Using equation (5.61) and equation (5.60)

$$0 = \frac{\mathrm{d}}{\mathrm{d}t}\left(c_1 z_1 + c_2 z_2\right) = c_1 \frac{\mathrm{d}z_1}{\mathrm{d}t} + c_2 \frac{\mathrm{d}z_2}{\mathrm{d}t} = \frac{z_2 - z_1}{r} i \left(c_2 u_{\theta_2} - c_1 u_{\theta_1}\right) \tag{5.70}$$

There exist a non trivial solution only if u_{θ_1} and u_{θ_2} are proportional i.e. only if $\beta = \delta$. In this case $c_1 = \Gamma_2$ and $c_2 = \Gamma_1$. This means that for $\beta = \delta$ the two

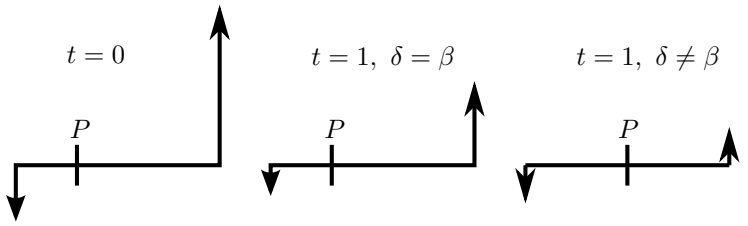

Figure 5.18: The rotation of Z implies circular motion around the point P of the two vortices if $\beta = \delta$. Otherwise the rotation center may move in time hence giving also a translational motion.

vortices rotate around a common center. Considering figure 5.18 increasing time means decreasing the speed of both vortices but for $\beta = \delta$ this conserves the rotation center. For $\beta \neq \delta$ one vortex may decrease its speed much relative to the other. This means the 'point of rotation' moves hence indicating that the vortices also translate.

5.4.2 Perspectives to erupted vortices

For two Gaussian vortices there are a range of parameters where the streamlines and the vorticity contours have the same topology which is also seen in a part of parameter space for two Gaussian vortices.

The analysis of Gaussian vortices confirm that the vortices defined from extrema of the vorticity is more 'robust' to change in parameters than the vortices defined from the streamlines. Hence, as viscosity 'drains' the erupted vortex for vorticity then the streamline vortex vanish before the vorticity vortex. In figure 5.19 an example of this is shown for two vortices of opposite circulation. Notice also that the vorticity centers are located closer together than the streamline centers. This is consistent with the simulations of an erupted vortex where a persistent 'offset' between the streamline vortex and the vorticity vortex is present. The streamline vortex is further away from the generating patch than the vorticity vortex - see for example figure 3.17f.

We have considered the instantaneous streamlines and vorticity contours for two Gaussian vortices. Increasing time causes the vortex cores to diffuse which in model parameters mean β and δ decrease towards zero. From figure 5.19 it seems that for two initial vortices of opposite circulation then first the streamline topology is similar to a single Lamb - Oseen vortex and then the same happens to the vorticity. The robustness of critical points of the vorticity compared to

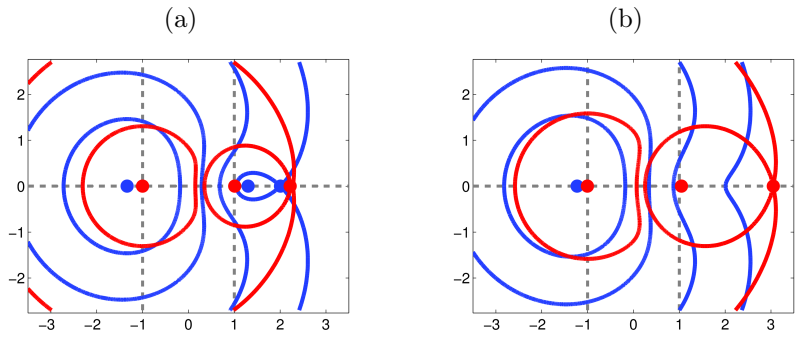

Figure 5.19: The contours of ω (red) and ψ (blue) are shown for $(\alpha, \beta, \delta) = (-3, 5, \frac{1}{2})$ in (a) and $(\alpha, \beta, \delta) = (-3, 2, 0.4348)$ using the time evolution of (β, δ) prescribed by equation (5.68). From (a) to (b) a saddle node bifurcation has occurred in the streamlines while the vorticity topology is unaffected.

the critical points of the streamlines are also seen in the numerics on eruption of boundary - layer.

The long term behaviour with a single critical point of center type is a manifestation of the strong result by Gallay & Wayne [39] that any integrable initial vorticity distribution of the two dimensional Navier - Stokes equation has an asymptotic solution being the Lamb - Oseen vortex with circulation determined by the total, initial vorticity. The long term Gaussian behavior is also found in a more special case by Agullo & Verga [3, 4] who investigate a stochastic representation of the Navier - Stokes equations in $\mathbb{R}^2$ with two point vortices as initial condition.

For two rotational symmetric vortices there is an alignment of all critical points when more than one exist. In the Gaussian case with vortices of opposite sign there are three critical points - a center with a center and a saddle on either side. In the simulations one observes an increasing alignment in the streamlines of the generating vortex center, the erupted vortex center and the corresponding saddle point - see figure 3.19e and 3.19f. In this aspect the simulations approach the behaviour of two Gaussian vortices.

Bibliography

[1] Milton Abramowitz and Irene A. Stegun. *Handbook of Mathematical Functions*. Dep. of Commerce, USA, 1964.

[2] D.J. Acheson. *Elementary Fluid Dynamics*. Oxford Applied Mathematics and Computing Science Series. Clarendon Press, 1990.

[3] O. Agullo and A. D. Verga. Exact two vortices solution of navier-stokes equations. *Phys. Rev. Lett.*, 78:2361–2364, 1997.

[4] Olivier Agullo and Alberto Verga. Effect of viscosity in the dynamics of two point vortices: Exact results. *Physical Review E*, 63(5):056304, 2001.

[5] S. V. Alekseenko, P. A. Okulov, and S. I. Shtork. Helical vortices in swirl flow. *J. Fluid Mech.*, 382:195–243, 1999.

[6] S.V. Alekseenko, P.A. Kuibin, and V.L. Okulov. *Theory of concentrated vortices*. Springer-Verlag Berlin Heidelberg, 2007.

[7] M. Amoretti, Durkin D., J. Fajans, R. Pozzoli, and M. Romè. Asymmetric vortex merger: Experiments and resuls. *Physics of Plasma*, 8:3865–3868, 2001.

[8] H. Aref, P. K. Newton, M. A. Stremler, T. Tokieda, and D. L. Vainchtein. Vortex crystals. *Advances in Applied Mechanics, VOL 39*, 39:1–79, 2003.

[9] P. G. Bakker. *Bifurcations in Flow Patterns*. Kluwer Academic Publishers, 1991.

[10] G.K. Batchelor. *An introduction to fluids dynamics*. Cambridge University Press, 1967.

[11] P. Billant, P Brancher, and J Chromaz. Three-dimensional stability of a vortex pair. *Physics of Fluids*, 11:2069 – 2077, 1999.

[12] L. K. Brandt and K. K. Nomura. The physics of vortex merger and the effects of ambient stable stratification. *Journal of Fluid Mechanics*, 592:413–446, 2007.

[13] L. K. Brandt and K. K. Nomura. Characterization of the interactions of two unequal co-rotating vortices. *Journal of Fluid Mechanics*, 646:233–253, 2010.

[14] M. Brøns. Topological fluid dynamics of interfacial flows. *Phys. Fluids*, 6(8):2730–2737, 1994.

[15] M. Brøns and A. V. Bisgaard. Bifurcation of Vortex Breakdown Patterns in a Circular Cylinder with two Rotating Covers. *J. Fluid Mech.*, 568:329–349, 2006.

[16] M. Brøns, L. K. Voigt, and J. N. Sørensen. Streamline topology of steady axisymmetric vortex breakdown in a cylinder with co- and counter-rotating end-covers. *J. Fluid Mech.*, 401:275–292, 1999.

[17] Morten Brøns. Streamline Topology: Patterns in Fluid Flows and their Bifurcations. *Advances in Applied Mechanics*, 41:1–42, 2007.

[18] R.E. Caflisch and M Sammartino. Existence and singularities for the Prandtl boundary layer equations. *Zeitschrift fur Angewandte Mathematik und Mechanik*, 80(11-12):733–744, 2000.

[19] C. Canuto, M. Y. Hussaini, A. Quarteroni, and T. A. Zang. *Spectral Methods - Fundamentals in Single Domains*. Springer Verlag, 2006.

[20] K. W. Cassel. A comparison of Navier - Stokes solutions with the theoretical description of unsteady separation. *Philosophical Transactions of the Royal Society of London Series A*, 358(1777):3207–3227, 2000.

[21] K. W. Cassel and A. V. Obabko. A Rayleigh instability in a vortex-induced unsteady boundary layer. *Physica Scripta*, T142, December 2010.

[22] K. W. Cassel, F. T. Smith, and J. D. A. Walker. The onset of instability in unsteady boundary-layer separation. *Journal of Fluid Mechanics*, 315:223–256, 4 1996.

[23] C. Cerretelli and H.K. Williamson. The physical mechanism for vortex merging. *J. Fluid Mech.*, 475, 2003.

[24] S. Childress, M. Landman, and H. Strauss. Steady motion with helical symmetry at large Reynolds number. In by H. K. Moffatt and A. Tsinober, editors, *Topological fluid mechanics, proceedings of the IUTAM Symposium, Cambridge University Press*. Cambridge University Press, 1990.

[25] M. S. Chong, A. E. Perry, and B. J. Cantwell. A general classification of three-dimensional flow fields. *Physics of Fluids A: Fluid Dynamics*, 2(5):765–777, 1990.

[26] S. J. Cowley, L.L. Van Dommelen, and S.T. Lam. On the use of Lagrangian variables in descriptions of unsteady boundary-layer separation. *Philosophical Transactions of the Royal Society of London Series A*, 333(1631):343–378, 1990.

[27] S.J. Cowley, L.M. Hocking, and O.R. Tutty. The stability of the solutions of the classical unsteady boundary - layer equation. *Physics of Fluids*, 28(2):441–443, 1985.

[28] W. R. Dean. Note on the notion of fluid in a curved pipe. *Philosophical Magazine*, 4:208–223, 1927.

[29] A. T. Degani, J. D. A. Walker, and F. T. Smith. Unsteady separation past moving surfaces. *Journal of Fluid Mechanics*, 375:1–38, 1998.

[30] Ivan Delbende, Maurice Rossi, and Olivier Daube. DNS of flows with helical symmetry. *Theor. Comput. Fluid Dyn.*, 26:141–160, 2012.

[31] A. Deliceoğlu. Topology of two-dimensional flow associated with degenerate dividing streamline on a free surface. *Euro. J. Appl. Math.*, 24(1):77–101, 2013.

[32] Norbert Didden and Chih-Ming Ho. Unsteady separation in a boundary layer produced by an impinging jet. *Journal of Fluid Mechanics*, 160:235–256, 10 1985.

[33] T. L. Doligalski, C. R. Smith, and J. D. A. Walker. Vortex interactions with walls. *Annual Review of Fluid Mechanics*, 26:573–616, 1994.

[34] T. L. Doligalski and J. D. A. Walker. The boundary layer induced by a convected two-dimensional vortex. *Journal of Fluid Mechanics*, 139:1–28, 1984.

[35] David G. Dritschel. Generalised helical Beltrami flows in hydrodynamics and magnetohydrodynamics. *J. Fluid Mech.*, 222:525–541, 1991.

[36] Boris Ettinger and Edriss S. Titi. Global existence and uniqueness of weak solutions of three-dimensional Euler equations with helical symmetry in the absence of vorticity stretching. *Siam J. Math. Anal.*, 41:269–296, 2009.

[37] Y. Fukumoto and V. L. Okulov. The velocity field induced by a helical vortex tube. *Physics of Fluids*, 17, 2005.

[38] Thierry Gallay. Interaction of vortices in weakly viscous planar flows. *Archive for Rational Mechanics and Analysis*, 200(2):445–490, 2011.

[39] Thierry Gallay and C. Eugene Wayne. Global stability of vortex solutions of the two-dimensional Navier-Stokes equation. *Communications in Mathematical Physics*, 255(1):97–129, 2005.

[40] F. Gargano, M. Sammartino, and V. Sciacca. High Reynolds number Navier-Stokes solutions and boundary layer separation induced by a rectilinear vortex. *Computers & Fluids*, 52:73–91, 2011.

[41] M. Germano. The Dean equations extended to a helical pipe flow. *J.Fluid Mech.*, 203:289–305, 2009.

[42] M. Golubitsky, I. Stewart, and D.G. Schaeffer. *Singularities and Groups in Bifurcation Theory.* Applied Mathematical Sciences. Springer, 1988.

[43] B.P. Gupta and R.G. Loewy. Theoretical analysis of the aerodynamic stability of multiple,interdigitated helical vortices. *AIAA Journal*, 12:1381–1387, 1974.

[44] G Haller. Finding finite-time invariant manifolds in two-dimensional velocity fields. *Chaos*, 10(1):99–108, 2000.

[45] G. Haller. Exact theory of unsteady separation for two-dimensional flows. *Journal of Fluid Mechanics*, 512:257–311, 2004.

[46] G. Haller. An objective definition of a vortex. *J. Fluid Mech.*, 525:1–26, 2005.

[47] G. Haller and G. Yuan. Lagrangian coherent structures and mixing in two-dimensional turbulence. *Physica D*, 147:352–370, 2000.

[48] J. C. Hardin. The velocity field induced by a helical vortex filament. *Physics of Fluids*, 25:1949–1952, 1982.

[49] J.N. Hartnack. Streamline topologies near a fixed wall using normal forms. *Acta Mechanica*, 136(1-2):55–75, 1999.

[50] Johan Nicolai Hartnack. *Structural changes in incompressible flow patterns.* PhD thesis, Department of Mathematics, Technical University of Denmark, 1999.

[51] J. K. Harvey and F.J. Perry. Flowfield produced by trailing vortices in the vicinity of the ground. *AIAA*, 9:1659–1660, 1971.

[52] H. Helmholtz. Über integrale der hydrodynamischen gleichungen, welche den wirbelbewegungen entsprechen. *Journal für die reine und angewandte Mathematik*, 55:25–55, 1858.

[53] J. C. R. Hunt, A. A. Wray, and P. Moin. Eddies, streams and convergence zones in turbulent flows. *Center for Turbulence Research Report CTR-S88*, pages 193–208, 1988.

[54] K. Ide, D. M. Small, and S. R. Wiggins. Distinguished hyperbolic trajectories in time-dependent fluid flows: analytical and computational approach for velocity fields defined as data sets. *Nonlinear Processes in Geophysics*, 9 (3-4):237 – 263, 2002. Publisher: European Geophysical Soc.

[55] Rutger H.A. Ijzermans, Rob Hajmeijer, and Pieter J. van Langen. Accumulation of heavy particles around a helical vortex filament. *Physics of Fluids*, 19:107102, 2007.

[56] Hidesato Ito. Flow in curved pipes. *The Japan Society of Mechanical Engineers*, 30:543–552, 2007.

[57] L. Jacquin, D. Fabre, D. Sipp, V. Theofilis, and H. Vollmers. Instability and unsteadiness of aircraft wake vortices. *Aerospave Science and Technology*, 7:577–593, 2003.

[58] J. Jeong and F. Hussain. On the identification of a vortex. *J. Fluid Mech.*, 285:69–94, 1995.

[59] F Jing. *Viscous Evolution of Point Vortex Equilibria*. PhD thesis, University of Southern California, Los Angeles, 2011.

[60] Fangxu Jing, Eva Kanso, and Paul K. Newton. Viscous evolution of point vortex equilibria: The collinear state. *Physics of Fluids*, 22:123102, 2010.

[61] Fangxu Jing, Eva Kanso, and Paul K. Newton. Insights into symmetric and asymmetric vortex mergers using the core growth model. *Physics of Fluids*, 24:073101, 2012.

[62] George Em Karniadakis, Moshe Israeli, and Steven A. Orszag. High-order splitting methods for the incompressible Navier-Stokes equations. *Journal of Computational Physics*, 97:414443, 1991.

[63] George Em Karniadakis and Spencer Sherwin. *Spectral/hp element methods for computational fluid dynamics, second edition*. Oxford University Press, 2005.

[64] H. Kudela and Z. M. Malecha. Eruption of a boundary layer induced by a 2d vortex patch. *Fluid Dyn. Res.*, 41:055502, 2009.

[65] L.D. Landau and E.M. Lifshitz. *Fluid Mechanics*. Pergammon Press, 1959.

[66] Michael J. Landman. On the generation of helical waves in circular pipe flow. *Phys. Fluids A*, 2:738–747, 1990.

[67] Michael J. Landman. Time-dependent helical waves in rotating pipe flow. *J. Fluid Mech.*, 221:289–310, 1990.

[68] Shijie Liu and Jacob H. Masliiyah. Axially invariant laminar flow in helical pipes with a finite pitch. *J. Fluid Mech.*, 251:315–353, 1993.

[69] D. Lo Jacono, M. Nazarinia, and M. Brøns. Experimental vortex breakdown topology in a cylinder with a free surface. *Phys. Fluids*, 11:111704, 2009.

[70] Dan Lucas and David G. Dritschel. A family of helically symmetric vortex equilibria. *J. Fluid Mech.*, 634:245–268, 2009.

[71] Hans J. Lugt. *The Dilemma of Defining a Vortex.* Springer - Verlag Berlin, 1979.

[72] C. Marchioro. On the Inviscid limit for a Fluid with a Concentrated Vorticity. *Commun Math Phys*, 193:53–65, 1998.

[73] J. D. Meiss. *Differential Dynamical Systems.* Differential Dynamical Systems. Society for Industrial and Applied Mathematics, 2007.

[74] P. Meunier, U. Ehrenstein, T. Leweke, and M. Rossi. A merging criterion for two-dimensional co-rotating vortices. *Physics of Fluids*, 2002:2757–2766, 2002.

[75] P. Meunier, S. Le CizÃ¨s, and T. Leweke. Physics of vortex merging. *C. R. Physique*, 2005:431–450, 2005.

[76] Igor Mezic, Anthony Leonard, and Stephens Wiggins. Regular and chaotic particle motion near a helical vortex filament. *Physica D*, 111:179–201, 1998.

[77] P.K. Newton. *The N-Vortex Problem: Analytical Techniques.* Applied Mathematical Sciences. Springer, 2001.

[78] A. V. Obabko and K. W. Cassel. Navier-Stokes solutions of unsteady separation induced by a vortex. *Journal of Fluid Mechanics*, 465:99–130, 2002.

[79] A. V. Obabko and K. W. Cassel. On the ejection-induced instability in Navier-Stokes solutions of unsteady separation. *Philosophical Transactions of the Royal Society of London Series A*, 363(1830):1189–1198, 2005.

[80] V. L. Okulov. The velocity field induced by helical vortex filaments with cylindrical or conic supporting surface. *Russian Journal of Engineering Thermophysics*, 5:63–75, 1995.

[81] V. L. Okulov. On the stability of multiple helical vortices. *J. Fluid Mech.*, 521:319–342, 2004.

[82] V. L. Okulov and J. N. Sørensen. Stability of helical tip vortices in a rotor far wake. *J. Fluid Mech.*, 576:1–25, 2007.

[83] F.W.J. Olver. The asymptotic expansion of Bessel functions of large order. *Philosophical Transactions of The Royal Society A*, 247:328–368, 1954.

[84] F.W.J. Olver. The asymptotic solution of linear differential equations of the second order for large values of a parameter. *Philosophical Transactions of The Royal Society A*, 247:307–327, 1954.

[85] L. Prandtl. Über Flüssigkeitsbewegung bei sehr kleiner Reibung. In A. Krazer, editor, *Verhandlungen des dritten internationalen Mathematiker-Kongresses in Heidelberg*. Leipzig, Teubner, 1904.

[86] Renzo L. Ricca. The effect of torsion on the motion of a helical vortex filament. *J. Fluid Mech.*, 273:241–259, 1994.

[87] Renzo L. Ricca. The contributions of Da Rios and Levi-Civita to asymptotic potential theory and vortex filaments dynamics. *Fluid Dynamics Research*, 18:245–268, 1996.

[88] Luigi Sante Da Rios. Sul moto d'un liquido indefinito con un filetto vorticoso di forma qualunque. *Rendiconti del Circolo Matematico di Palermo*, 22:117–135, 1906.

[89] S.K. Robinson. A review of vortex structures and associated coherent structures in turbulent boundary layers. In A Gyr, editor, *Structure of Turbulence and Drag Reduction, IUTAM Symposium*. Springer- Verlag Heidelberg, 1989.

[90] S.K. Robinson. Coherent motions in the turbulent boundary-layer. *Annual Review of Fluid Mechanics*, 23:601–639, 1991.

[91] C. Roy, N. Schaeffer, S. Le Dizès, and M.C. Thompson. Stability of a pair of co-rotating vortices with axial flow. *Physics of Fluids*, 20(9):094101–8, 2008.

[92] P.G. Saffman. *Vortex dynamics*. Cambridge University Press, 1992.

[93] L. G. Sarasua, A. C. Sicardi Schifino, and R. Gonzalez. The stability of steady, helical vortex filaments in a tube. *Physics of Fluids*, 11:1096–1103, 1998.

[94] W. Sears and D. Telionis. Boundary-layer separation in unsteady flow. *SIAM Journal on Applied Mathematics*, 28(1):215–235, 1975.

[95] T. K. Sengupta, S. De, and S. Sarkar. Vortex-induced instability of an incompressible wall-bounded shear layer. *Journal of Fluid Mechanics*, 493:277–286, 2003.

[96] J. N. Sørensen. Instability of helical tip vortices in rotor far wakes. *J Fluid Mech.*, 682:1–4, 2011.

[97] M. C. Thompson, K. Hourigan, A. Cheung, and T. Leweke. Hydrodynamics of a particle impact on a wall. *App. Math. Model.*, 30(11):1356–1369, 2006.

[98] G.N. Throumoulopoulos and H. Tasso. Ideal magnetohydrodynamics equilibria with helical symmetry and incompressible flows. *J. Plasma Physics*, 62:449–459, 1999.

[99] E.R. Tuttle. Laminar flow in twisted pipes. *J. Fluid Mech.*, 219:545–570, 1990.

[100] L.L. Van Dommelen and S.J. Cowley. On the Lagrangian description of unsteady boundary-layer separation .1. General theory. *Journal of Fluid Mechanics*, 210:593–626, 1990.

[101] J. D. A. Walker. Boundary-layer due to rectilinear vortex. *Proceedings of the Royal Society A*, 359(1697):167–188, 1978.

[102] S. Wiggins. *Introduction to Applied Nonlinear Dynamical Systems and Chaos*. Texts in Applied Mathematics. Springer, 2003.

[103] J. C. Williams. Incompressible boundary-layer separation. *Annual Review of Fluid Mechanics*, 9(1):113–144, 1977.

[104] L. Zabielski and A.J. Mestel. Steady flow in a helically symmetric pipe. *J. Fluid Mech.*, 370:297–320, 1998.

[105] L. Zabielski and A.J. Mestel. Unsteady flow in a helically symmetric pipe. *J. Fluid Mech.*, 370:321–345, 1998.